Round 3: For this test the model was buried in the ground and the charge was increased to four ounces. As in the previous two firings, seizing of the guide tube about the rod did not occur. The pressure vessel raised out of the ground slightly when the charge was fired and it was noted that the vessel failed at the bottom head weld. The pressure vessel bulge and bottom head deformation resembled the contours which were present on the SL-1 pressure vessel after the excursion.

Round 4: The pressure vessel was rewelded and the charge weight increased to eight ounces. The model, which had been buried in the ground, lifted slightly during the firing but the actual height the model rose was not determined. There was sufficient collapse of the guide tube to indicate that conditions during this round were very nearly equivalent to the reactor incident, The extension rod no longer slid freely in the housing. The deformation in the lower section of the model was attributed to the repeated firings. However, the deformation just below the flange was due to the effect of the water hammer which was very nearly equivalent to that produced in the SL-1. The two side pressure gage holes were found to have been distorted elliptically, similar to the steam pipe hole in the original pressure vessel. The deformation of the bottom head was much more severe than it had been during round 3 and it resembled the deformation observed in the original vessel. The model pressure vessel failed at the bottom head weld and had a 1/4 inch wide split 15 inches long which started 6 inches from the bottom head. Figure III-40 shows three nozzles, #1, 7 and 9, split longitudinally. All nozzles were expanded adjacent to the head, the same effect observed in the original vessel. A pressure trace was obtained by a pressure gage mounted on the head. In Figure III-41 the oscilloscope sweep time was set for 500 milliseconds. The trace shows the pressure-time history of the accelerated water column hitting the bottom side of the head and the tremendous increase in pressure due to the compression of the water column. The discontinuity of the trace at approximately 10 milliseconds does not represent a pressure plateau but that the pressure produced exceeded the range of the pressure measuring equipment. It appears from the figure that the maximum pressure obtained was on the order of several thousand psi. After compression of the accelerated water column against the underside of the pressure vessel head, the pressure decreased to an average value of 550 psi and was maintained for nearly a second. This value corresponds to the estimated pressure required to accelerate the water column which created the water hammer in the SL-1 itself. It also indicates that the pressure under the water column remained essentially constant until all of the water was expelled. This constant pressure apparently did not allow the column of water to fall back into the core. The decrease in the pressure as the water escaped is roughly compensated by continued heat transfer to gas. Thus, the pressure remained essentially constant during the escape of the water*.

*Data from a second pressure sensing device substantiated the average decay pressure of 550 psi for those conditions.

Phase III. After the optimum charge size was obtained the firing was repeated with the head off to determine the water velocity and profile. The results of this phase were limited to the firing of a four ounce charge. The pressure vessel ruptured, so that further testing was impossible. The water velocity associated with this shot was 130 ft/sec.

Phase IV was not conducted. In this test the pressure vessel was to have been turned down to the scaled wall thickness and the optimum charge size fired in the closed system.

Conclusions: The results of the firing of the eight ounce charge in the closed vessel closely approximated the results of the incident. The velocity of the water column for this firing was estimated to be 25% greater than the 130 ft/sec. measured for the four ounce charge. The average pressure measured behind the water column and its estimated velocity at impact made calculations possible which supported the postulated maximum pressure of 7000 to 10,000 psi acting on the guide tube. This pressure and the period over which it acted are partially confirmed by the instrument trace. The experiment indicated that all of the water above the thermal shield was expelled through the nozzles. Damage to the model was similar to that produced by the SL-1 excursion. The desired measurements, although plagued by numerous troubles, substantiated the postulated behavior.

1.7 Core and Thermal Shield Deformation

1.7.1 Preliminary Observation Underneath Core

Prior to removing the vessel from its support cylinder at the SL-1 site, a 2 inch diameter hole was drilled through the support cylinder pressure vessel and thermal shield. The hole entered the vessel several inches below the main core support structure.

Photographs were taken by the use of a 1-3/4 inch diameter boroscope looking upward at the core. Visual observation was conducted as extensively as possible in trying to picture the appearance of the core.

Examination of the photographs and visual observation revealed the following information:

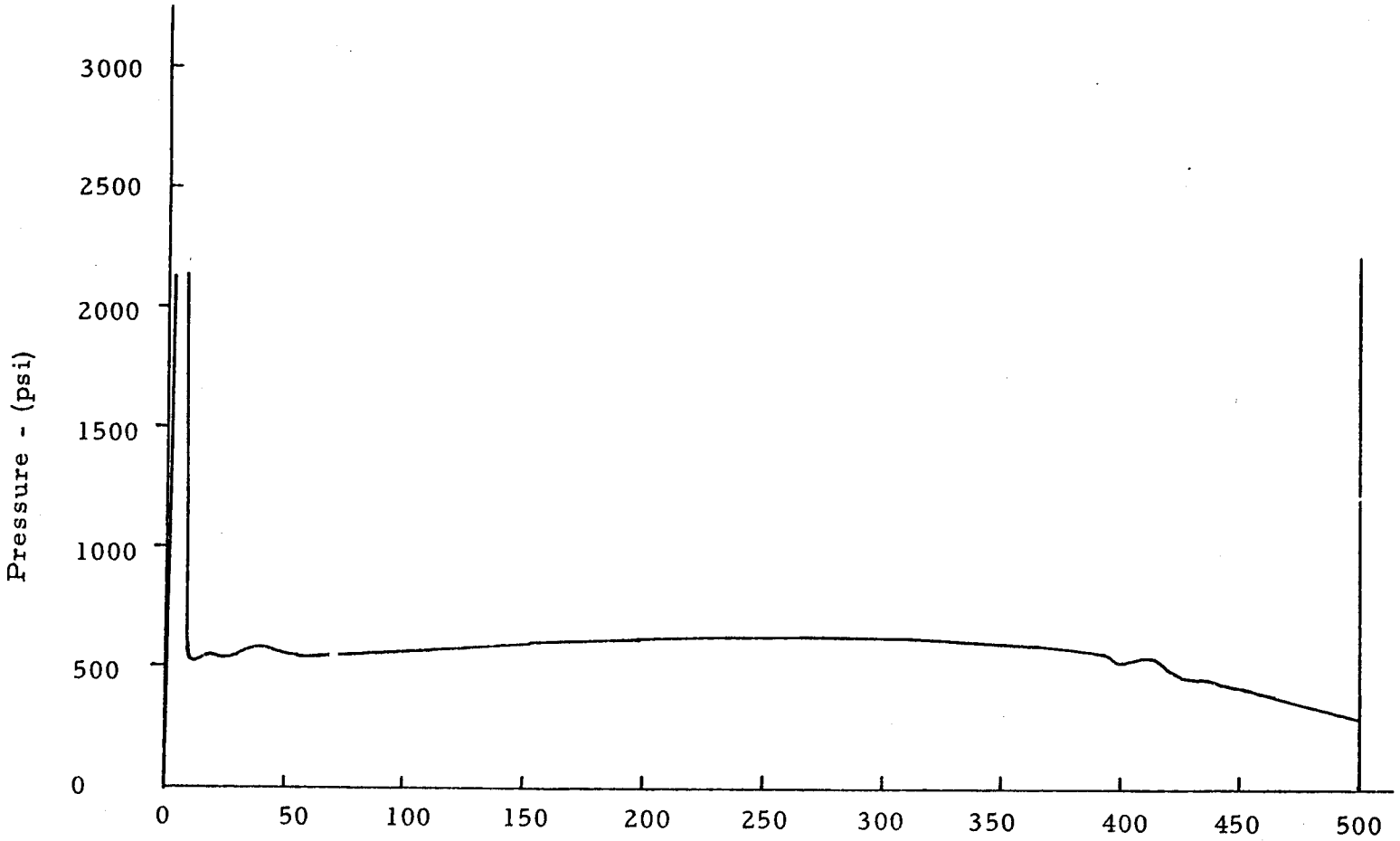

Fig. III-41

Pressure - Time History
at Head for Half Pound Charge

1) The support structure had lifted up from the support bracket at two observable locations (Figure III-42).

2) Much of the support structure appeared to be out of its original position.

3) The outer fuel elements were partially collapsed and were thrust outward toward the thermal shield.

4) A large hole appeared to exist in the center of the core area.

1.7.2. Observations and Measurements of Core after Removal of the Reactor Head

After loose elements, plates and other debris were removed from the region above the active core and prior to the critical experiment, direct measurements were obtained remotely in the Hot Shop. These included the measurements of the vertical position of the significant parts of the top of the core from the top of the studs on the main pressure vessel flange. The tops of shrouds and control rods were measured and found to be between 3-1/2 inches to 4-1/2 inches above their as-built location in the core. The uncertainty in the displacement, which was believed to be $> \pm 1$ inch, is due to the uncertainty of the as-built dimensions, to the location and extent of elongation of the pressure vessel studs, and to the measurements themselves.

This measured displacement of the core helps to explain why the control rod extension of shield plug #5 was seized by its collapsed guide tube approximately 6 inches above normal scram position. (At the time of the accident this plug was completely installed, bolted down with seal housing attached.) Further confirmation of the upward rise of the core and thermal shield is indicated by the damage sustained to the guide pin support bracket of the auxiliary stillwell (nozzle #11). (Figure III-35).

Observation inside the core (Figure II-52) shows vividly the results of the radial forces collapsing all the cruciform shrouds and binding a major number of the peripheral fuel elements between the shrouds and the thermal shield. Shrouds Nos. 1, 2 and 9 were removed from the core structure and revealed the damage to the lattice support structure which included the shearing of the bolt stud threaded to the core support bracket. A cross shaped stanchion was bent outward and the shrouds disengaged from the stanchion by the rivets which were sheared. Figure III-43 shows three tee-shaped stanchions, two with the lattice support pads sheared off and one still in place. All rivets on all stanchions, as shown in the figure, have been sheared.

Observation of the thermal shield shows that three of the six hold-down bolts have been sheared while the other three are still intact with the lattice pads sheared from the tee-shaped stanchions. The two alignment pins and their support brackets were intact and undamaged.

U-5059-3

Figure III-42 Bottom view of core. Note support bracket.

U-5001-316

Figure III-43, Core, Tee-Stanchions

1.8. Cadmium Blades and Shrouds

1.8.1. Shroud and Blade Recovery Examination

The control rod blades and their related shrouds were examined visually in the Radioactive Materials Laboratory (RML). Each assembly will be discussed independently except where they were recovered in pairs.

Shroud No. 1: One section of the shroud was torn away from the remainder, breaking along the weld seam (Figure III-44). Fuel element 17 was tightly bound in the collapsed shroud and element 44 had been captured in the shroud until the assembly was raised by the manipulator grip on the dummy cartridge which released element 44 (Figure III-45). The control blade was extended 4 inches below the bottom of the shroud and prominent rub marks can be plainly seen on the lower section of the exposed part of the blade as shown in Figure III-46. These marks are of pre-incident origin and also show some attack by corrosion.

Shroud No. 2: The assembly was received with the tee-section of the shroud and cadmium blades, as well as stanchions and support hardware attached (Figure III-47). A definite water level indication still remained visible above the upper row of relief holes. The three sections of cadmium blade appeared loose in the shroud. All edge rivets were missing from the shroud and the edge weld of the blades appeared to be partly fractured. Figure III-48 shows a weld seam separation on #2 control blade. The three blades were five inches* above the bottom of the shroud. The tee shroud was deformed but not collapsed. Subsequent to the visual examination this shroud assembly was sectioned and sampled for further analyses.

Shrouds No. 3 and No. 4: The shrouds and blades of control rods 3 and 4 arrived in the RML together. Element 54 was entrapped between the two shrouds as shown in Figure III-49. The lower part of plate E-255, element #10, was attached to shroud No. 3 by having been pressed into relief and rivet holes while heat softened. Both shrouds were collapsed radially outward with fuel plate material splattered inside the shroud. Seam welds were cracked and all rivets were sheared.

Shroud No. 5: This shroud had fuel plate E-674, element 50, very lightly attached to the face of the shroud by its being pressed into the relief holes (Figure III-50). The control blade extended 4-3/4 inches below the bottom of the shroud, but impact marks by relief holes indicate that the blade had moved downward 1-1/4 inches after impact. Rub marks are very pronounced along a major portion of the control blade and are of pre-incident origin (Figure III-51). Figure III-52 shows marks from the source cartridge and element 9 attached to shroud. The bottom section of the blade below the shroud also shows a considerable amount of sliding and abrasion marks. The shroud was collapsed radially outward and all rivets sheared. Seam welds were also partially fractured.

* Shrouds 2 and 6 each contained three cadmium strips which were not movable remotely, and therefore not control rods in the usual sense.

U-5001-255

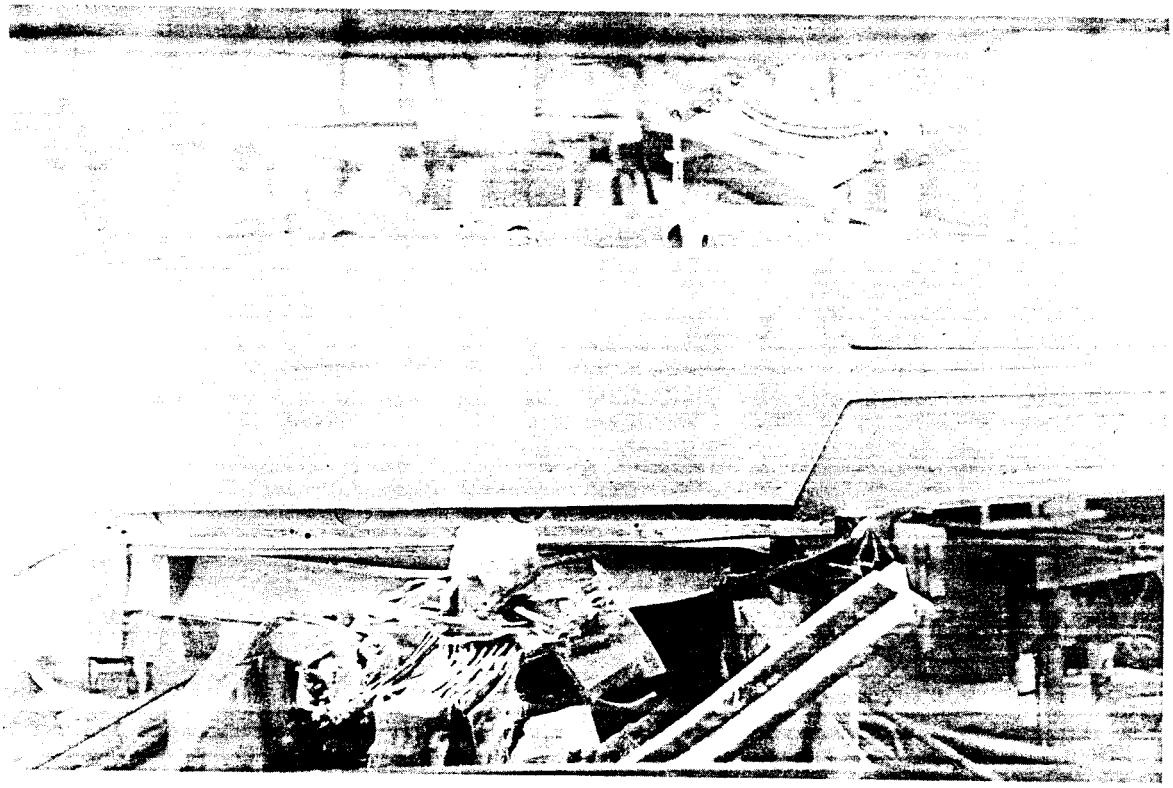

Figure III-44 Shroud and blade assembly #1. Blade exposed.

U-5001-257

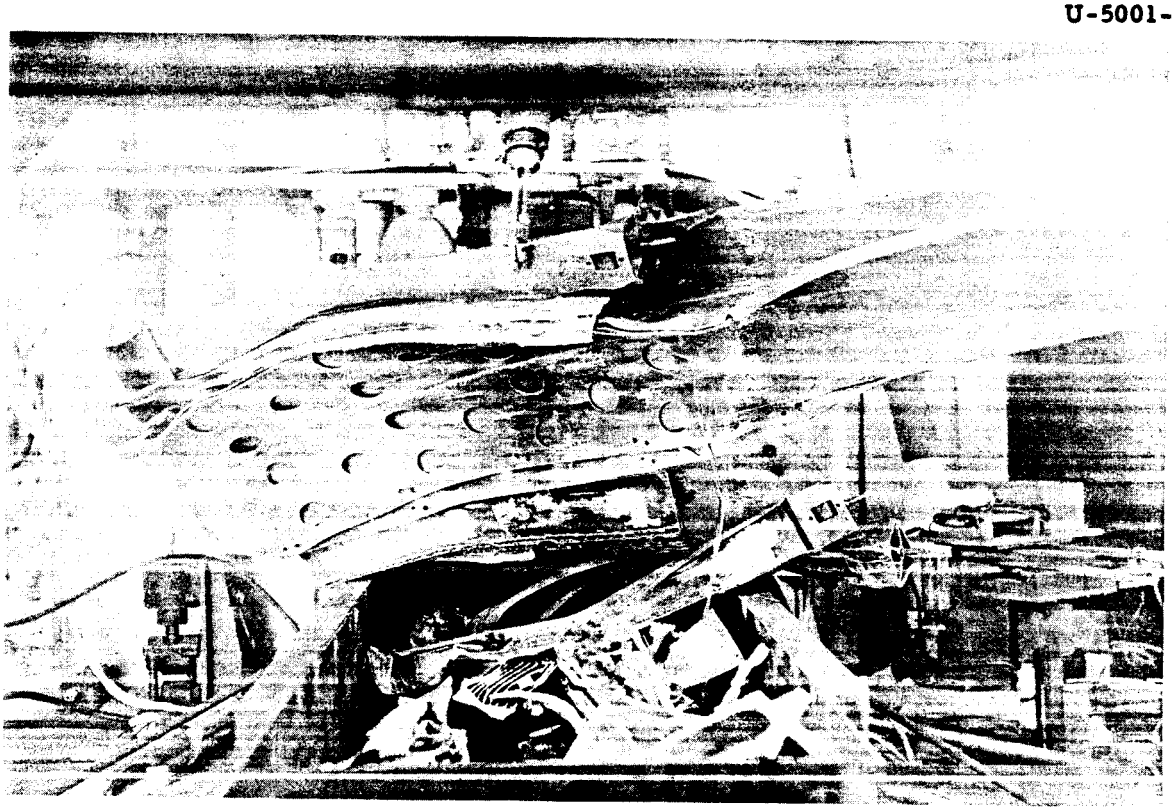

Figure III-45, Shroud and blade assembly #1.

U-5001-326

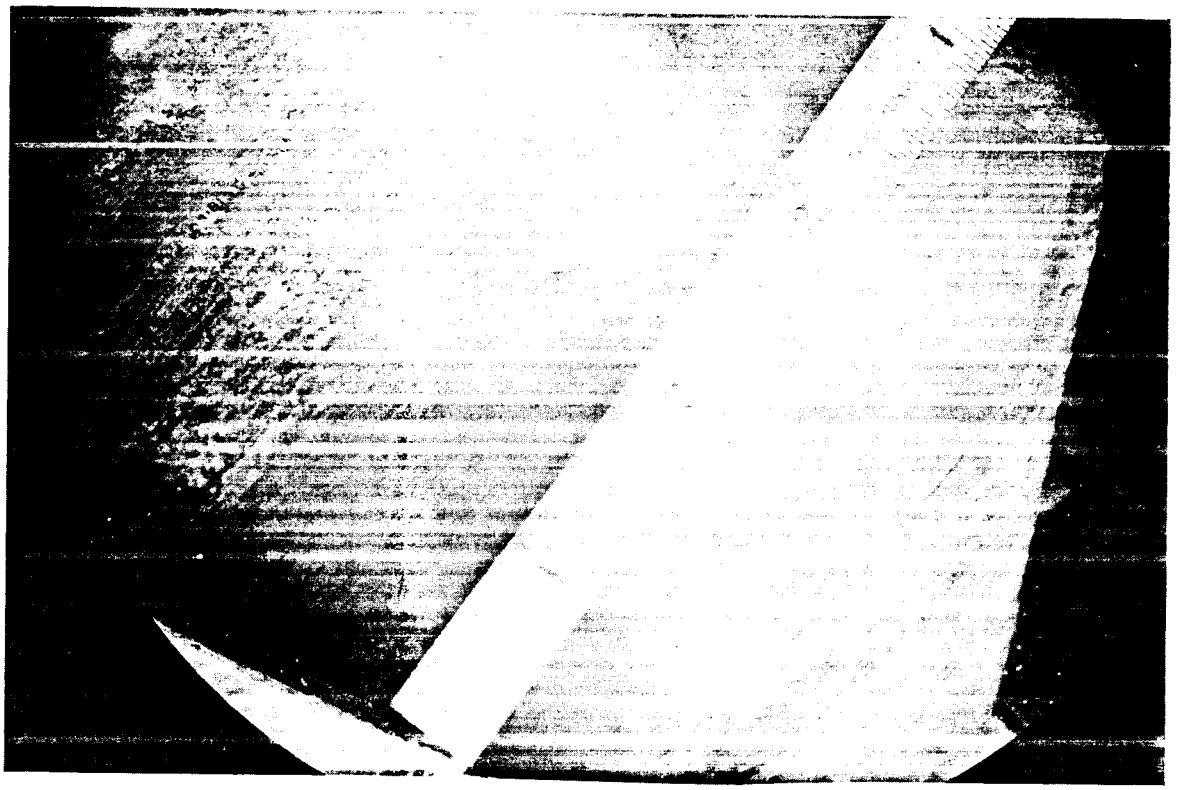

Figure III-46, Blade #1, note longitudinal marks.

U-5001-307

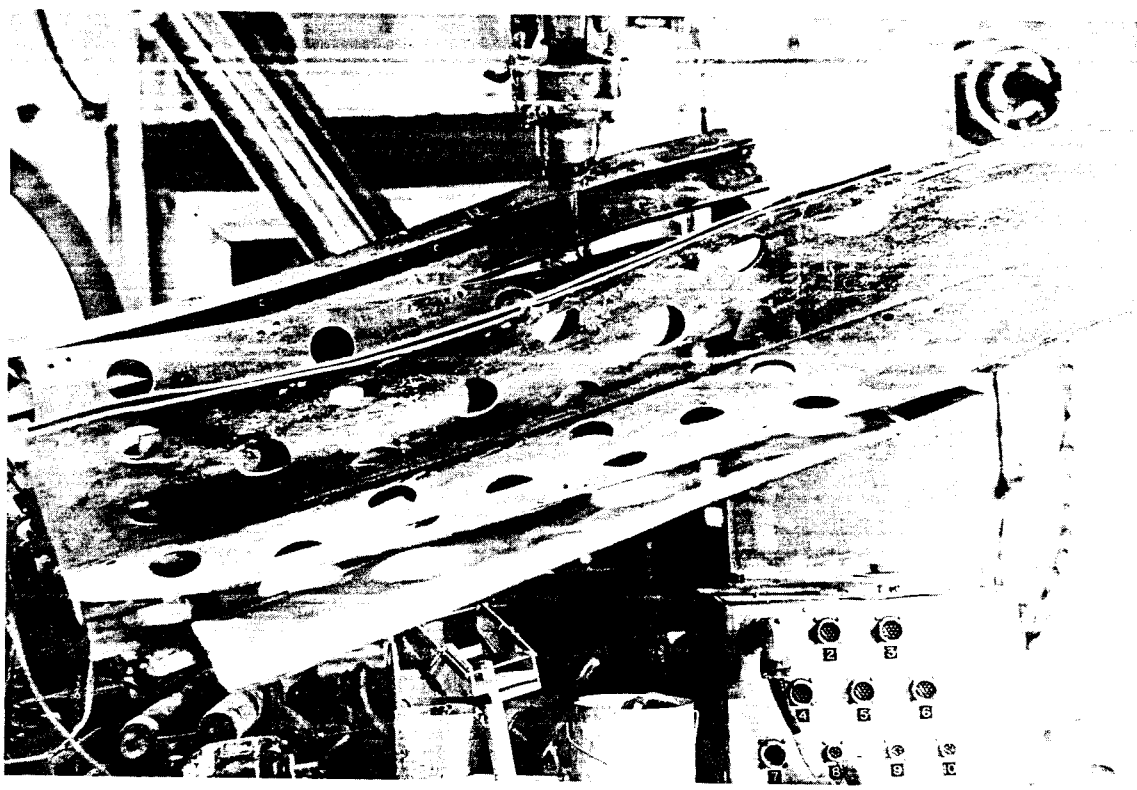

Figure III-47, Shroud and blade assembly #2.

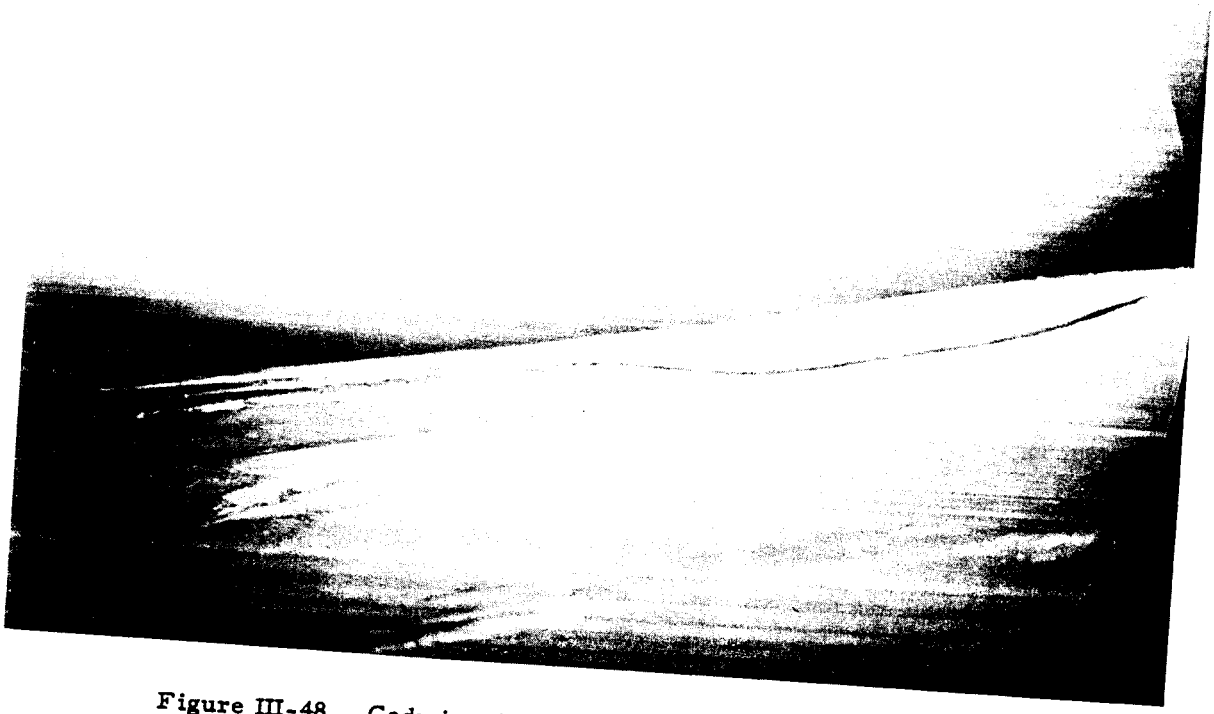

Figure III-48 Cadmium blade from assembly #2. Seam weld separation.

-329

Figure III-49, Shroud No. 3 and No. 4 assemblies.

U-5001-339

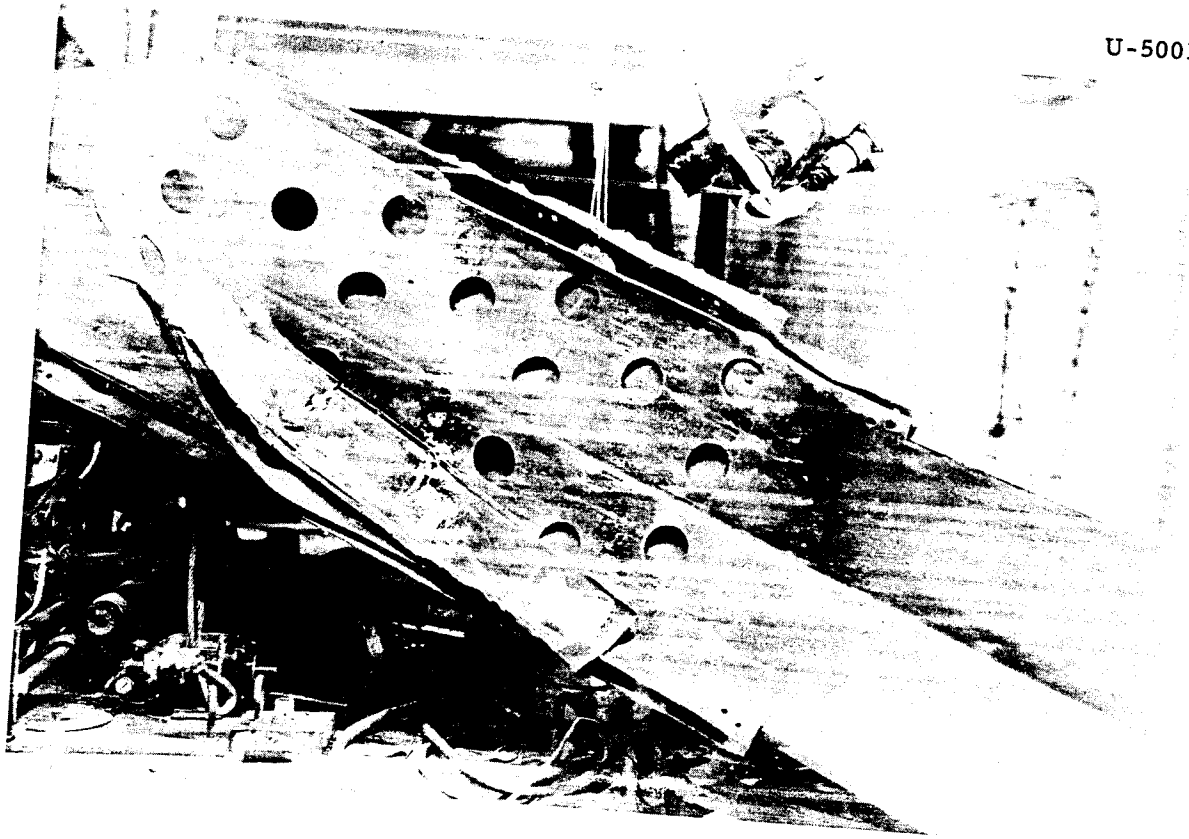

Figure III-50, Shroud Assembly #5.

U-5001-343

Figure III-51, Shroud Assembly #5.

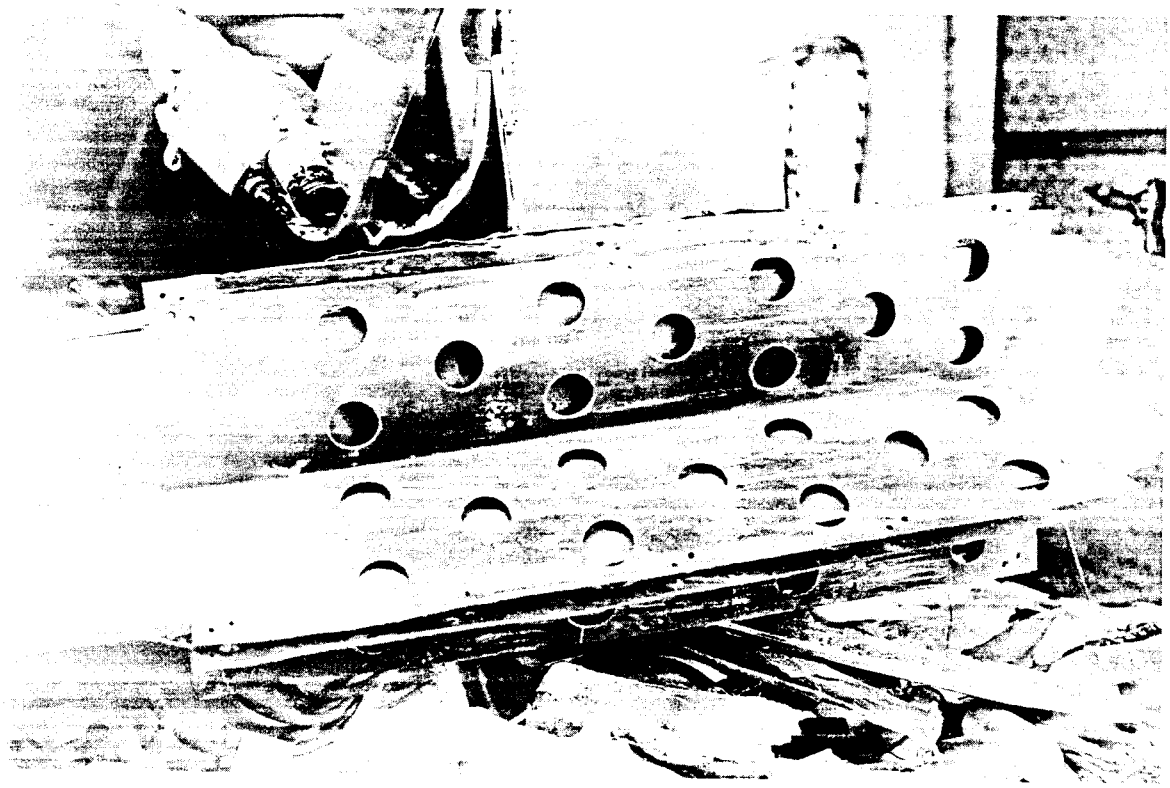

Figure III-52, Shroud Assembly #5.

U-5001-346

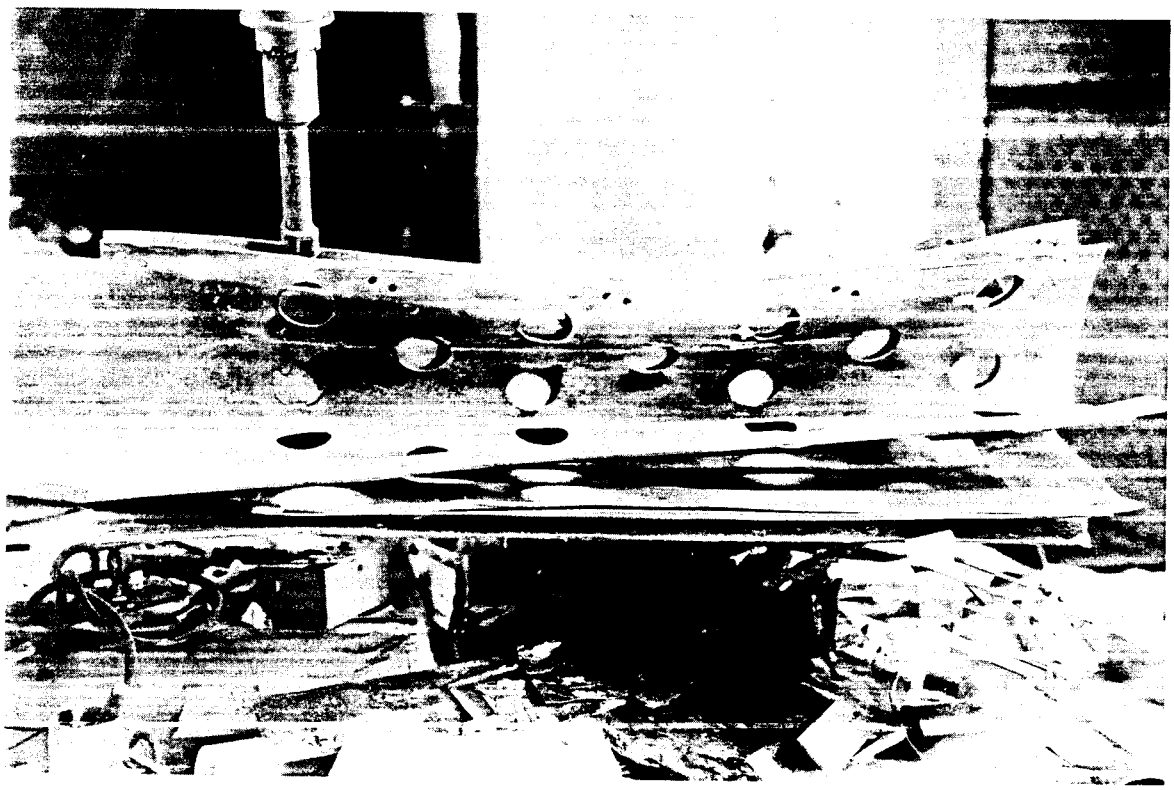

Figure III-53, Shroud Assembly #6.

Shroud No. 6: No fuel cartridges were attached to this shroud assembly. Figures III-53 and 54 show the separation of the cadmium blade edges. The welds at the upper end of the shroud appear to be partially fractured. One cadmium blade was 2-1/2 inches up from the bottom of the shroud, and the other two blades were 5 inches above the bottom of the shroud. One of the cadmium blades had the lifting fixture blown off. The tee-shroud was not collapsed but was deformed and all the rivets were sheared.

Shrouds No. 7 and No. 8: These two control-rod and shroud assemblies arrived together for examination and held elements 11, 43 and 61. (Figure III-55. A 14 inch section of an outer plate from element 3 was plastered on #7 shroud. The fuel plates were melted in the area of the relief holes One relief hole was completely filled with molten metal. The #7 control blade extended 3-3/8 inches below the bottom of the shroud as shown in Figure III-56. Rub marks were very prominent on the lower end of the control blade and some pitting has resulted from corrosion.

Shroud #7 was collapsed outward, all rivets were sheared and seam welds were partially fractured.

Shroud #8 was not collapsed but was deformed; all rivets and seam welds were partially fractured.

No. 9 Control Blade and Shroud: The control rod cruciform blade, its shroud and the connector housing were lifted from the top of the core and removed from the pressure vessel intact and without difficulty. The following observations were made:

The gripper fingers, although sheared from the control rod connector, still held the connector housing to the control blade assembly. Only a small force with the manipulator was required to release the housing from the fingers.

The bottom of the extension (follower) of the cruciform control blade was bound in the shroud 4-1/2 inches* above the bottom end of the shroud (Figure III-58).

The control blade was firmly bound by the collapsed shroud and the blade had not moved after the shroud collapsed. This fact is verified by the imprint of the shroud relief holes on the surface of the control blade (Figure III-59).

Collapse of the shroud occurred before surface melting of the fuel (Figure III-59). The impression of the shroud relief hole on the control blade is vividly shown with fuel element splattered over the imprint.

Two series of rivet holes are along each edge of the shroud. The outer rivet holes were the ones used, as most of them indicated some extent of deformation. The inner holes show no observable deformation. No rivets have been recovered from or detected on the shroud.

* In the normal scram position, the bottom of the 17 inch follower would extend 15-1/2 inches below the shroud.

U-5001-347

Figure III-54, Cadmium Blade, Assembly #6.

U-5001-348

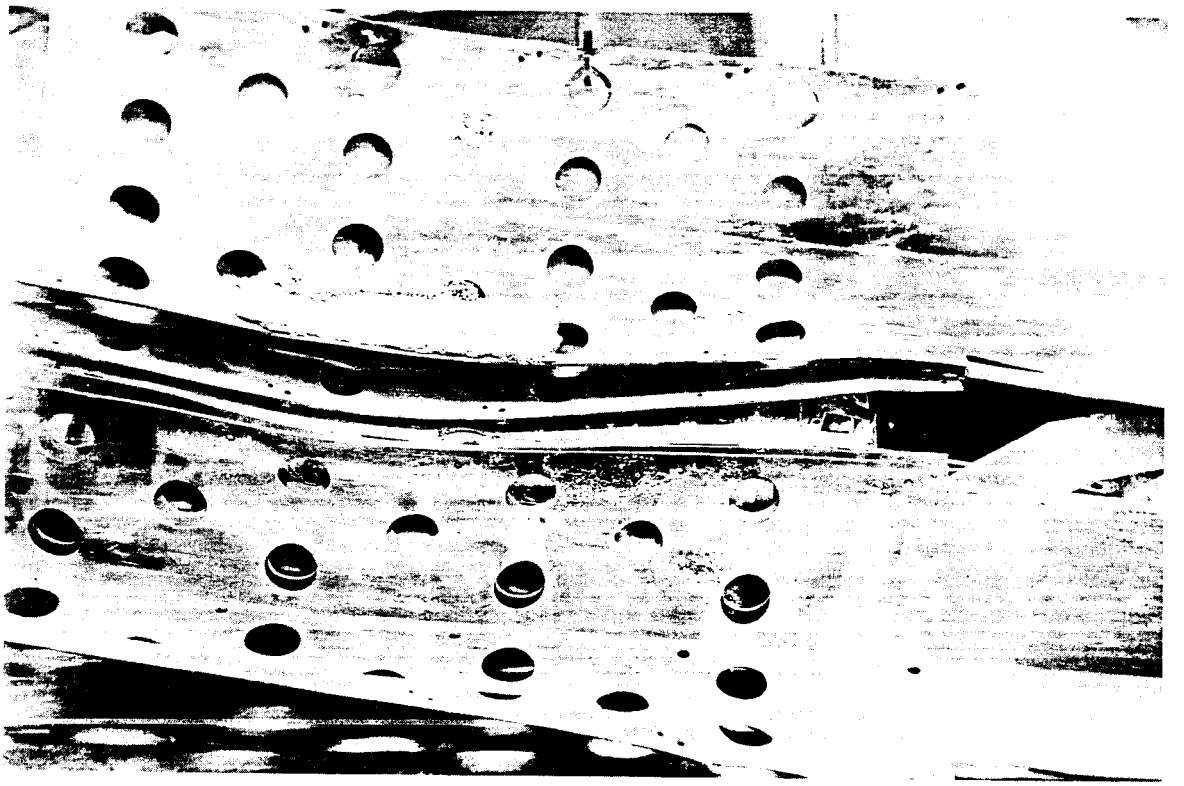

Figure III-55, Shroud Assemblies No. 7 and No. 8

U-5001-356

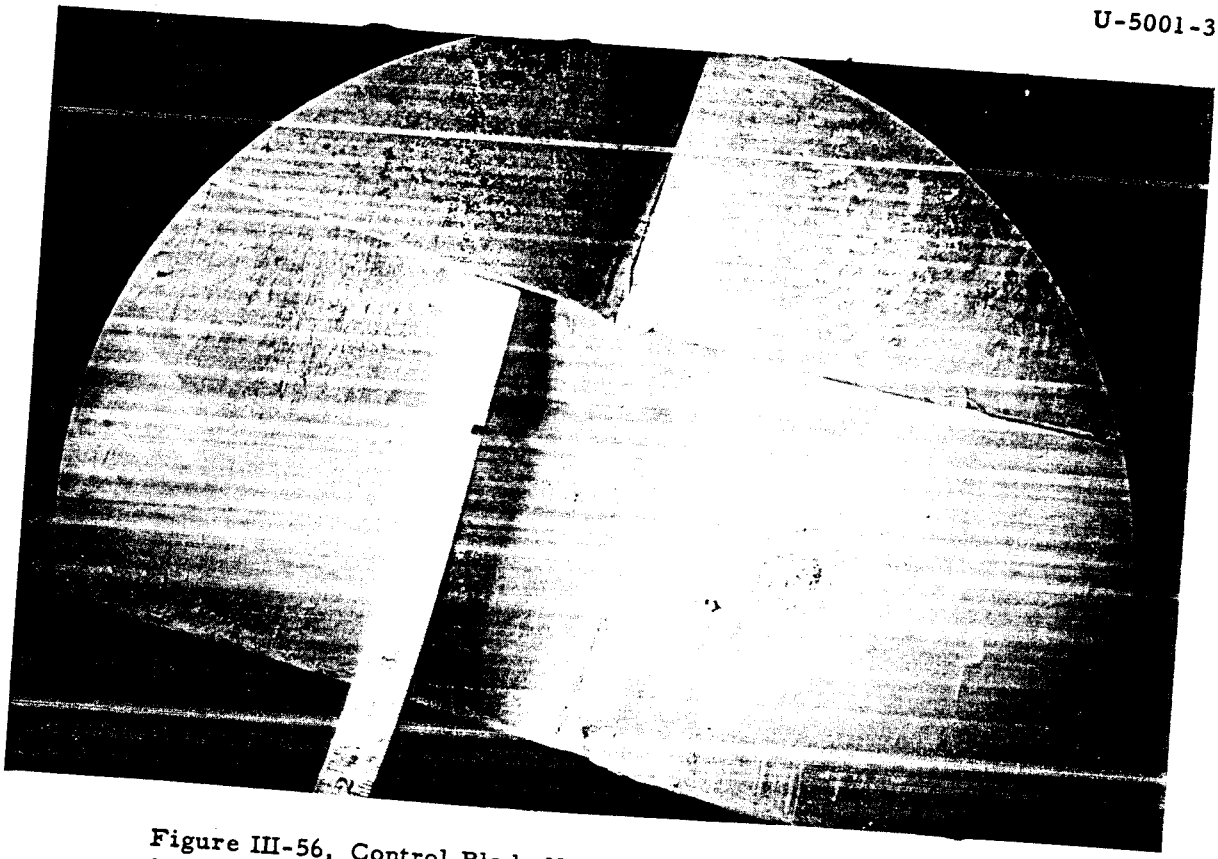

Figure III-56, Control Blade No. 7 extending 3-3/8 inches below bottom of its shroud.

U-5001-233

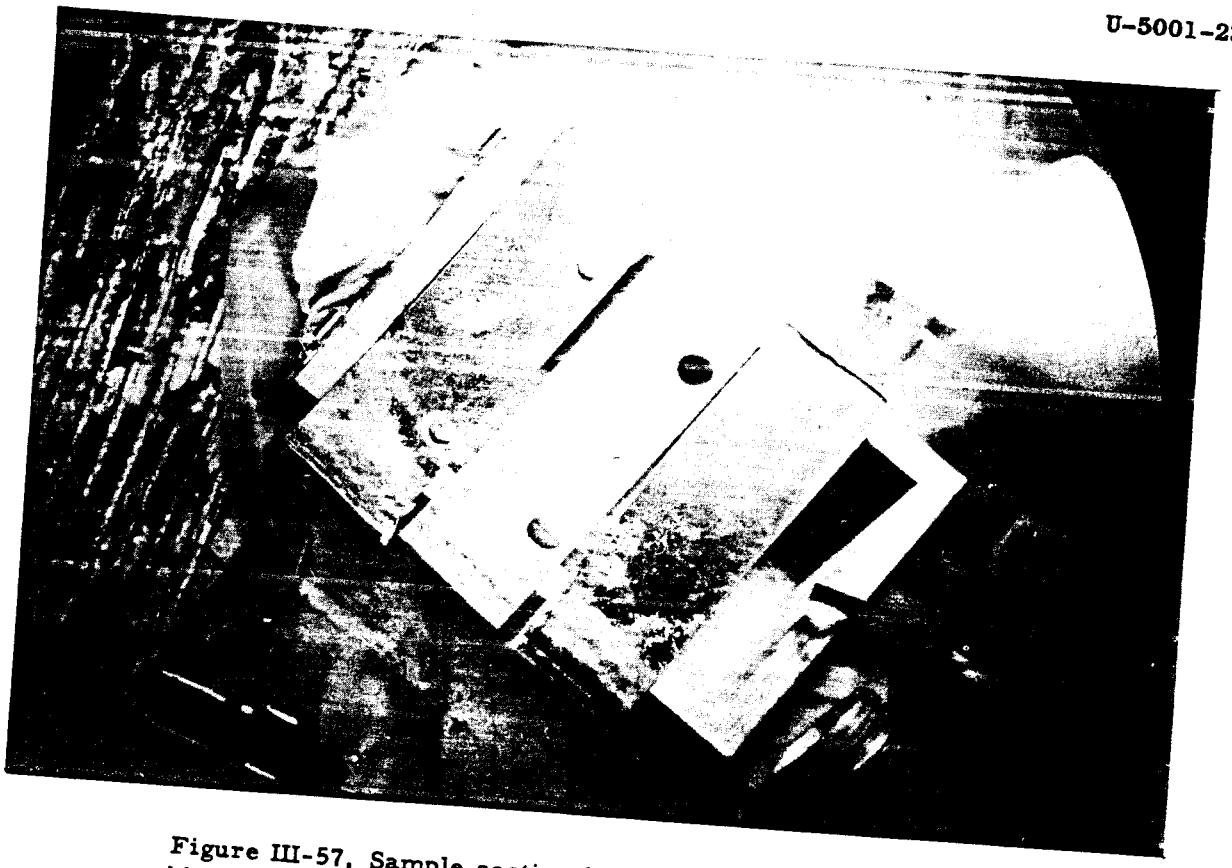

Figure III-57, Sample section from control blade #9.

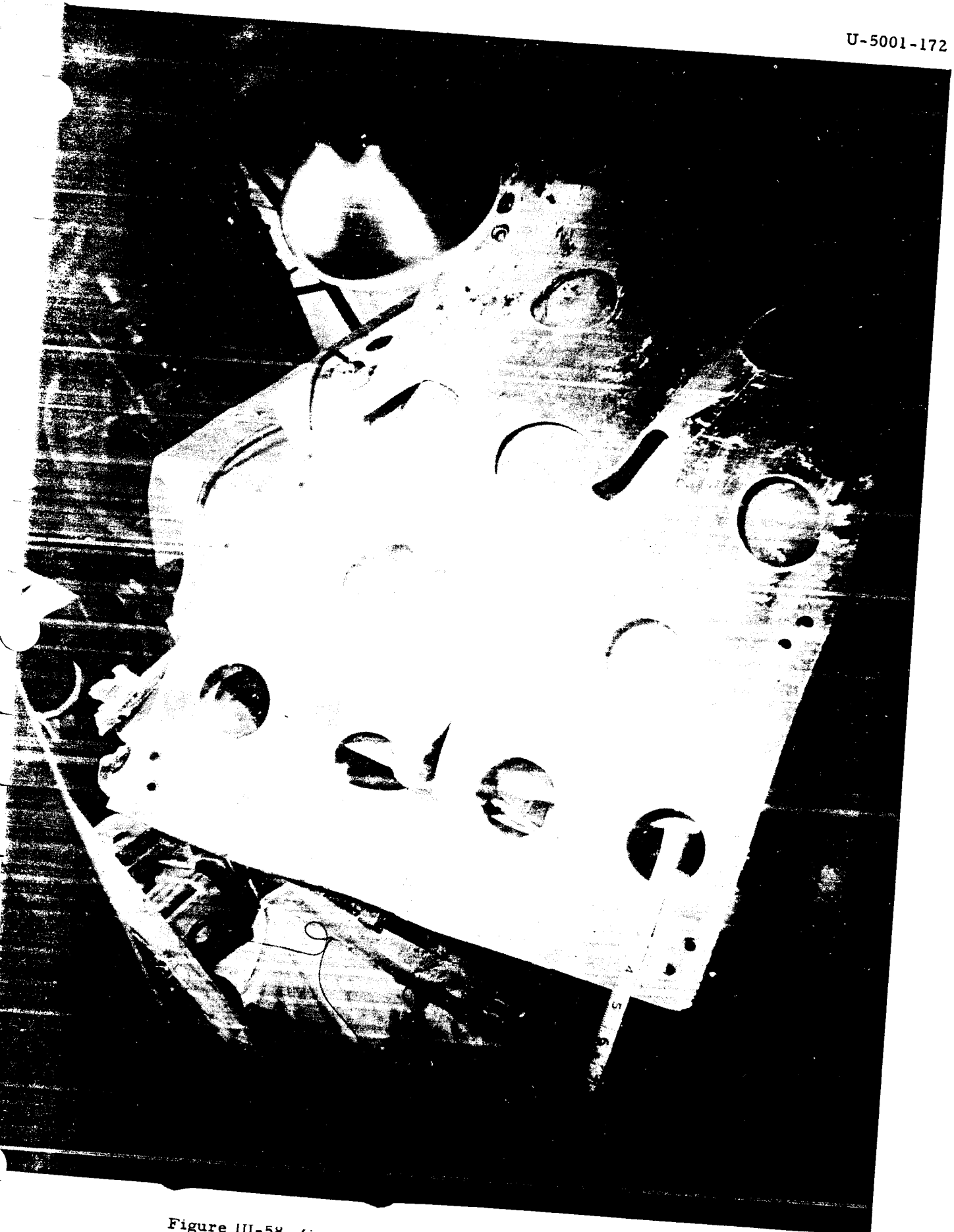

Figure III-58, Control Blade #9 bound in its shroud.

U-5001-188

Figure III-59, Shroud relief hole imprint on control blade #9 and metal spatter.

U-5001-176

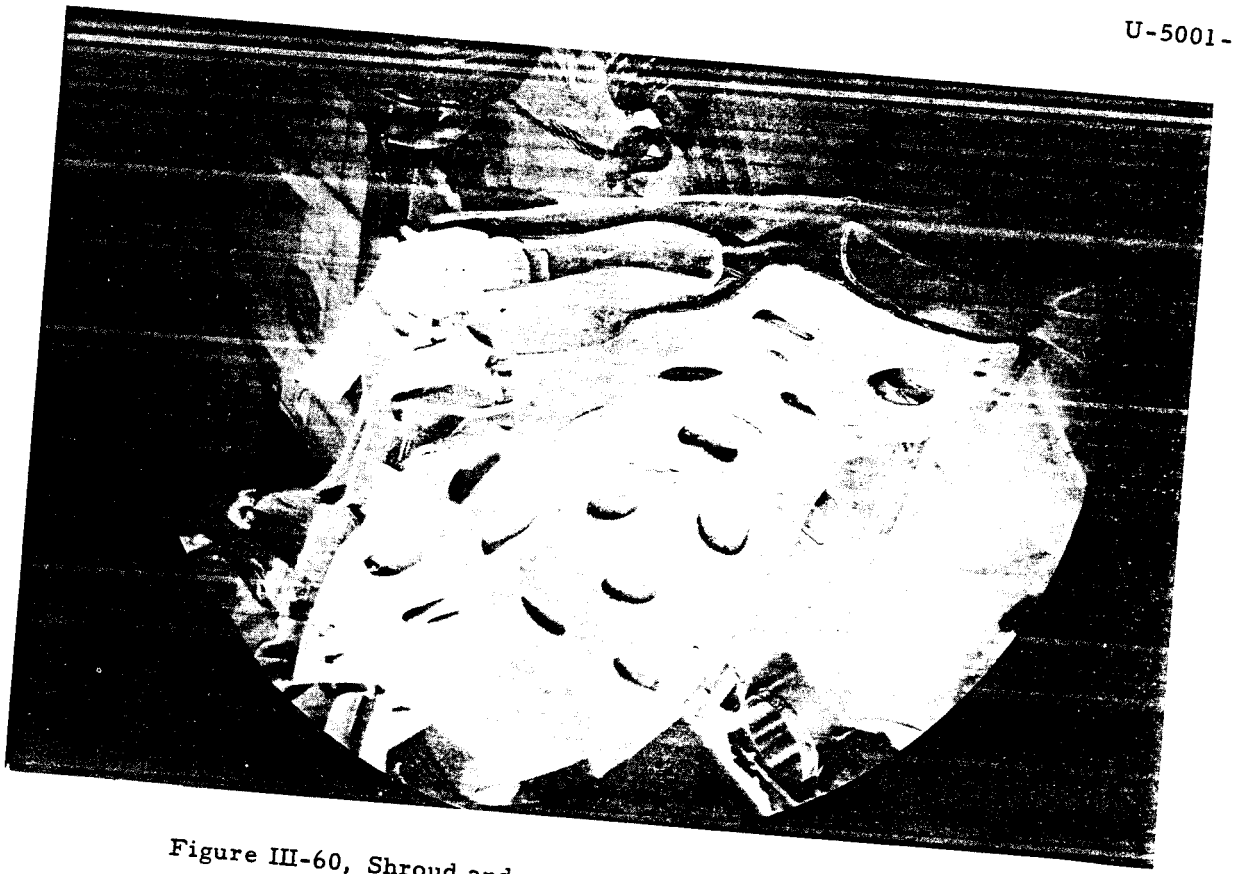

Figure III-60, Shroud and control blade #9.

Many scouring marks have been detected on the control blade. These marks appear to be of pre-incident origin since many of them are covered with splattered metal.

The control rod blade and shroud had undergone severe deformation (bending) and collapse principally in the region of the active core. Many areas of the shroud surface originally in the active core region were splattered with fuel plate material. Figure III-60 is a view showing distortion of the shroud and blade and metal spatter.

The overall length of the control blade was approximately 53" from the lower end of the tapered section. The length of the follower was measured to be 17±1/4 inches. The trailing edge of the cadmium plate sandwiched in the aluminum clad could be seen because of a weld fracture in the lower section of the blade (Figure III-61).

The control rod shroud was removed from the cruciform control rod blade. The cadmium and aluminum alloy cladding were separated along the blades edges on the lower half section of each of the four blades, as shown in Figure III-62. As the shroud was pulled away, it was noted that the aluminum clad seam welds tore apart easily by use of the manipulator grips. Previous attempts were made to section the shroud along the seam welds with an abrasive wheel. This procedure was slow and it was difficult to follow the shape of the deformed shroud. All sectioning or removal of the shroud from the control blade was subsequently accomplished by tearing the seam welds with the General Mills manipulator.

Sectioning and sampling for radiochemical and metallurgical analyses were completed on the control rod cruciform. Four 2 inch wide strips were sectioned from three of the blades. One was left intact. These four strips from each blade were sectioned corresponding to 1/4, 1/2, 3/4 and maximum flux. Macroscopic observation indicated the cadmium metal and its alloy clad were in good condition (Fig. III-57).

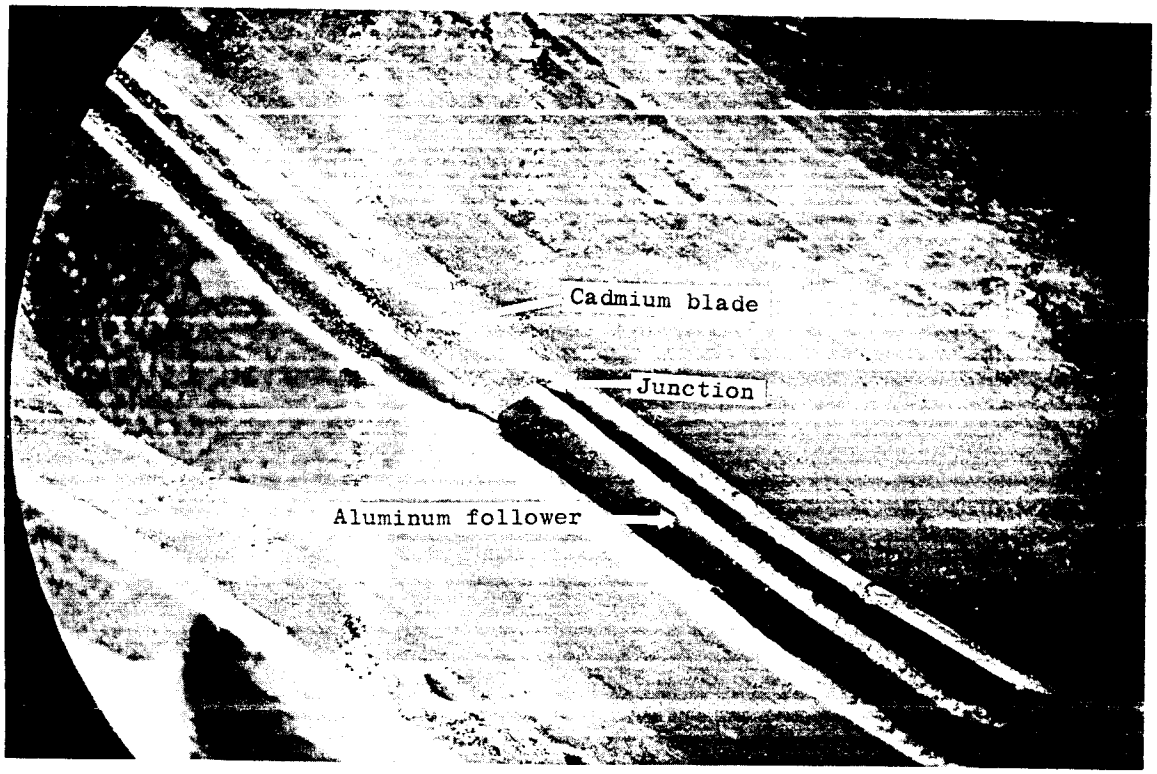

Figure III-61 Cadmium blade showing weld seam separation

U-5001-203

Figure III-62, Lower end of #9 control blade.

Chemical and Related Evidence

Identification of Deposits

Throughout the Phase 3 recovery a comprehensive program of chemical analysis was carried out. All foreign material and unexpected deposits and coatings were carefully identified, with particular emphasis on those inside the pressure vessel. It is believed that the major sources of such material were the shielding material from the head of the pressure vessel, and the thermal insulation around it. The plate which covered the shielding material was disrupted by the accident, and the gravel fines, boron oxide, and steel punchings were widely scattered. The insulation was similarly distributed. These conditions are shown in Figures II-1, 2, 3, and 4, Section II. The water expelled from the pressure vessel by the accident washed some of this material into the pressure vessel through the open nozzles, the gap formed between the vessel head and flange, and the sheared pipes. The leaching and oxidation of the steel punchings by this water represent a significant source for much of the iron oxide found. The gravel fines account for the silicon dioxide residue, while the boron oxide is judged to be the source of the white crystalline deposits which were identified to be mostly boric acid. Lead found in the debris came from the lead shot which was used during the recovery operation for shielding.

The type of deposits found within the pressure vessel can be seen in Section II, Figure II-33. Figures III-63 and 64 are photographs of the deposits on shield plug #5 and shield plug #4, respectively.

A tabulation of samples scraped from various areas of the pressure vessel and core is shown in Table III-2. Analysis of these samples was by optical emission spectroscopy and X-ray diffraction powder patterns.

An analysis was made of a block of the thermal insulation originally around the pressure vessel. Contrary to expectations, emission spectrography gave magnesium and calcium as major constituents with silicon, aluminum and iron present. The sample was then analyzed by X-ray diffraction means and showed calcium carbonate as the prime crystal structure with magnesium, iron, and aluminum silicate also present. The expected magnesium oxide was not present in the X-ray diffraction patterns. This is in contrast to the composition of 85% magnesia given in "Design of the Argonne Low Power Reactor", ANL 6076.

Burnable Poison Strips

The SL-1 core had been loaded with 39 full and 16 half strips of burnable boron-aluminum, as shown in Figure III-65. During the pre-incident

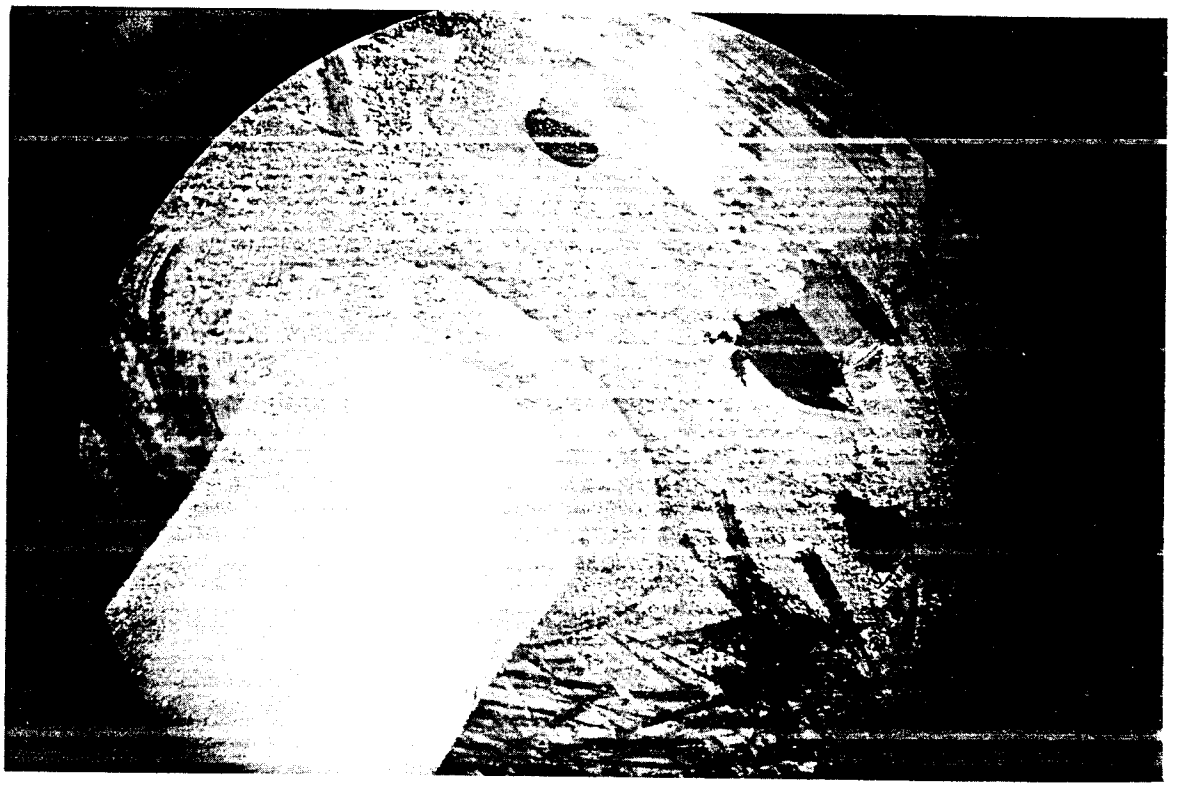

Figure III-63 Showing Vaporized Deposits on Shield Plug #5

U-5001-222

Figure III-64, Deposits on Dummy Rod Assembly #4

TABLE 2

Analysis of Samples from the Pressure Vessel & Core

Sample Description	Sample Origin	X-Ray Identification	Principal Constituents 10%	1-10%	0.1-1.0%	Not Detected
Scrapings of white deposit	Hold-down Box	--	Al	--	Fe, Si, Mg, B	U
Scrapings of white deposit	Under-side of pressure vessel head	H_3BO_3, B_2O_3	--	--	--	--
Scrapings of white deposit	No. 4 control rod assembly (Figure III-	Al, H_3BO_3 B_2O_3, γ-Al_2O_3 α-$Al_2O(OH)_2$ αAl_2O_3(?)	Al	--	Fe, B, Cu, Si, Mg	--
Scrapings of white deposit	No. 7 Shroud	H_3Bo_3, -Al_2O_3, $\alpha Al_2O(OH)_2$	Al	--	Fe, Mg, B	--
Scrapings of white deposit	No. 6 T-Shroud	$Mg(NO_3)_2$(?)	Mg, B	--	Al, Fe	--
Scrapings of white deposit	Pressure Vessel Wall (Figure II-33	B_2O_3, H_3BO_3	--	--	--	--
H_2O leach of above samples	(See above)	--	Mg, B	--	--	U
H_2O leach residue from above	(See above)	--	(Same as above samples)			--
Metallic Slag	No. 9 Shroud	--	Al	--	B, U, Fe, Si, Cu, Ni, Mg, Mn	--
Corrosion Scale	Around each head-bolt hole	--	(Commercial Anti-Galling Compound)			
Cd control rod blade + Al Clad	No. 9 control rod	--	Al	Na, Mg, Si	B, Fe, Ni, Mn, Cr	--
Cd control rod blade + Al Clad	Oxide from Clad	Al, α-$Al_2O(OH)_2$	--	--	--	--

shutdown, fuel element 42 had been removed and replaced with element 62. The micro-examination of the boron-aluminum strips from element 42 showed the surfaces of both strips to be irregular and pitted with some boron particles having diameters of approximately 0.004 inches. Most of the boron particles, however, had diameters in the order of 0.0005 inches. Thicknesses of each of the two strips measured were in the 0.022 to 0.027 inch range.

The recovered boron strips were heavily corroded and embrittled. Figure III-66 indicates the severe corrosion of the full boron strip near the midpoint of element 45. Figure III-67 shows the deterioration of the boron strip from element 20 (strip at left in four pieces) and a more complete view of strip #30 from element 45. The corrosion was identified by X-ray diffraction and proved to be basic aluminum oxide (Boehmite) which has an orthorhombic crystal structure. A total of 29 boron strips (or portions thereof) were recovered and identified. These strips produced 2.88 kilograms for a recovery of 55.6%.

Table III-3 is a listing of the boron strips, the original weights, and related comments about their condition at recovery.

A considerable number of fragmented boron strips were recovered with the debris from the reactor pressure vessel. These pieces were not included in the inventory because of their lack of identification and difficulty in separation. Figure III-68 shows pieces of boron strips atop the cutter loaded with debris from the bottom of the core. An unanswered question is what percentage of flaking of the boron strips occurred during the incident and what took place during the preceeding normal operation as reported in CEND-1005.

BORON STRIP LOADING

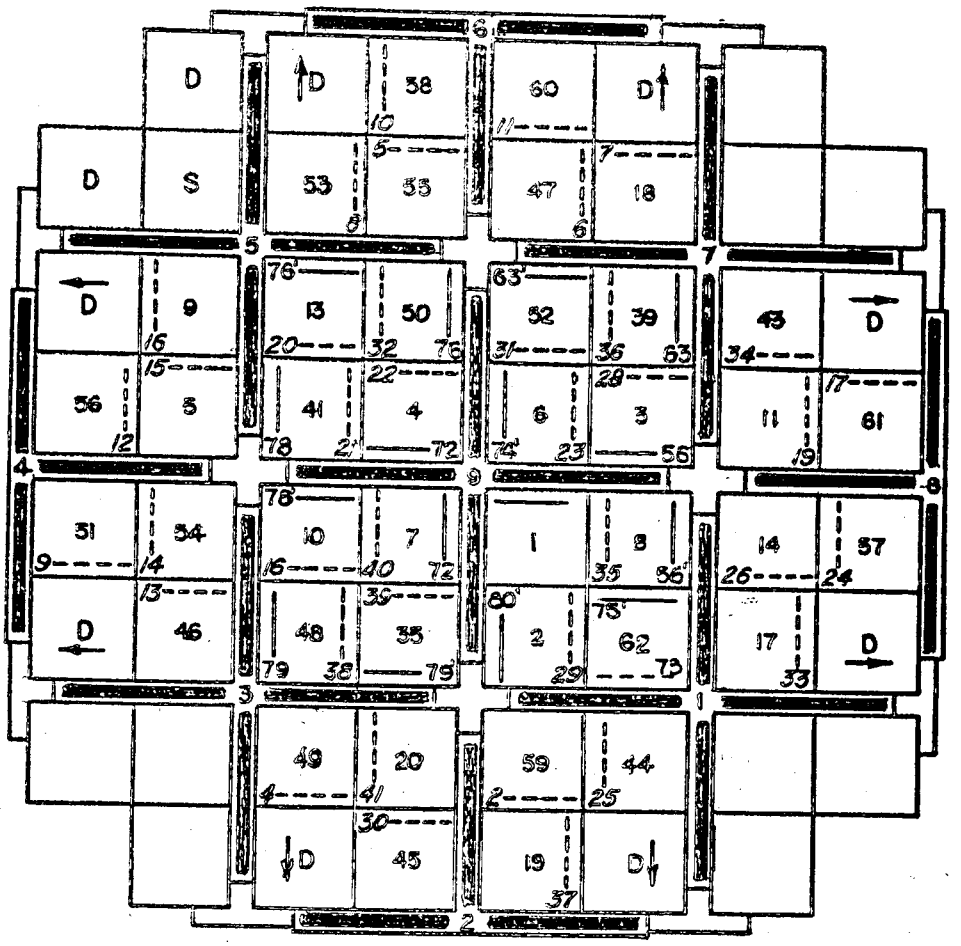

KEY:

FULL STRIP OF BORON - DASH LINE
HALF STRIP OF BORON - SOLID LINE
D - DUMMY ELEMENT
S - SOURCE

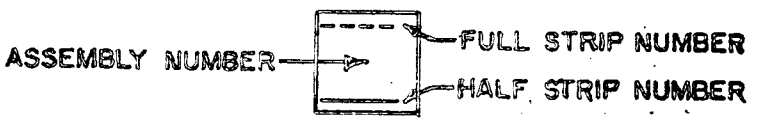

The position of the full and dotted lines indicate the orientation of the assembly and the position of the boron within a cell of four assemblies.

The direction of the side plates of the dummy elements are shown by an arrow.

SL-1 LOADING FOR 40 ELEMENT CORE

Figure III-65

Figure III-66, Corrosion and Deterioration of Boron Strip on Fuel Element #45 Side Plate

U-5001-336

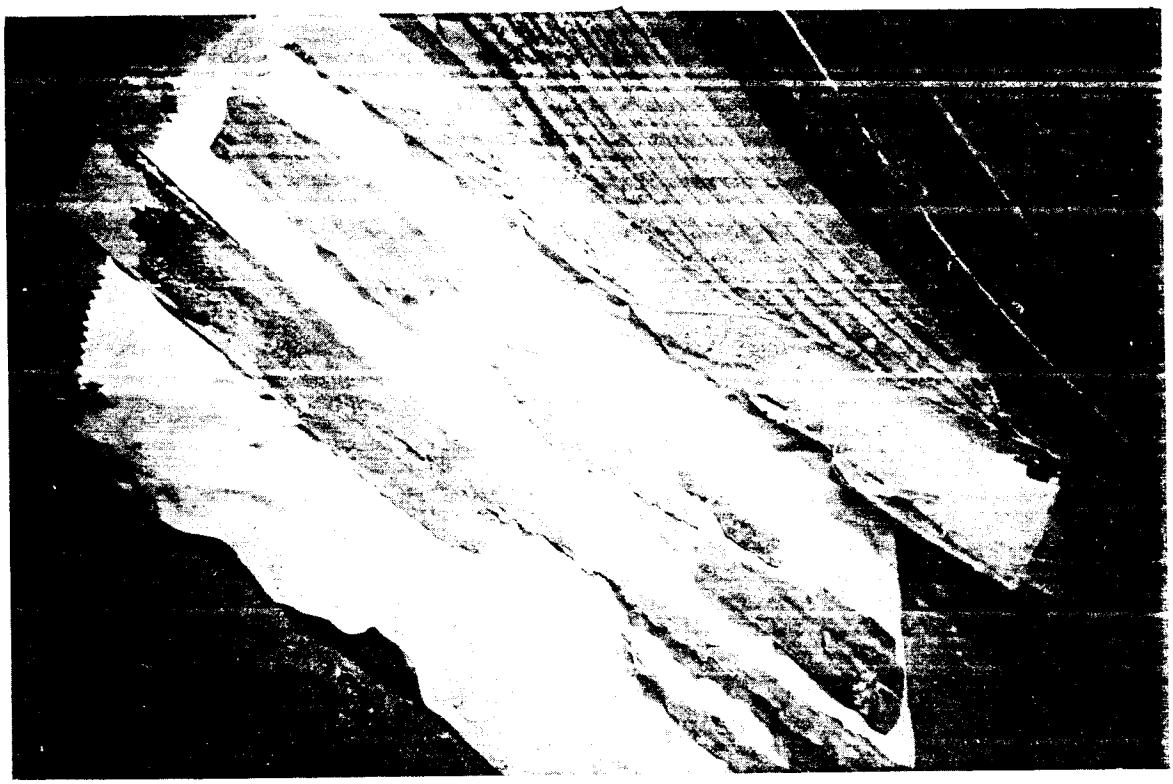

Figure III-67, Portions of Corroded Boron Strips

Figure III-68 Cutter Loaded with Debris from Bottom of Pressure Vessel

U-5103-3

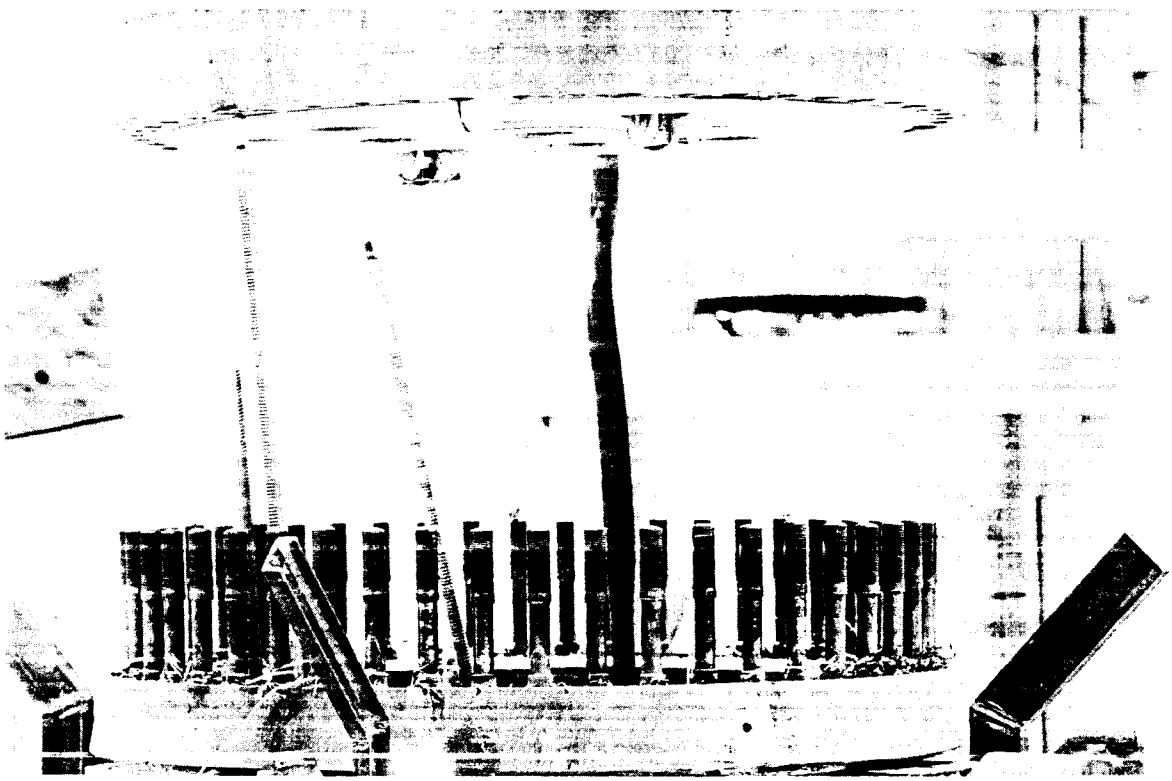

Figure III-69 Deposit Underneath Reactor Head Surface

TABLE III-3

Boron Strip Recovery Data

Element Number	Boron Strip Number	B-Al Strip Weight Grams	Remarks
1	1/2 strip	45.776	
2	29	111.609	
	80A	46.66	
3	28	116.046	
	56A	44.740	
4	22	117.726	Recovered upper 10 inches
	72A	47.749	
5	15	115.766	Recovered upper 15 inches Corrosion on left side
6	23	119.314	Recovered upper 4 inches
	74	47.260	Heavy corrosion
7	40	116.031	Recovered upper 9 inches
	72B	47.750	Twisted - crumpled
8	35	116.887	Recovered upper 13 inches de-
	56B	47.740	terioration on 3" of lower right
9	16	113.606	Recovered upper 15" break heavily corroded & embrittled
10	18	117.580	
	78A	44.756	
11	19	110.180	Recovered whole; deterioration on left edge
13	20	116.769	
	76B	39.655	
14	26	116.365	
17	33	112.468	Recovered upper and lower 8" center portion corroded away
18	7	111.433	
19	37	111.520	Recovered whole - Deterior- ation on right side and center
20	41	112.602	Recovered 6"
35	39	117.893	
	79B	46.248	
39	36	119.751	Recovered upper 5" - Deterior-
	63	44.456	ation on lower 2" of right side

TABLE III-3
Con't

Boron Strip Recovery Data

Element Number	Boron Strip Number	B-Al Strip Weight Grams	Remarks
41	21	117.157	
	78B	44.756	Recovered upper 16" - Deterioration on right side
43	34	113.960	
44	25		Recovered 20" - lower end corroded away
45	30	114.176	
46	13	118.603	Recovered upper 12" - Badly corroded right edge 12"
47	6	112.384	Recovered completed - Deterioration on both sides
48	38	112.036	Recovered upper 18" - Last 6" deteriorated on left side
	79A	120.775	
49	4	46.248	
50	32	112.630	Recovered upper 8" - Lower end corroded away
	76A	117.739	
51	9	48.655	Recovered upper 12" - Deterioration of 2" lower right side
		111.980	Recovered upper 12"-Last 3" left side deteriorated completely. Deteriorated along right side.
52	3		
	63	116.524	
53	8	44.456	
54	14	111.530	Recovered upper 12" - Right edge deteriorated
55	5	112.926	Recovered complete - slight deterioration along left side
56	12	114.877	Recovered whole - slight deterioration along left side
57	24	109.242	
58	10	118.148	Deterioration on left edge
59	2	112.112	Center section missing - Deterioration along edge. Tied to 53
		113.831	

TABLE III-3
Con't

Boron Strip Recovery Data

Element Number	Boron Strip Number	B-Al Strip Weight Grams	Remarks
60	11	112.551	Slight deterioration on left side
61	17	110.762	Recovered whole. Slight deterioration along one edge.
62	73	96.043	
	75A	45.507	
		5182.944	Grams of B-Al plate (half and full) prior to incident
		4453.532	Grams of full B-Al plate prior to incident
		2880.0	Grams recovered B-Al plate

2.3 Boric Acid Deposit Analyses

In Part 2.1 of this section it was pointed out that the white crystalline material found on the reactor components and the interior of the pressure vessel was identified as predominantly boric acid, H_3BO. Before the Phase 3 investigation, it had been postulated that the boric acid injection system might have been operated, adding boric acid solution to the system by way of the upper spray ring. Investigation proved that this was not the case, however. The 120 gallon storage tank was expected to contain boric acid with a concentration of 100 grams H_3BO_3 per gallon of water or a 2.6% boric acid solution. Since an analysis of a liquid sample from the storage tank after the incident showed it to be a 2.9% boric acid solution and the total volume of solution was accounted for, it was concluded that the boric acid found within the pressure vessel came from another source.

A review of the design manual, "Design of The Argonne Low Power Reactor", ANL 6076, showed that directly above the reactor vessel head was a region 15 inches high through which the nozzles for the control rods passed. The remaining volume was packed with a shielding mixture containing 100 pounds of steel punchings, 30 pounds of boron oxide, and some gravel fines for each cubic foot of volume. The total of these shielding materials was approximately 26 ft^3. This volume was enclosed by a ring of sheet metal capped with a plate. There was, therefore, approximately 780 pounds of boron oxide available to hydrolyze to boric acid.

A visual examination of the top of the pressure vessel, the inner walls and the fuel elements and shrouds produced evidence that the boric acid, leached from shielding atop the reactor, ran down these surfaces. Figure III-69 shows evidence of boric acid deposits on the top cap. This residue, deposited as boric acid, ran under the ring over the top cap and into the core through the opening between the top cap and the pressure vessel. Upon removal of the top cap it was noted that the complete under side area (approximately 23.5 square feet) was covered with the boric acid deposit. An analysis showed that 40 grams of boric acid had been deposited in this region.

Boron deposits were found on the shield plug surfaces which faced the reactor head prior to removal in the recovery operation. Scrapings from #4 dummy weight, which was believed to be a typical water deposit sample, were found to be 40% boron oxide compounds. Of this percent, 40% were water-soluble borates and 60% were water-insoluble. It was found that a 2% acetic acid solution dissolved these boric acid deposits considerably more rapidly than did pure water.

The definition of an apparent water level ring and its apparent changes are exhibited in Figure II-34, Section II. These deposits, identified as mostly boric acid, point to the fact that there was water in the core after the first expulsion. The deposits on the underside of the head and on the shield plugs indicate that there was sufficient afterheat to produce the volatilization action of the boric acid.(1)

4 Chemical Explosives

The possibility of a chemical explosive initiating or causing the SL-1 accident was investigated with the assistance of the Stanford Research Institute.(2) Their recommendations included analysis of the reactor debris for quantities of organic residues and remnants of inorganic explosives.

Representative samples of the reactor debris were extracted with carbon tetrachloride for organic residues, and with distilled water for residues from inorganic explosives. These extracts were subjected to infra-red spectrometry and qualitative chemical tests for the presence of organic material, nitro, and nitrate groups.

edgwick, N. V., Vol. I. "Chemical Elements and Their Compounds".
ee Appendix C

Standard colorimetric tests for nitro and nitrate groups were made on solvent blanks, known standards, and the debris extracts. These tests indicated no more than the expected traces of such groups in the extracted samples.

Infra-red analysis of extract samples and their residues indicated the following: "No organic materials were observed in the samples which were not present in the starting material (solvent)." (1)

In addition, visual examination of reactor components at all stages of disassembly gave no indication of any quantity of elemental carbon, which would have been expected to have been present.

2.5 Aluminum-Water Reaction

Considerable attention has been given the possibility that a metal-water reaction was associated with the SL-1 accident. Studies by L.F. Epstein[2,3], R.C. Liimatainen, et.al.,[4], F.J. Shipko[5], and W.F. Zelezny[6] indicate that a rapid, potentially dangerous chemical reaction between a metal and water in a nuclear reactor is possible. The conditions, however, for such a reaction are rather specific.

Violent chemical reaction between metals and water resulting from a temperature excursion in a nuclear reactor can occur only if the metal is molten. For a system such as the SL-1 reactor core (i.e., Al-U alloy and water) the important reaction must take place between liquid metal and water vapor. Below a certain critical temperature (about 1170-1225°C for Al), the rapid, violent reaction does not occur. (2)

It is also necessary that the metal to water ratio in the reacting region approach the stoichiometric ratio as given by: $2\ Al + 3\ H_2O \rightarrow Al_2O_3 + 3\ H_2$. An excess of either reactant would tend to subdue the reaction. (3)

1. R. Abernathey (Phillips Petroleum Company, NRTS) - private communication.
2. Epstein, L.F., Nuclear Science & Eng. 10, 247-253 (1961)
3. Epstein, L.F., Metal Water Reactions; VII, GEAP-3335 (1960)
4. Liimatainer, R.C., et.al., Studies of Metal-Water Reactions at High Temperatures, ANL-6250 (1962)
5. Shipko, F.J., & R.M. Haag, Thermal Stability of Hydrous Aluminum Oxides, KAPL-1740 (1957)
6. Zelezny, W.F., Metal Water Reactions, IDO-16629 (1960)

Experiments performed at atmospheric pressure have indicated that the reaction of molten Al-U alloys with water vapor is not an explosive (self-propagating) hazard at this pressure. [6]

No doubt some reaction occurred between metal and water during the SL-1 incident. Liimatainen, et.al., have observed as much as 25% complete reaction in their studies (private communication).

The fine screenings of the debris from the bottom of the pressure vessel, described in Section III-3.3, were analyzed for the presence and amount of alpha-alumina, α-Al_2O_3, the product of an aluminum-water reaction. The samples were prepared by acid dissolution and filtration, which facilitated extraction of the insoluble residue. The residue represented 68 weight percent or 23.7 kilograms of the total fines. A screening process was then performed on two samples of the residue which separated the samples into four grades of screenings. Table III-4 is a presentation of the screening data.

X-ray diffraction powder samples were prepared from the two finest grades and produced powder patterns of α Al_2O_3 and α-$Al_2O(OH)_2$. The quantitative determinations were obtained with the use of standard samples and an X-ray diffractometer. The results showed that sample A (<200 mesh, Table III-4) contained 29% α-Al_2O_3 and the sample B (<60->200, Table III-4) was composed of 52% α-Al_2O_3. The screening process had produced 2.21 weight percent and 11.15 weight percent of A and B, respectively. The 34550 grams of original fines then included 1.49 kilograms of α-Al_2O_3.

TABLE III-4

Insoluble Residue Data

Sample	Total Weight	Sample Size (Screen Mesh)	Screened Sample Weight	wt. %	Visual Identification
56	25.9593	<12->18	17.2891	66.6	lead shot
		<18->60	4.8905	18.8	sand, insulation material
		<60->200	3.3234	12.8	fine grit
		<200	0.4563	1.8	fine powder
57	21.3805	<12->18	16.6910	78.1	lead shot
		<18->60	2.1455	10.0	sand, insulation
		<60->200	1.9551	9.1	fine grit
		<200	0.5889	2.8	fine powder
56 + 57	47.3398	<12->18	33.9801	71.78	
		<18->60	7.0360	14.86	
		<60->200	5.2785	11.15	
		<200	1.0452	2.21	

3. Fuel Elements

Examination of the fuel elements was conducted to determine the extent and areas of damage to the assemblies, the extent of damage from thermal effects, the amount of fissionable material remaining and the uranium migration from the fuel matrix in areas of heat affected zones.

3.1 Extent of Melting

In order to determine the amount of fuel plate destroyed and where the loss occurred in the core, each fuel assembly, plate or section of plates was individually examined.

Appendix D is a tabulation of individual fuel plates and/or complete intact fuel assemblies listing percent of area destroyed and percent of area left unmelted.

Forty-seven percent of the fuel in the center 16 elements was destroyed. Relative to the total core, 20% of the fuel was destroyed.

Figure III-70 is a schematic view showing approximately the damaged areas of the core (averaged throughout the vertical direction). The darkened areas represent intact or unaffected parts of fuel elements; the light areas represent the destroyed portions of the fuel assemblies. The four center-most elements were severely destroyed so that only the top 4 to 6 inches of fuel plate remained intact, with slightly less destruction adjacent to the central control blade.

By August of 1961, the only amount of significant fuel material recovered external to the reactor was four (4) small pieces on the fan room floor. See Figure III-71. Examination of these pieces showed that most of the fuel matrix melted and virtually exploded away from its clad, leaving behind a small amount of sponge-like fuel material. Most of the clad and side dead edge was relatively unaffected. The corrosion film still was evident on the pieces but for the most part it had spalled off. The trailing dead edge of one piece shown in the figure was unaffected and the corrosion film remains intact.

An upper portion of fuel plate from element #7, one of the center 16, was recovered from the debris in the bottom of the pressure vessel. See Figure III-72. Here again is seen the unaffected (leading) dead edge, though fuel matrix exploded away leaving portions of the aluminum clad. The dead-side edge was splattered with fuel material.

The corrosion film was intact on the leading dead edge and partly spalled off in the heat affected areas. Most of the corrosion film has been identified as an alumina hydrate and constitutes a small percentage of the insoluble material from the debris recovered from the pressure vessel. See Section III-2.5.

Examination showed the debris from the pressure vessel contained a large quantity of fuel material fragments. See Figure III-78. The small pieces, identifiable as fuel plate material, has a sponge-like appearance. Figure III-73 is a photograph showing fuel material which was ejected from fuel element #3, one of the center 16 elements, and has practically filled the relief hole of shroud #7.

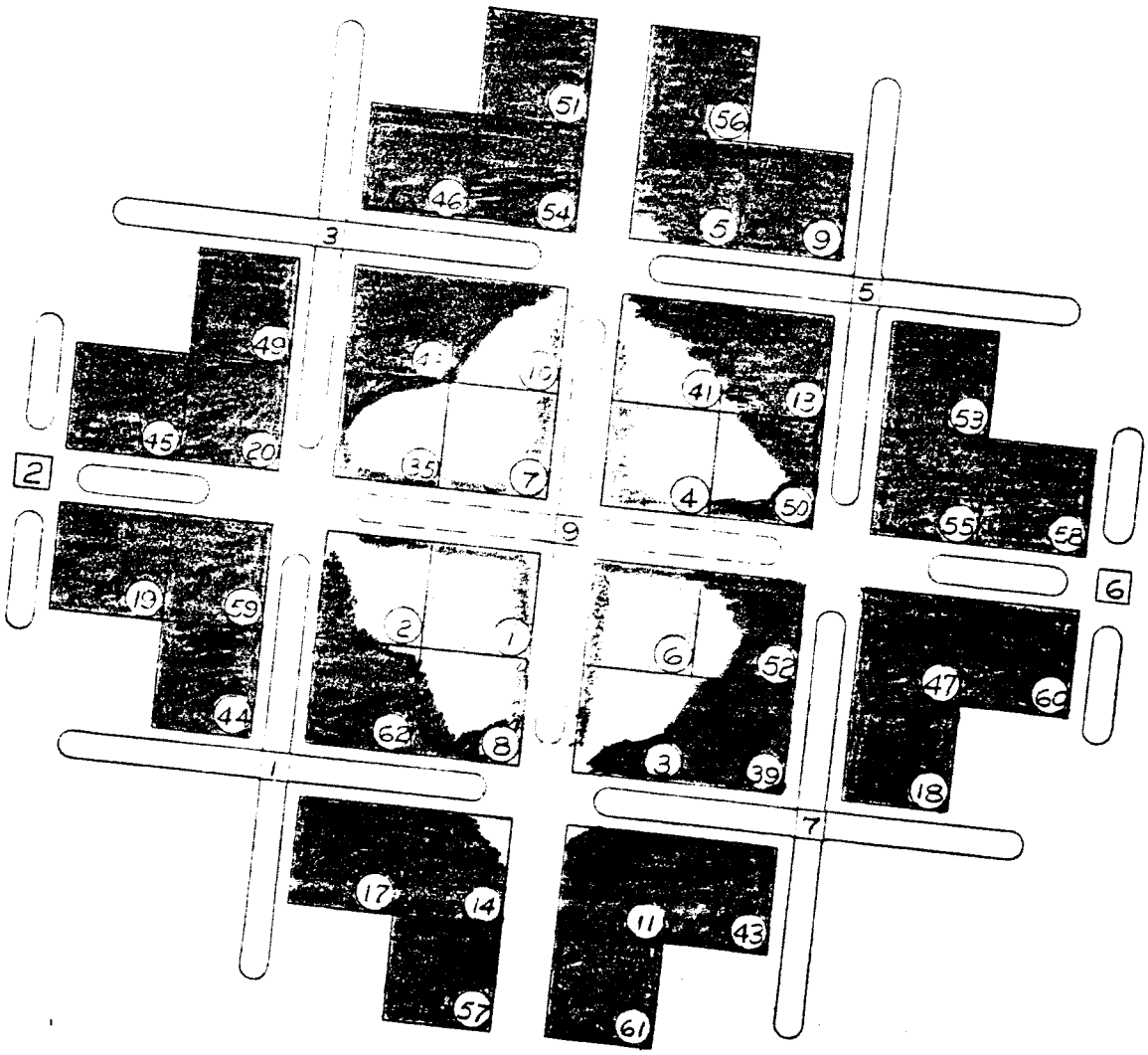

Darkened areas - Unaffected plates

Light areas - Destroyed plates

Figure III-70, Schematic View of Core, Showing Areas of Destruction

U-5001-64

Figure III-71 Sections of Fuel Plate Recovered from Fan Room Floor

U-5001-274

Figure III-72, Section of Fuel Plate from Element #7

Figure III-73 Fuel Material Spatter from Element #3

U-5001-206

Figure III-74 Extraneous Material in Fuel Element #52

Figure III-74 shows the lower end of fuel element #52 with the spaces between plate filled with some molten material, sponge-like material and unmelted pieces.

The sponge-like appearance of fuel material results from a relatively fast cooling rate of a molten metal in contact with water or water vapor. The glazed appearance of a fuel material usually results from a slow cooling rate and may or may not be in contact with water or water vapor until such time that resolidification has begun. In only three instances has glazed appearance of melted fuel material been observed. See Figure III-75.

The preponderant amount of observed sponge-like material to the small amount of glazed material indicates that a relatively fast cooling rate was experienced during the excursion.

3.2. Temperature Ranges

Observation and examination (other than metallurgical) of recovered parts of fuel plates and fuel assemblies indicate a wide temperature range was experienced by the various core components.

A rather unusual aspect of the excursion is that no appreciable amount of glazed molten material was recovered or observed. During the examination of fuel assemblies for damage and fuel inventory, a small amount of unidentified molten material having the glazed appearance was found attached to a piece of burnable poison strip as shown in Figure III-75. Temperature of this melt was probably in the range between 1350°-1450°F.

A section of fuel plate recovered from a center section fuel assembly, shown in Figure III-76, is typical of damage sustained to many individual fuel plates that were blown off their assemblies. The darkened area, Figure III-76, indicates the leading dead edge with the corrosion coating relatively unaffected. It is estimated that it experienced only a moderate rise in temperature; probably in the range of 300°-450°F.

The light area, the corrosion coating having spalled off, shows undisturbed plate. This indicates a heat affected zone in the temperature range between 1000°-1150°F.

The disturbed area, characterized by the folds in the clad, probably reached a temperature between 1250°-1320°F. The fuel matrix in this region was above molten temperature, 1350°-1450°, and was ejected from the clad plate. There is no evidence of molten material having flowed out between the plates, although there is a small amount of sponge-like material along the edges of the plates.

Figure III-77 is a stereomicroscopic photograph at low power of a cross-section through a fuel plate. The clad is virtually unaffected. The fuel matrix has increased in thickness, due to swelling, while other portions have been ejected from the plate. The large voids seen in the figure indicates regions where the fuel matrix has vaporized and reached temperatures of at least 2060°C (3740°F).

U-5001-297

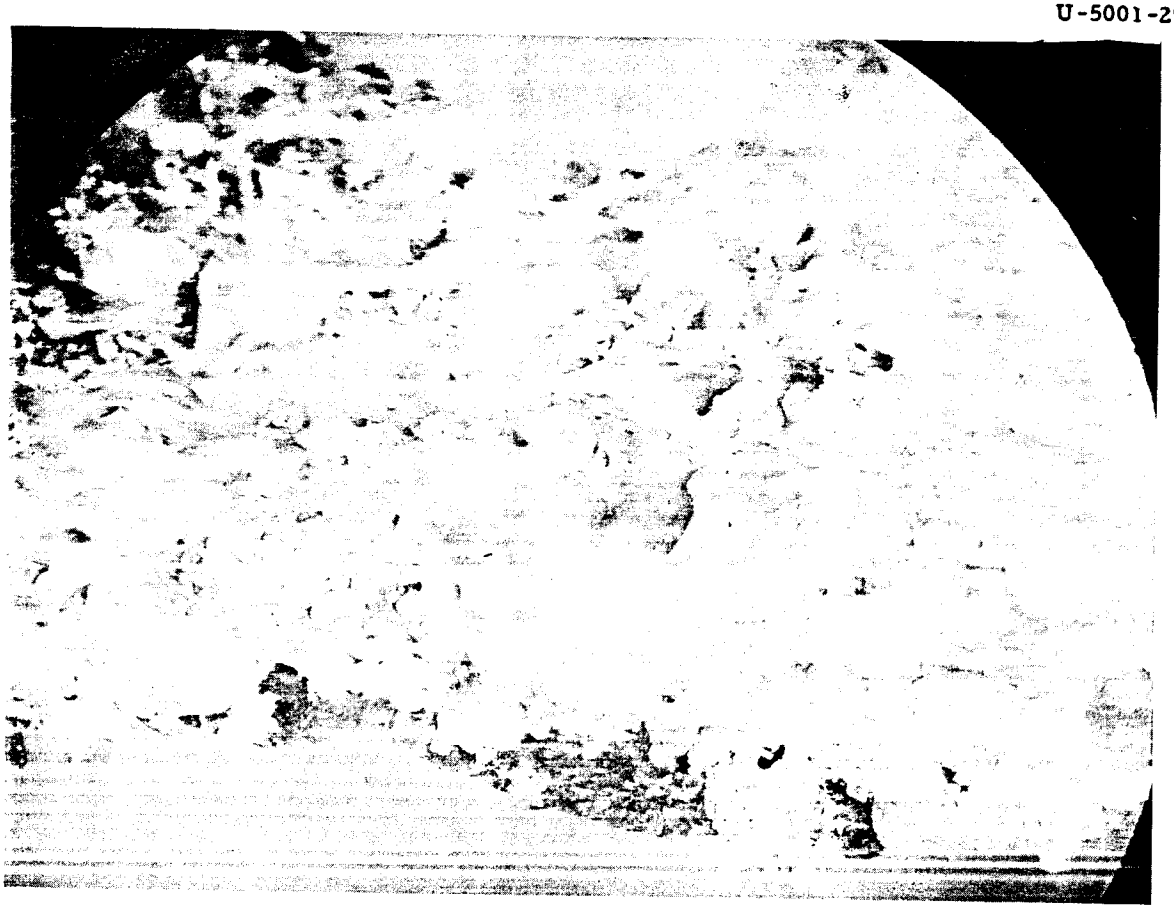

Figure III-75, Molten Metal on Boron Strip

U-5001-224

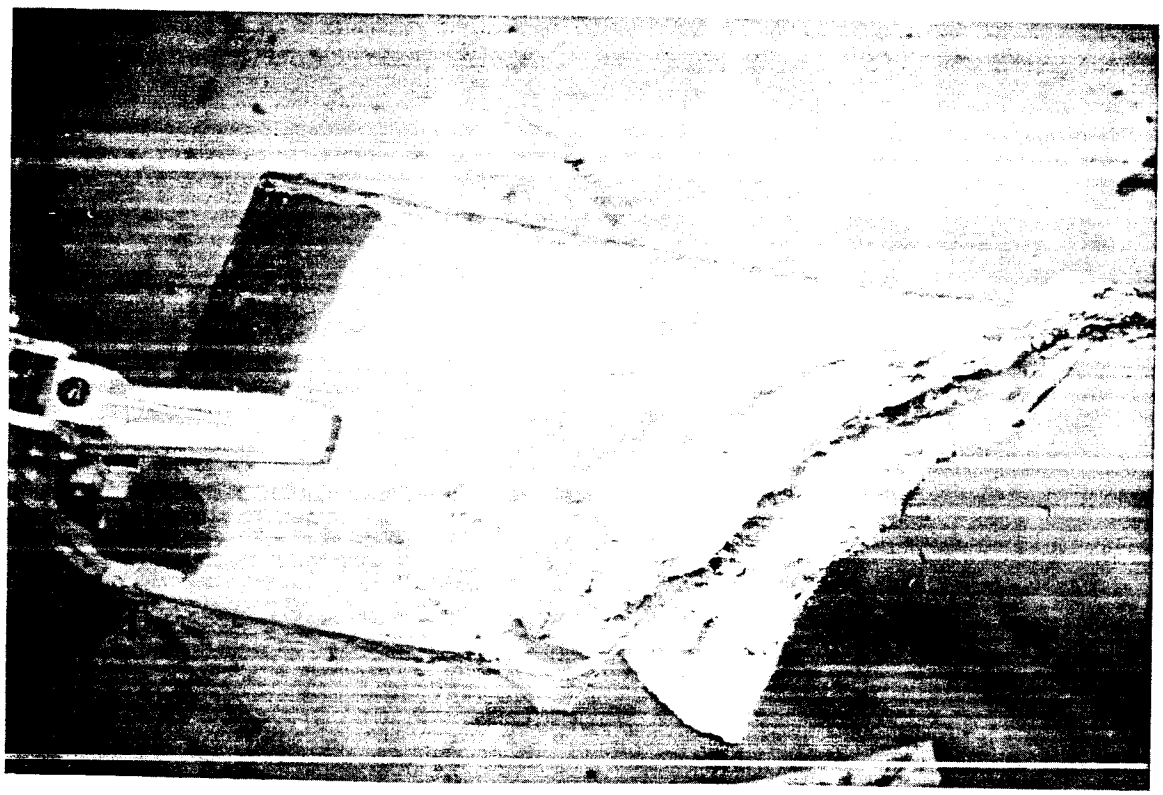

Figure III-76, Fuel Plate from Fuel Element #4
Showing Heat Affected Zones

U-5001-366

Figure III-77 Cross-Section Through Fuel Plate Showing Swelling of Plate

U-5001-238

Figure III-78 Screened Debris Recovered from the Pressure Vessel

Uranium Inventory

The physical operations in making a fuel inventory of the SL-1 core and pressure vessel contents consisted of weighing each fuel element, fuel plate, or plate fragment remotely in the Radioactive Materials Laboratory. A Toledo scale of 20 Kg. capacity was used for weighing. Weights are considered accurate to ±1%. To obtain the weight of active fuel material, the following allowances were made for non-fueled material:

Side plates = 241.0 grams each, 27.8 in. long; or 8.7 grams per inch
Dead-ends = 18.6 grams each
Dead-side edge, including weld area = 33.6 grams, or 1.2 grams per inch--except for the last plate which is 26 grams, or 0.94 grams per inch.

Using these relationships, the active weights of fragments and incomplete elements were determined. The uranium weights reported are those referenced to the original loading and do not account for burnup (i.e. 100% recovery would give a total U-235 weight of 14.1 Kg, the original inventory).

Debris from the reactor pressure vessel was collected and sized by screening into three (3) sizes. The coarse material was sized greater than 1/4 inch; the medium was less than 1/4 inch - greater than 12 mesh; and fines were less than 12 mesh. (See Figure III-78).

The following Table III-5 gives data for recovered fuel material from fuel elements, plates and fragments, and reactor vessel debris. The initial fuel element loading is included. It should be noted that in nine cases the recovery weight significantly exceeds the initial U^{235} loading. This discrepancy results from molten fuel material which was deposited between the plates or splattered onto other plates giving the additional weight. These elements are indicated with (*), and an example can be seen in Figure III-74.

Uranium in the reactor vessel debris is calculated on the basis of enriched U as in the initial material, allowing for ~15% operational depletion prior to the incident, since it is assumed this material originated from the high burnup regions.

A table listing recovered fuel plate condition with respect to melting, is shown in the Appendix D.

TABLE III-5

SL-1 Fuel Inventory

Fuel Element Number	Initial U^{235} Loading	Active Plate Material Recovered	Final U^{235} Recovered*
1	351.5	1121.2	83.39
2	353.0	3908.0	290.65
3	349.6	2506.0	186.38
4	350.3	1046.7	77.85
5	353.3	4480.4	333.23
6	351.9	1543.4	114.78
7	351.0	1206.8	89.75
8	351.7	1152.5	85.72
9	351.0	4700.0	349.56
10	352.9	2392.6	177.95
11	353.9	4707.0	350.08
13	350.4	4676.4	347.80
14	351.6	3975.4	295.77
17	348.1	4700.0	349.56
18	351.3	4700.0	349.56
19	350.1	4821.0	358.56*
20	349.8	4427.0	329.25
35	355.9	1718.0	127.78
39	354.0	4647.0	345.61
41	348.4	2206.4	164.10
43	353.9	4700.0	349.56
44	350.6	4768.0	354.62*
45	349.6	4867.0	361.98*
46	351.7	4700.0	349.56
47	352.8	4700.0	349.56
48	352.7	4657.0	346.36
49	348.9	4700.0	349.56
50	344.1	1912.9	142.27
51	346.0	4700.0	349.56*
52	346.6	3669.0	272.88
53	345.8	4700.0	349.56*
54	345.0	4717.0	350.82*
55	347.0	4700.0	349.56
56	351.8	4807.0	357.52*
57	348.6	4867.0	361.98*
58	349.7	4700.0	349.56
59	348.5	4803.0	357.22*

TABLE III-5

SL-1 Fuel Inventory

(Cont'd)

Fuel Element Number	Initial U^{235} Loading	Active Plate Material Recovered	Final U^{235} Recovered*
60	346.3	4700.0	349.56
61	349.3	4700.0	349.56
62	348.9	4387.0	326.27
		TOTAL	11,534.85
Miscellaneous Fuel Material not Identifiable as to Fuel Plate No.		4961.4	369.00
		TOTAL	11,903.85

Reactor Vessel Debris Uranium Recovery

	Total Weight Recovered (grams)	Wt % U	Uranium Weight Recovered
Fine Screenings	34550	1.6 ± 0.9	552.8 ± 311.0
Medium Screenings	12970	3.2 ± 1.6	415.0 ± 207.5
Coarse Screenings	4480	1.0 ± 1.0	44.8 ± 44.8

Total U from Debris:	1,013.6 ± 453.0
Total U^{235} (Allow ~16% ± 3% depletion of 93.20% enrichment)	1,124.6 ± 510.0
Total U^{235} accounted for:	13,029.0 ± 548.0
Total Initial U^{235} loading:	14,007.50 grams
% Total Accounted for:	93.0 ± 3.9

*Calculated at 7.44 w/o of Active Plate Weight

3.4 Fuel Element Thermal Effect

Much of the damage incurred in the core was the result of thermal effects associated with melting and vaporization of fuel plate material.

Figure III-79 shows two fuel element assemblies which have been subjected to some thermal effect as evidenced by the spalling off of dark oxide from the surfaces of the plates. Most of the fuel plates were separated from each other and the spot welded side plates partly blown away. Both upper and lower end boxes were either blown off or physically separated. No bonding of surfaces had occurred.

Figure III-80 shows a side plate from an element. All spot welds were broken due to impact shear and not as a result of heat effect.

Figure III-81 shows fuel element #4 which was destroyed principally from the effects of melted and vaporized fuel material. One of the side plates, however, remains intact and the dead edge of each plate is shown still spot welded to it. The heat transfer in this region must have been very poor even though contact was metal to metal. The fuel plates, although appearing to have fused together at the lower end, were actually without bond and plates were separated easily by use of slave manipulator hands.

Figures III-82 and 83 show one of the center 16 fuel elements, fuel element #3, which was over 50% destroyed. The center of greatest destruction is approximately 3 to 4 inches below the midpoint of element. However, both side plates remain relatively intact, the two flux wire assemblies were unaffected, and residue of fragmented and melted material was blown both upward and downward into the spaces between the fuel plates. Figure III-83 shows that a portion of the outer fuel plate is missing. The missing portion of plate was found attached, but unbonded, to the neighboring shroud. The portion of plate was intact, distorted and partly splattered with metal.

Even for those fuel elements or plates which had undergone some degree of destruction from melting or vaporization of the fuel, parts adjacent to them remained relatively intact, principally due to the water acting as an insulation blanket and thereby effectively reducing heat conduction.

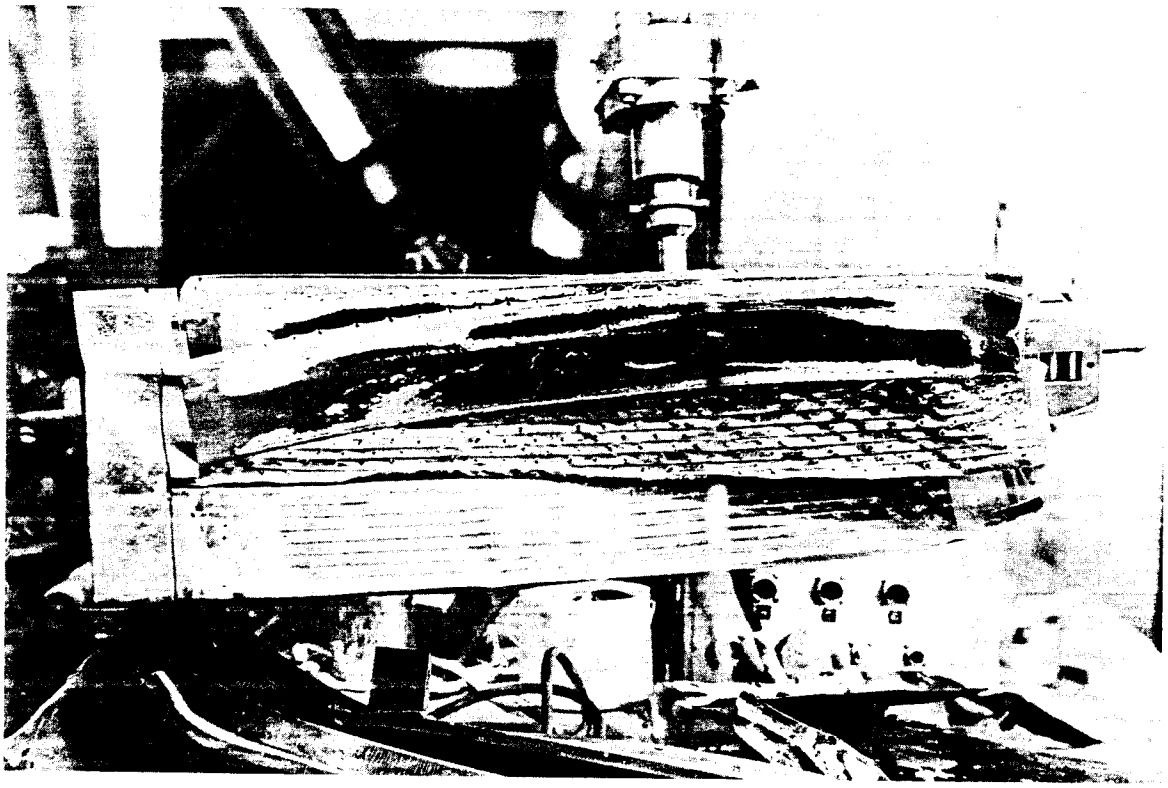

Figure III-79 Fuel Elements #60 and 18, Showing Heat Affected Areas

U-5001-280

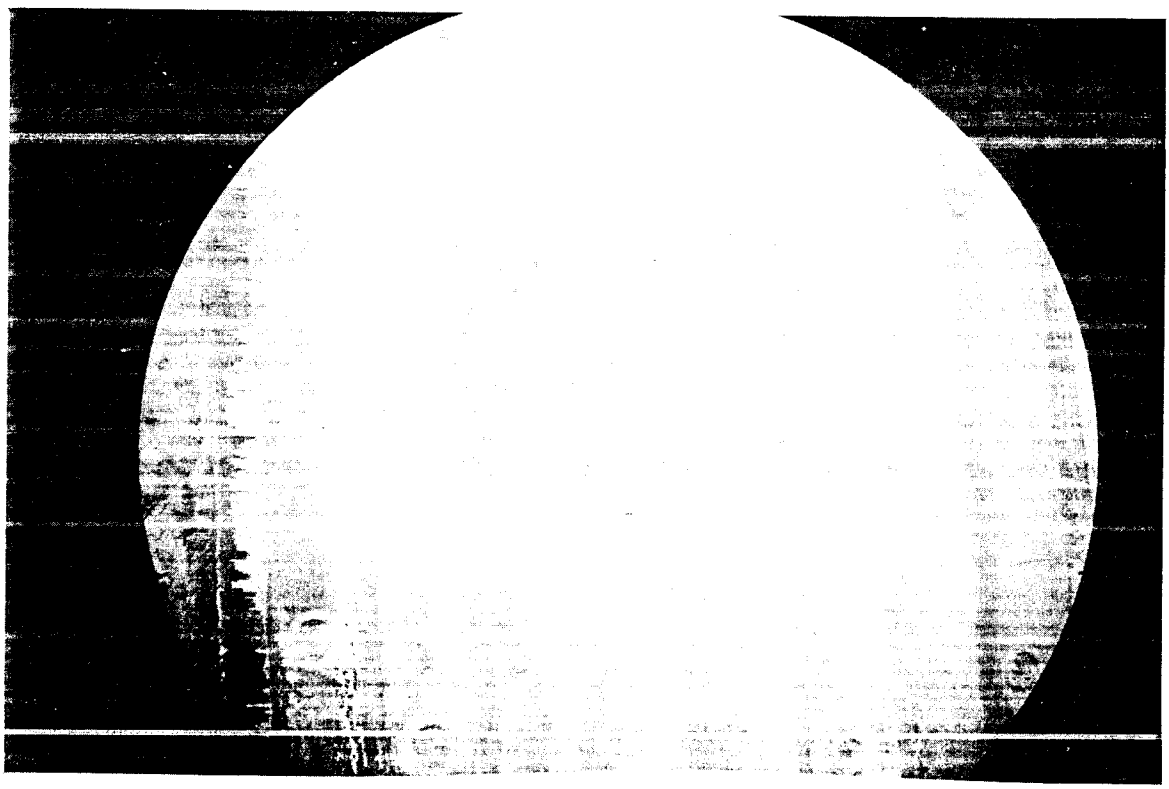

Figure III-80 Fuel Element Side Plate Showing Fracture of Spot Welds

U-5001-155

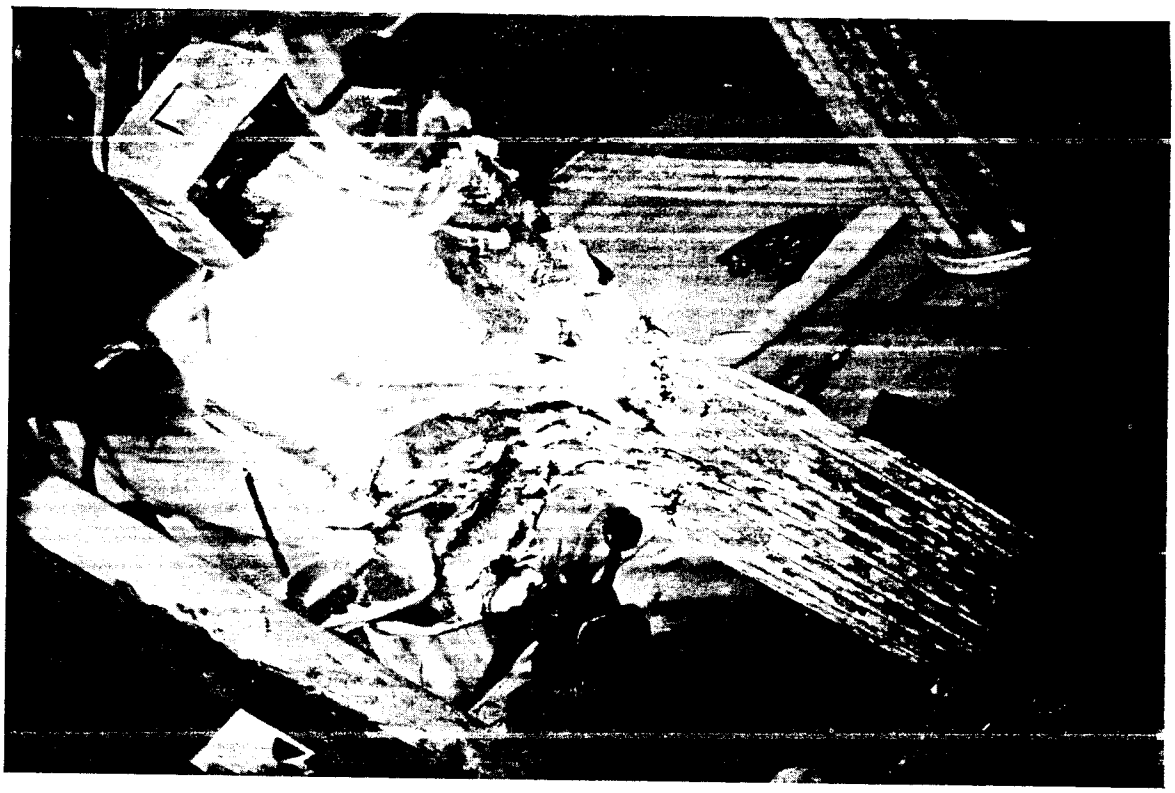

Figure III-81, Upper Section of Fuel Element #4

U-5001-266

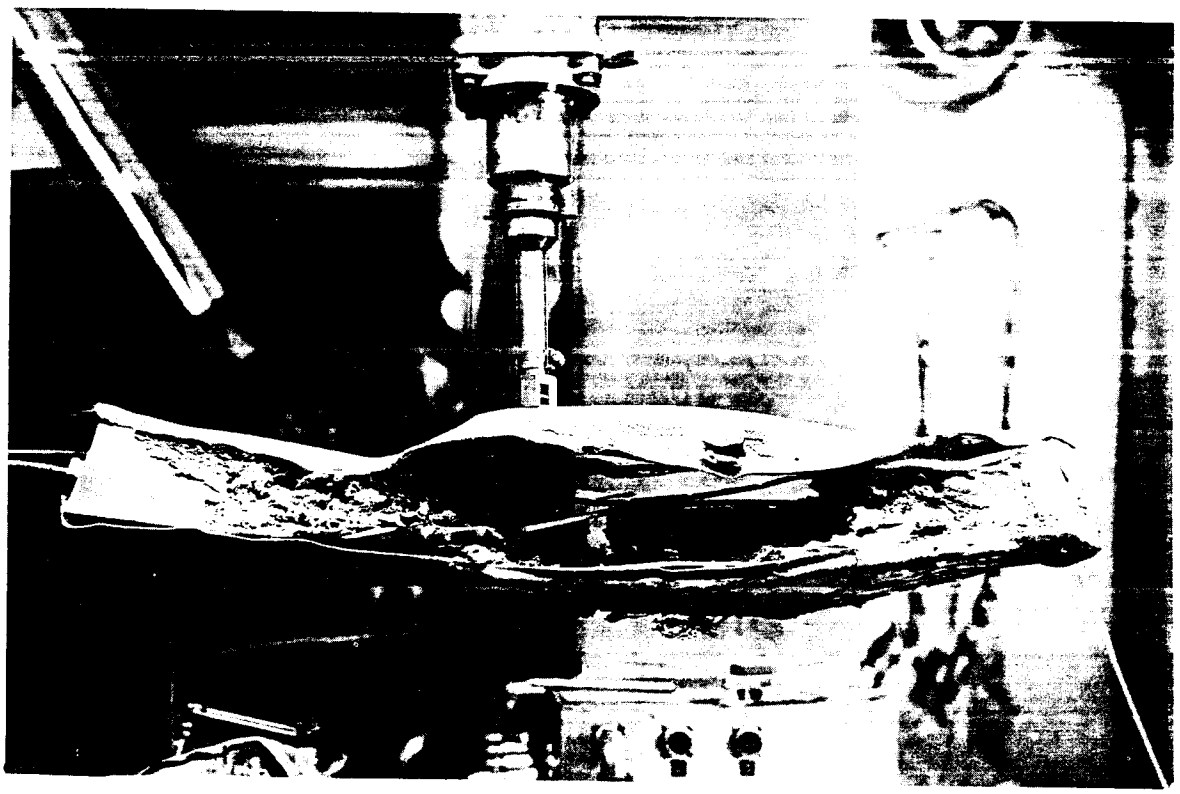

Figure III-82, Fuel Element #3

U-5001-267

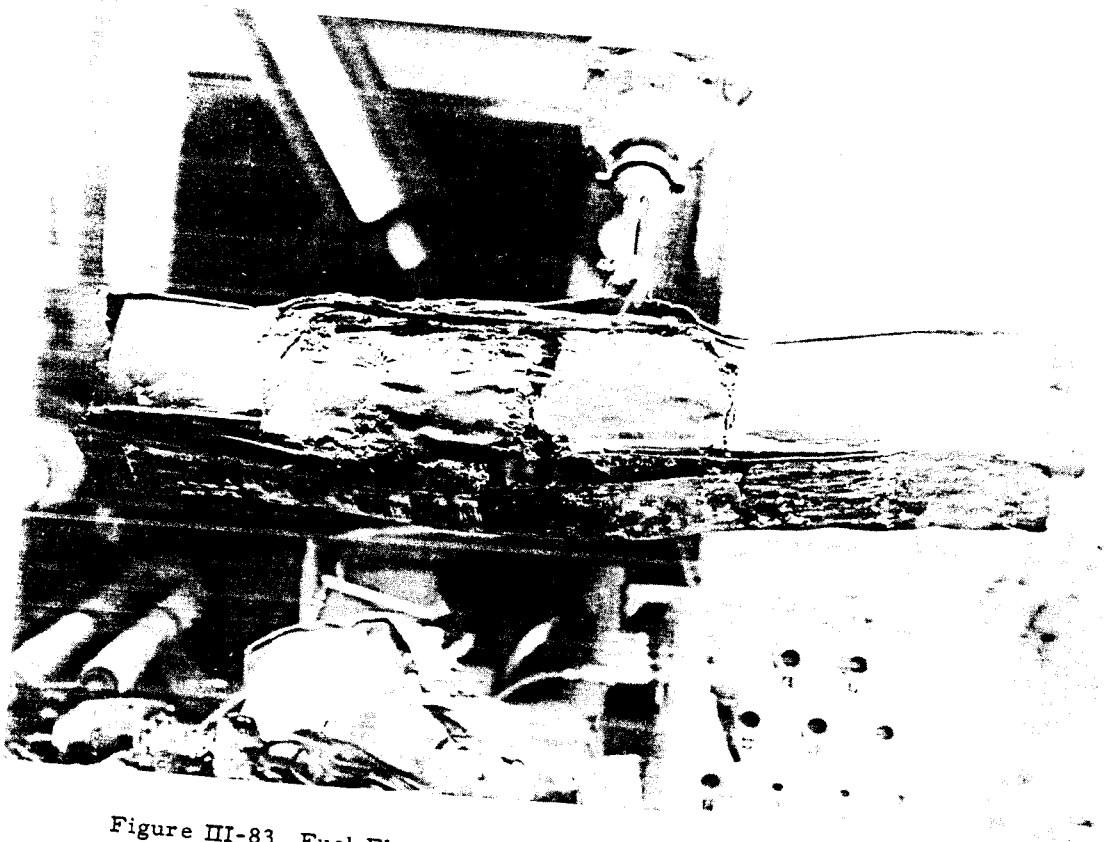

Figure III-83, Fuel Element #3

U-5001-207

Figure III-84, Fuel Element #52, Showing Melted Region and Flux Wire Undamaged

3.5 Flux Wire Thermal Effects

Aluminum flux wires, containing alloy pellets, had been placed between the plates of some elements prior to the incident. Attempts were made to extract and identify each of these wires from the damaged elements without breaking apart the elements. The wires were generally restricted by the mechanical deformation of the elements; and in the majority of cases the plates had to be separated to extract the wires.

Despite the high temperatures attained by the plates, none of the flux wires appeared to have been damaged by the heat. Figure III-84 is a view of a severely melted region of element #52, showing intertwined flux wire to be undamaged except for mechanical bending. Deposits of spattered fuel have been found on the wires, and some wires were fractured. Most fractures appeared to have been entirely mechanical, although some of the breaks may have been induced by the action of a hot piece of fuel element coming in contact with the wire.

The wires, 0.188 inches in outside diameter, were in 0.310 inch wide water channels. Quite likely contact of the wires with the fuel plates occurred at relatively few points along the length of the wire. Heat transfer from the plates to the wires thus had to occur primarily through the water, which effectively provided an insulating blanket for the flux wires.

3.6 Aluminum-Uranium Ratio

In an effort to determine the fuel loss from areas of melting, the ratio of aluminum to uranium in selected areas of fuel plates was determined. 1/4" diameter punchings were taken from plate E-8 of fuel element #5 (Figure III-85) and from plate E-83 of fuel element #6 (Figure III-86). The punchings from plate E-8 were taken from upper, center, and lower regions shown in the photograph (Figure III-85). Punchings from plate E-83 were from the threshold of melt area. Photos in Figure III-87 shows the molten area and the swelling of plate E-83. Table III-6(a) shows the existing data from the above areas.

TABLE III-6(a)

Aluminum/Uranium Ratios

Plate No.	Sample Region	Wt % Al	Wt % U	Al/U Ratio
E-8	Upper end	84.8	8.87	9.6
E-8	Center	95.7	0.69	138.7
E-8	Lower End	90.7	5.68	15.9
E-83	Threshold of Melt	80.9	7.23	11.2
E-83	Threshold of Melt	79.4	8.20	9.7
E-83	Threshold of Melt	87.7	7.99	10.9
E-316	New Fuel	90.56	7.98	11.35

Ratios of Al to U less than control samples of non-irradiated fuel plate can be explained by swollen regions forcing fuel between the cladding to enlarged thicknesses. Greater ratios indicate uranium loss from fission or possible volatilization.

Another set of punchings from plate E-550 of fuel element #39 was analyzed for Al and U. The punchings were selected to give an axial profile of uranium loss from element #39. The punching locations are shown by reference number in Figure III-88. The analytical results are given in Table III-6 (b)

TABLE III-6 (b)
Aluminum-Uranium Ratios
Plate E-550/Fuel Element 39

Punching No.	wt/% Al	wt/% U	Al/U Ratio
41	95.67	1.42	67.4
42	89.49	8.06	11.1
43	88.67	7.07	12.5
44	83.86	5.54	15.1
45	92.85	3.42	27.2
46	90.79	4.39	20.7
47	93.63	2.64	35.5
48	89.18	5.84	15.3
49	90.02	5.85	15.4
50	88.35	7.71	11.5
316 New Fuel	90.56	7.98	11.35

U-5001-304

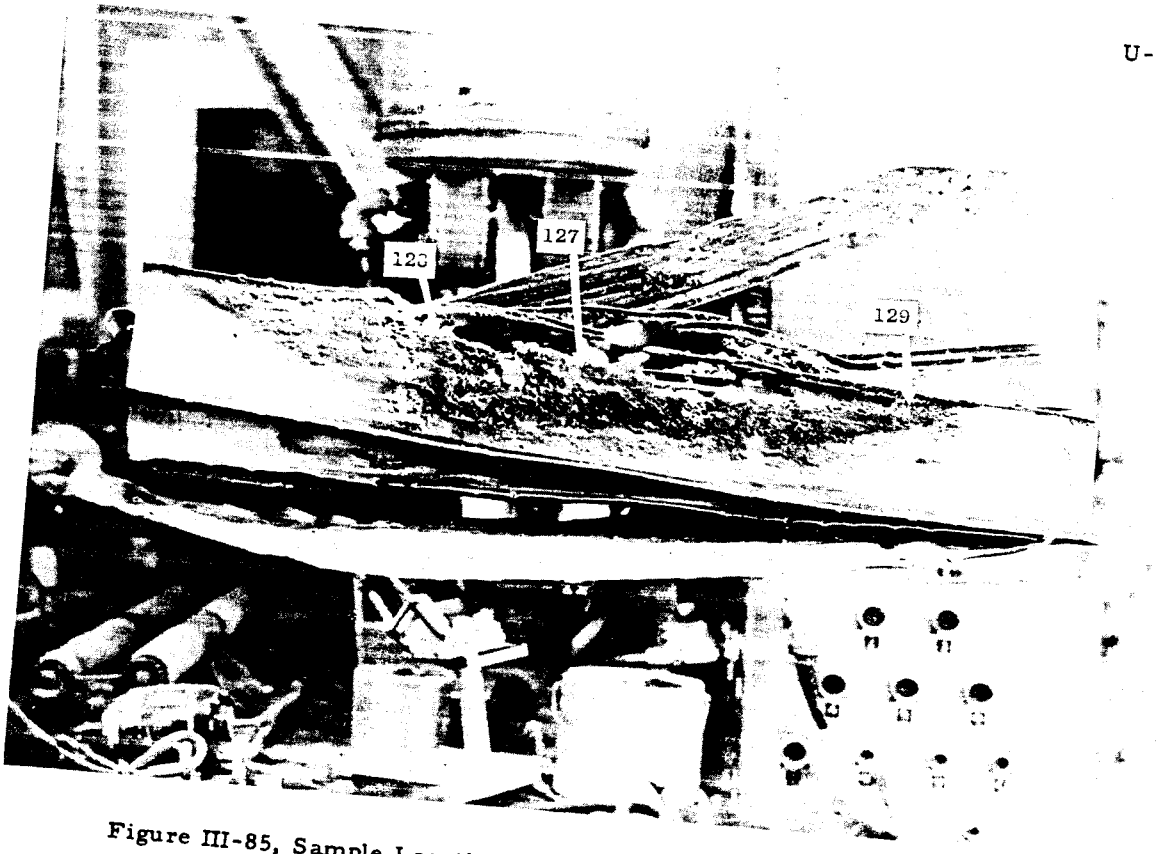

Figure III-85, Sample Locations on Fuel Element #5

U-5001-362

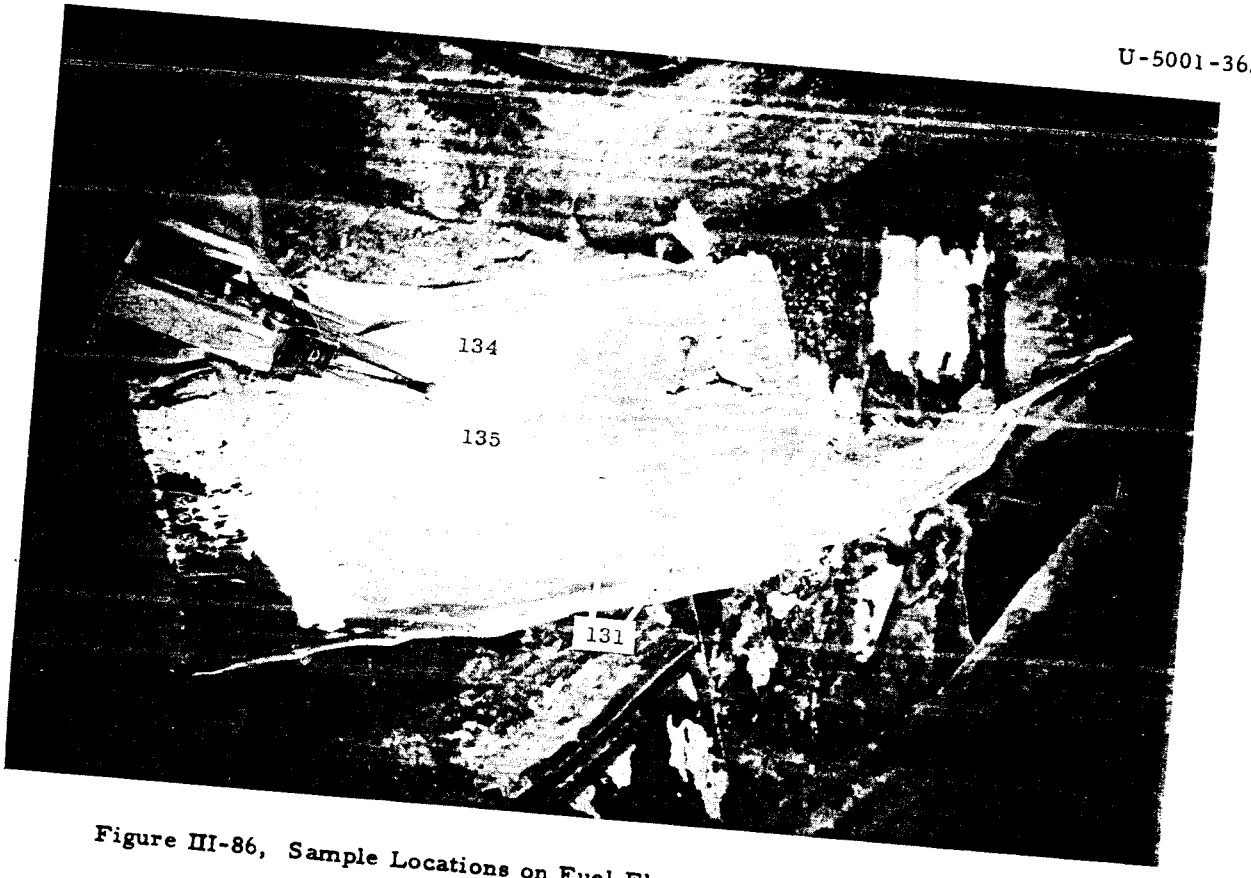

Figure III-86, Sample Locations on Fuel Element #6

U-5001-365

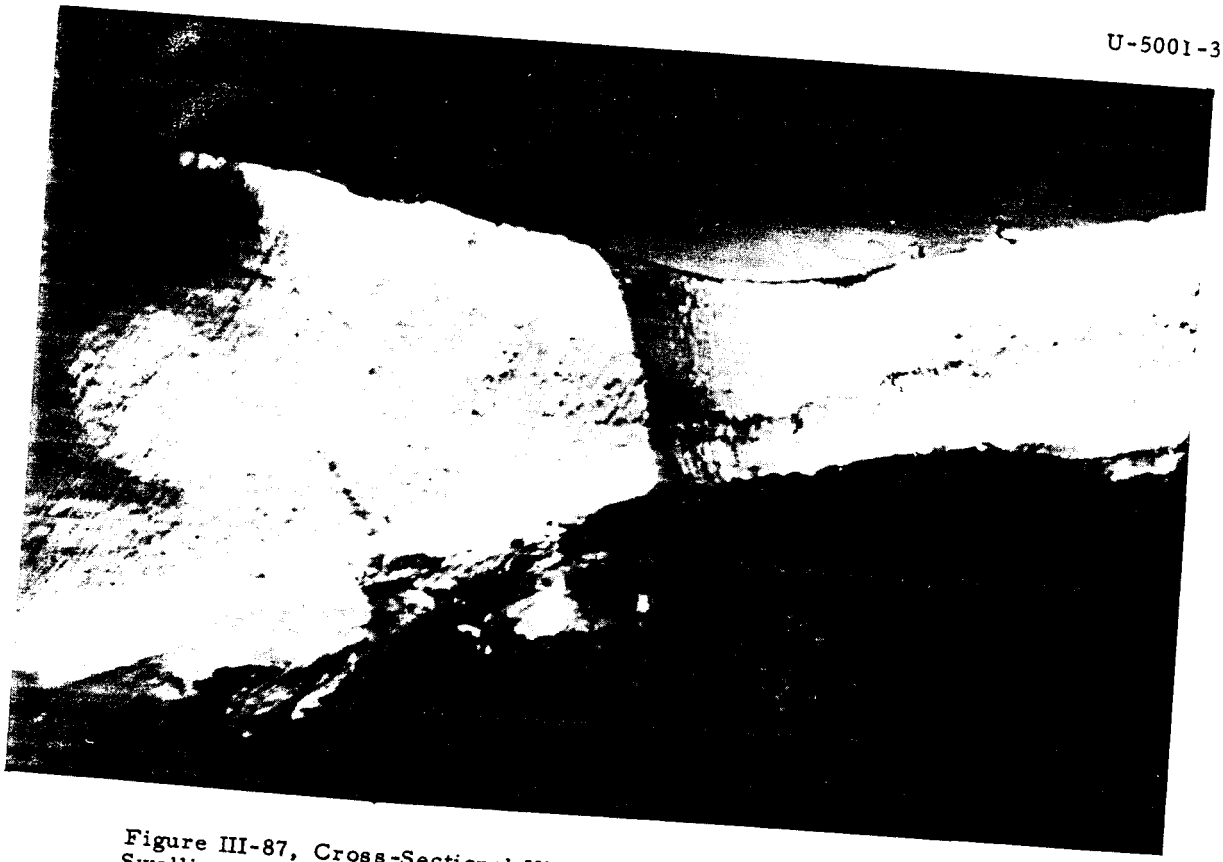

Figure III-87, Cross-Sectional View of Fuel Plate Swelling from Fuel Element #6

U-5001-375

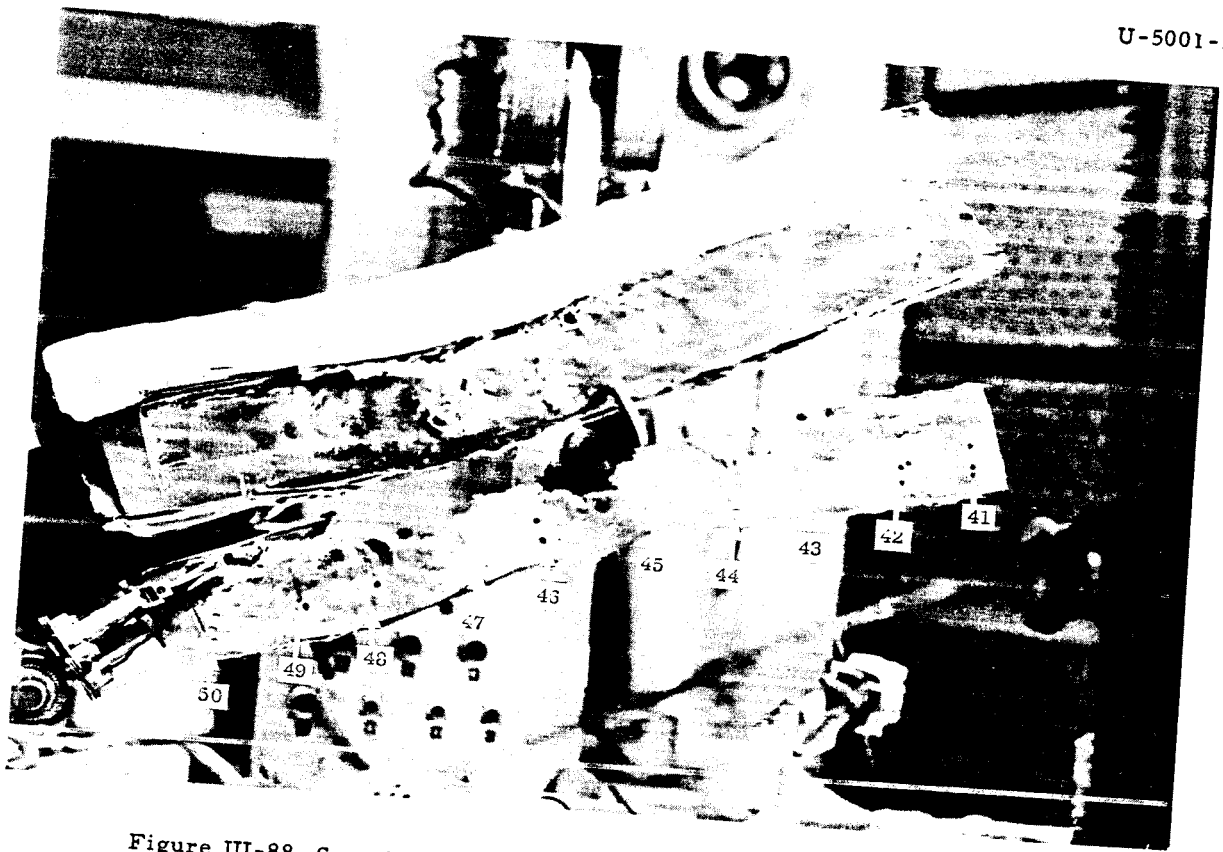

Figure III-88, Sample Locations on Fuel Element #39

4. Nuclear Evidence

4.1 Flux Wires

Just prior to the SL-1 incident, 45 flux wires had been placed between fuel plates at various regions throughout the core. Each wire contained either 10 or 13 small cobalt - aluminum pellets, spaced three inches apart (476 pellets total). Each pellet was 3/32-inch long by 40 mils in diameter, weighed approximately 5 milligrams, and contained cobalt in the concentration of 0.5% by weight, for a net of 25 micrograms of cobalt per pellet. It was intended that these wires would receive approximately a 35 megawatt-day exposure during normal reactor operation. The pellets had received no exposure prior to the incident, and therefore provided a direct measurement of flux and energy densities for the incident.

The wires containing the pellets were enclosed in protective aluminum sheaths with an identifying number printed on the plate attached to the top of the sheath. All of the wires have been recovered in whole or in part. In some cases the identifying tags were broken off or the wire was broken in several pieces making it impossible to identify wires or sections thereof. However, approximately 352 pellets have been recovered, identified, and analyzed. Figure III-89 shows the locations of the wires in the core.

Since the exposure received by the pellets was about 10^{-4} of that for which they were designed, the activity was quite low. The surface of the pellets was badly contaminated with the usual fission products which normally masked the cobalt activity. (Typical wires read about 25 R per hour gamma at one foot) Some attempts were made at chemically separating the small amount of cobalt from the fission products, but this method generally proved unreliable. Most of the pellets were counted whole after being cleaned ultrasonically. Cobalt activity, accurate to about ± 10%, was obtained from the pellets in the high flux regions using nominally two hour count times on a 3 x 3 NaI (Tl) crystal at a distance of three centimeters from the source (256 channel gamma analyzer). Pellets from the lowest flux regions had cobalt activity barely discernible from the fission product background following 10 hour counting times.

It can be shown that the measured cobalt activity (A) in $\frac{dis}{min}/gm$ of cobalt, corrected back to the time of the incident, when multiplied by 1.06×10^{7} gives the equivalent 2200 m/sec flux in n/cm^2 for short exposure times and a Co^{60} half life of 5.3 years.

A more useful quantity pertaining to the effect of the flux on the fuel plates is the nuclear energy generated per unit mass of fissile material. Using a flux disadvantage factor of 0.91 for the fuel and a value of 3.2×10^{10} fissions to produce one watt-sec (joule) of total nuclear energy (of which only 86% is immediately deposited in the plates), the following conversion factor is obtained:

$$\frac{MW\ sec}{Kg\ U235} = 4.1 \times 10^{-14} \ (\phi t) \ \frac{n}{cm^2}$$

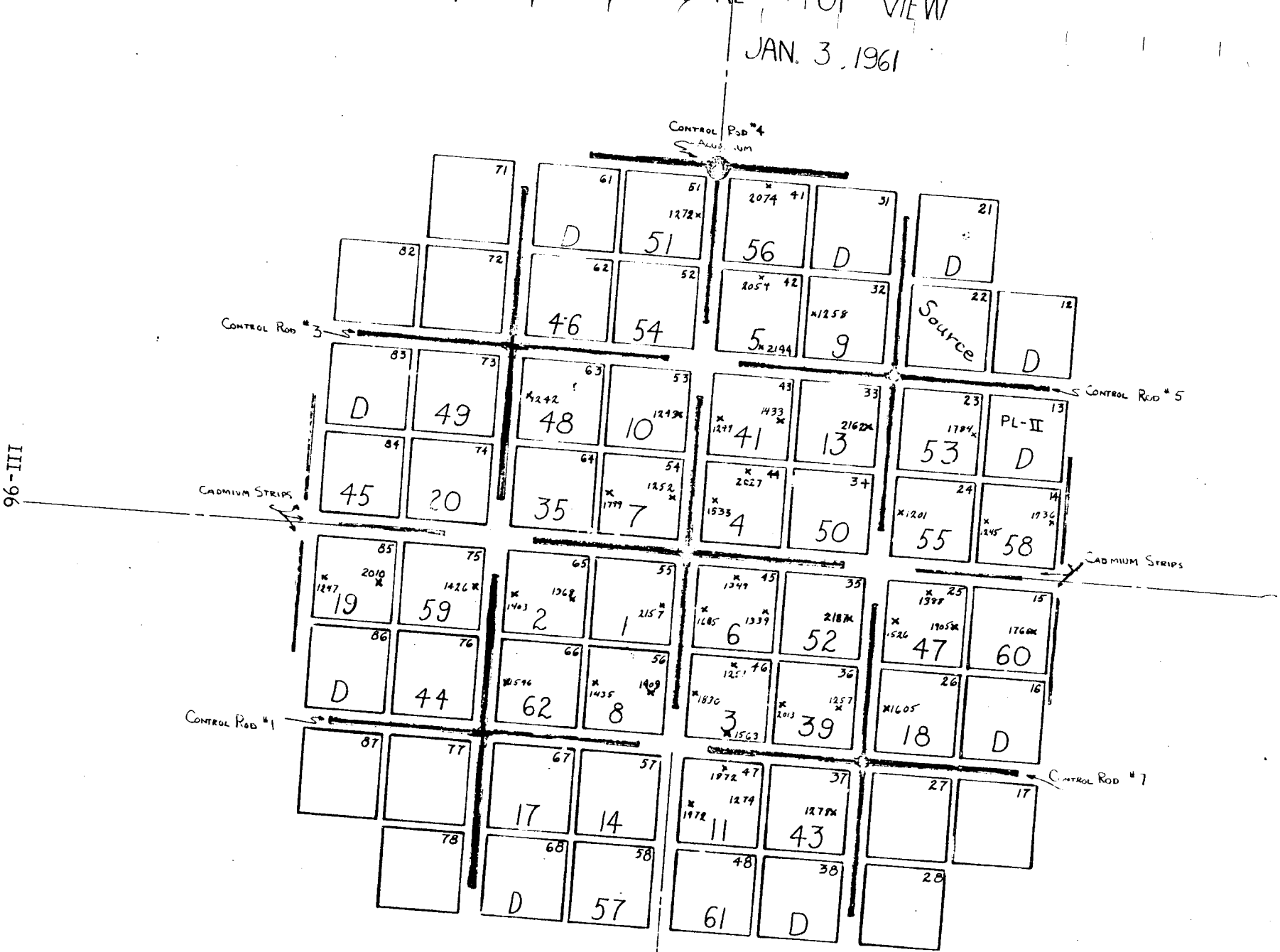

Figure III-89 Flux Wire Locations in Core

× 1252 — FLUX WIRES

D — DUMMY ELEMENTS

Knowing the original fuel loading per element (350 gm of U^{235}) and the approximate burnup (8% average over core, 20% peak), the energy generated per element or per cm^3 of a portion of the fuel meat can be easily calculated. In determining the total energy generated, the average over the longitudinal flux distribution was obtained for the active fuel. Corrections for the radial variation of the flux were made for cases in which a single wire from an element was located significantly off the centerline of the element (C. W. Luke, Combustion Engineering, Incorporated, private communication). This radial correction in no case was taken to be greater than 20%.

The energy generated per element for those elements containing flux wires is shown in Figure III-90. The tabulated results of flux recorded on each pellet is given in Appendix E . The longitudinal flux distribution was peaked downward in the center section of the core because of the partially inserted central control rod, while near the outer portion of the core, the flux distribution was a flattened and chopped cosine. Typical longitudinal flux distributions are shown in Figures III-91 and 92 . A summary of the most significant data obtained from the flux wires is given Figure III-93 .

Using this data, the total power generated in each typical section is summed:

Center Section	Totals
4 at 6.3 ± 1.0	25.2 Mw-sec
8 at 4.7 ± 0.5	37.6 Mw-sec
4 at 3.7 ± 0.8	14.8 Mw-sec
Center Total	78 ± 7 Mw-sec

Outside Section (No Cd strips)	
4 at 3.3 ± 0.4	13.2 Mw-sec
4 at 2.1 ± 0.4	8.4 Mw-sec
4 at 1.9 ± 0.3	7.6 Mw-sec

Outside Section (with Cd strips)	
4 at 2.0 ± 0.5	8.0
4 at 1.9 ± 0.5	7.6
4 at 1.3 ± 0.4	5.2
Outside Total	50 ± 4 Mw-sec

Total Energy of Excursion: 130 ± 10 Mw-sec

Positive flux wire data for the very center of the core, the highest flux region, were not obtained. All of the pellets from this region were either lost during the excursion or unidentifiable. One wire, found intact, but without an identification tag, was interpreted as having been in one of the four center elements. From its activation, a peak energy

SL-1 CORE (TOP VIEW SCHEMATIC)

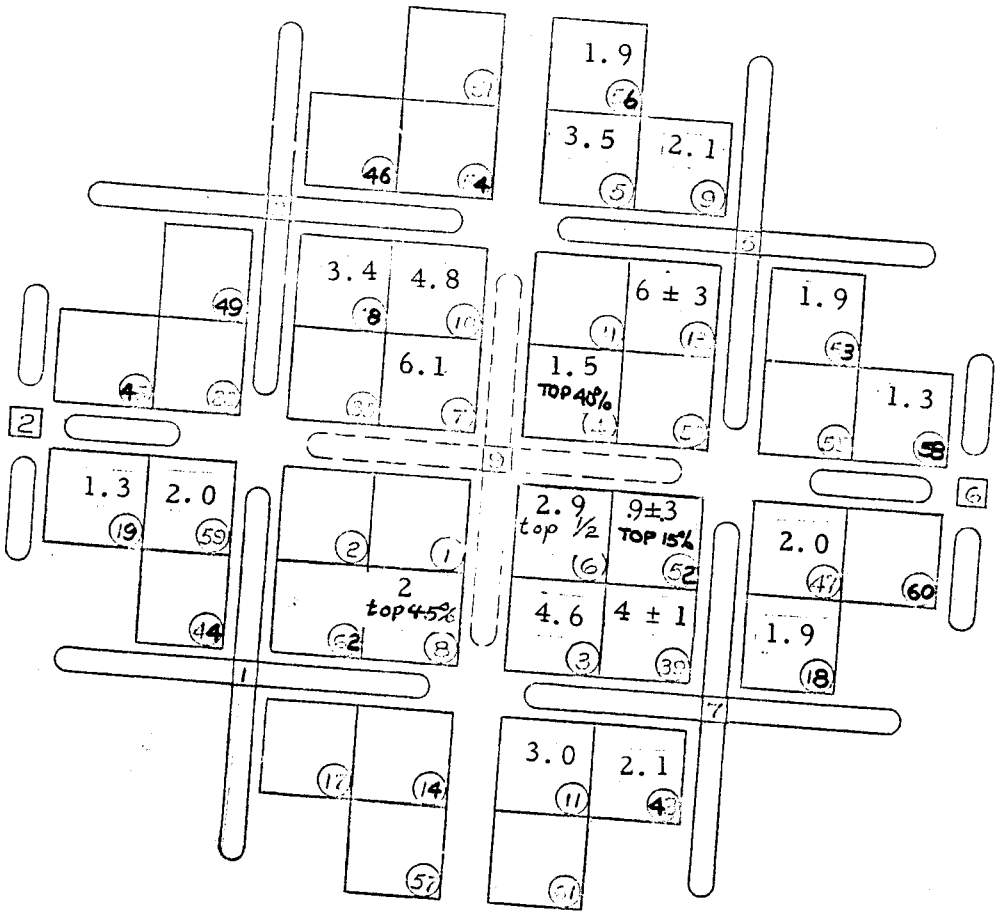

Figure III-90 Energy Released per Element - in Mw-sec.

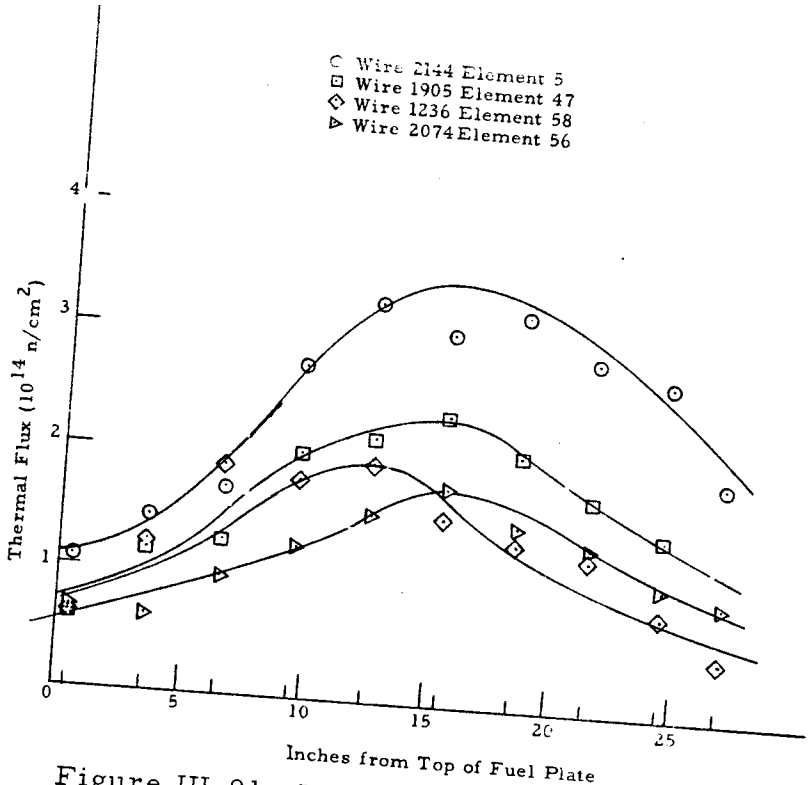

Figure III-91 Longitudinal flux distributions in outer 24 elements (in water)

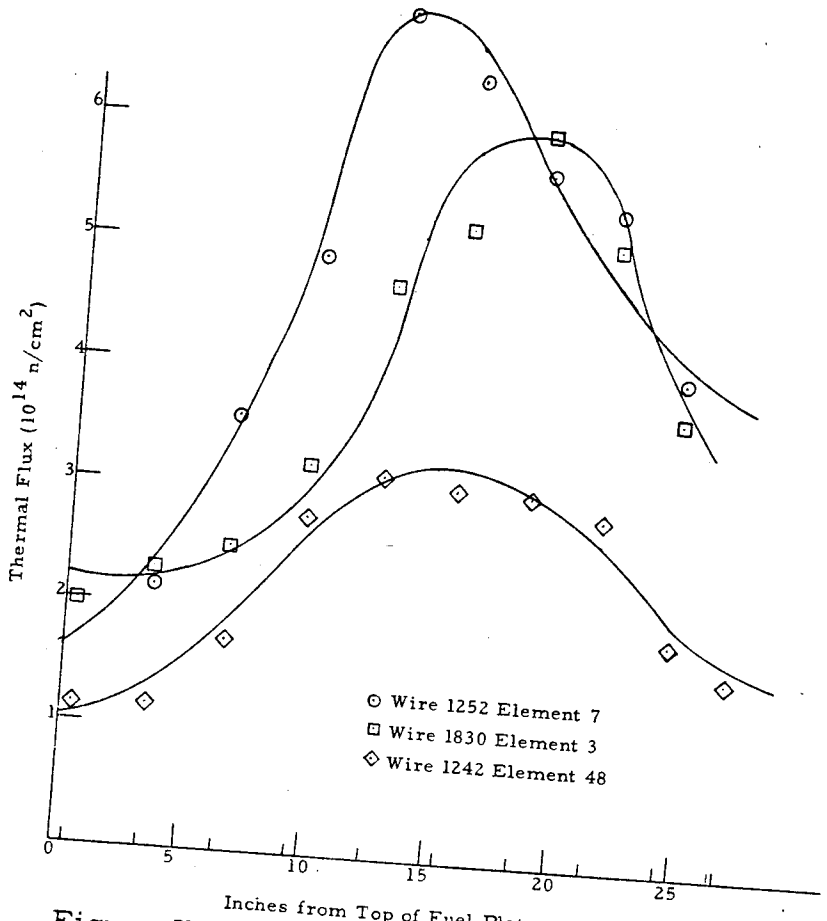

Figure III-92 Longitudinal flux distributions in center 16 elements (in water)

Quadrant of Core - energy generated per element in Mw-sec and estimated inventory of U-235

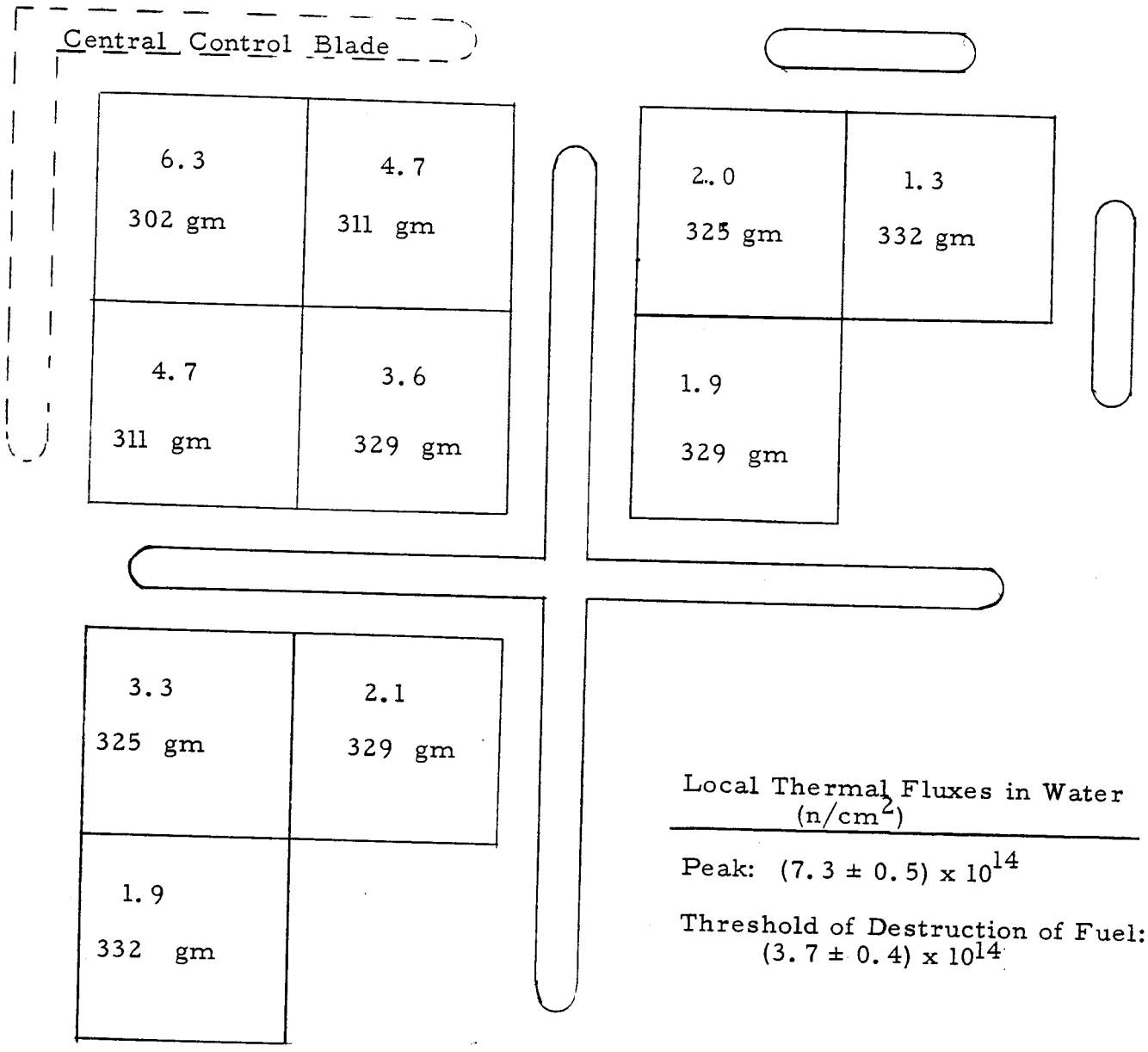

Figure III-93 Energy distribution during SL-1 excursion

density of between 30 snd 35 Mw-sec/Kg of U-235 has been deduced. The accuracy of most of the other data has a standard deviation of approximately 15%. The peak to average energy density ratio was approximately 3/1.

4.2 Other Activation Data

Initial Data

Soon after the incident, some thermal and fast neutron activation data were obtained from materials on or near the three victims. The reported fluxes are given in Table III-7, below Samples for which previous exposure history was uncertain have not been included.

TABLE III-7

	Sample	Activation Product	Neutron Flux (n/cm^2)
1.	Cigarette lighter (1) screw from first victim	Cu-64	9×10^9 (thermal)
2.	Watch band buckle (1) from second victim	Cu-64	2×10^{10} (thermal)
3.	Ring from third (1) victim	Au-198	9×10^9 (thermal)
4.	Scalp hair (2) first victim	P-32	2×10^{12} (fast)
5.	Pubic hair (2) first victim	P-32	8×10^9 (fast
6.	Scalp hair (2) second victim	P-32	2×10^{13} (fast)
7.	Pubic hair (2) second victim	P-32	5×10^{11} (fast)
8.	Scalp hair (2) third victim	P-32	9×10^{12} (fast)
9.	Nuclear accident dosimeter (1) at top of stairway	Au-198	6×10^7 (thermal)

Stellite Bearing from #4 Shield Plug

The #4 shield plug had seen no previous service in the reactor (except during the initial critical experiment). Normally, the Stellite bearing was located one foot below the pressure vessel head, surrounded by 0.2 inch thick stainless steel guide tube wall with the extension rod through its center. The bearing was found in its guide tube in the fan room.

The Stellite was 55% cobalt, and showed barely measurable activity when recovered in July, 1961. The surface of the bearing was machined

1. SL-1 Reactor Accident Report, Combustion Engineering, Inc. May 15, 1961, IDO-19300
2. SL-1 Reactor Accident Autopsy Procedures and Results, LAMS-2550

away to remove contamination. An activity of approximately 20 $\frac{dis}{min\text{-}gm}$ was measured over most of the bearing. This corresponds to 4×10^8 n/cm^2 thermal flux. The stainless steel guide tube would provide about 10% attenuation, while the self-shielding effect of the bearing is about 40%. The flux which impinged on the bearing was probably not isotropic, and was apparently no greater than 10^9 n/cm^2. A direct upward streaming beam of neutrons would have been ineffective in activating the bearing.

Shield Plug Flanges and Caskets

Samples of the shield plug flanges were analyzed for Co-60 activity as were the "Flexitallic" gaskets. The previous history of the latter was uncertain. This fact and the shielded location of the gaskets made it impractical to attempt to derive useful information from them.

The flange material from the shield plugs known to have been in the reactor head for all previous operation indicated total thermal fluxes of about 3×10^{12} n/cm^2. This value, which reflects activation during normal operation and not during the incident is consistent with flux measurements taken four feet above the reactor head during normal operation (IDO 19005, Vol. II, 4×10^3 n/cm^2 - sec at 1.3 MW).

Instrument Support Pipe

Approximately five months before the incident, a stainless steel pipe was attached to instrumented element #1 so as to provide support for the thermocouple wiring. Though the activation on this pipe from the incident was negligible, the pipe was useful in obtaining a flux profile during normal reactor operation between the top of the core and the top of the #8 nozzle. The pipe was analysed for Co-60 activity and the results are shown in Figure III-94.

These data show that a factor of 1.5×10^4 existed between the flux at the top of the core and the flux at the top of the nozzle during normal operation. This condition existed with four feet, four inches of water containing approximately 15% steam voids above the core. During the initial excursion, seven feet of water containing no voids was above the core. Thus, an attenuation factor of considerably greater than 1.5×10^4 existed between the top of the core and the top of the nozzle during the initial SL-1 excursion.

PL-II Sample

A sample of structural material for the newly designed PL-II core had been placed on top of one of the dummy elements during the pre-incident shutdown period. A portion of this sample was blown out of the pressure vessel and recovered early in the cleanup operation. The indication of excursion energy derived from the activation of the cobalt (0.1%) in this sample gave one of the earliest estimates of the total energy of the excursion, though this result has been superseded by the more accurate flux wire data. The 250 ± 80 Mw-sec obtained by various methods of extrapolating the measured 2.5×10^{13} n/cm^2 flux from the PL-II sample to the core was higher than the flux wire results by 1-1/2 standard deviations.

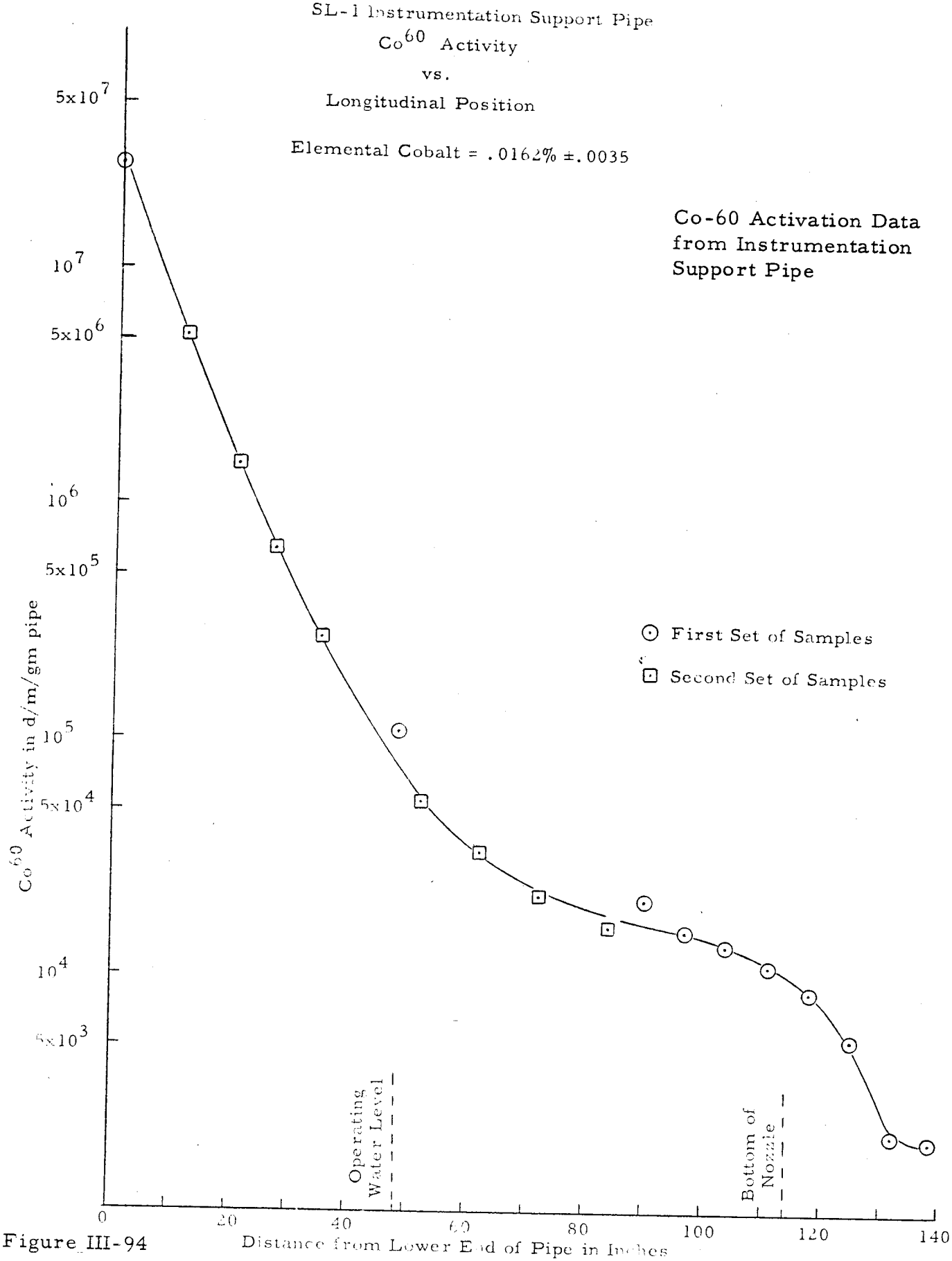

Figure III-94

However, the flux of 2.5×10^{13} n/cm^2 is useful in estimating what the fluxes might have been further away from the core.

Film Badge Activation

The film badges of the victims were not recovered until nearly seven months after the incident. The nuclear accident dosimeters in the badge packets had no measurable activity because of the long decay time. The most promising material in the badge was silver, with its resultant 250 day Ag-110 activation product, resulting from a 2.8 b thermal cross section. Each badge contained about 1/6 gram of silver, which was thoroughly decontaminated. A disintegration rate of 20 dis/minute, about 1/2 of normal background, could have been detected. This value corresponds to a thermal flux of 1.5×10^{10} n/cm^2, which is therefore an upper limit to the thermal fluxes experienced by the badges.

4.3 Fission Product Release

At the time of the incident, the SL-1 had been shut down 11 days since its last power operation, with most of its operation having been spread out over a three year period. The main gaseous fission products remaining at this time were I-131, I-132, and Xe-133. These represented a small fraction of the total inventory of gamma emitting fission products, the I-131 being only 6% of this inventory at the time of the incident.

The gross gamma-emitting fission product inventory, calculated by the Way-Wigner formula (1), is listed in the table below at various significant times during the SL-1 post-incident history.

Time	Gross Gamma Fission Product Inventory
Incident, January 3, 1961	500×10^3 curies
March 1, 1961	200×10^3 curies
June 1, 1961, cleanup began	120×10^3 curies
August 1, 1961, cleanup of fan room	90×10^3 curies
December 1, 1961, reactor in Hot Shop	65×10^3 curies
April 10, 1962, critical experiment	50×10^3 curies

On June 1, 1961, the average gamma radiation level throughout the operating room (exclusive of local hot spots and the area immediately over the reactor) was approximately 60 R/hr. four feet above the floor. This field could be produced by about 1800 curies scattered over the floor (uniformly) and 300 curies in the ceiling above the reactor. Since significant shielding of the radiation by various equipment, shield blocks, etc. occurred, and with due consideration for the local hot spots, particularly the top of the reactor, it is believed that the curie release represented by a 60 R/hr. field would be twice as great as calculated, or about 4000 curies, representing 3% of the fission products.

(1) Glasstone, Principles of Nuclear Reactor Engineering, P. 118-120.

As an independent check, the activity of the truckloads of debris removed from the operating room and fan room was measured with a survey meter from a distance so as to simulate a point source. Each load of debris was approximately corrected for self absorption (factor of 1.5 to 2.0). The total gamma activity of all the debris, including the building walls and equipment, was measured to be about 2400 curies, corrected to June 1, 1961. This represents about 2.1% of the total gamma fission product inventory, and is probably an underestimate.

Very little of the particulate fission products that left the vessel actually escaped outside of the building, and the gaseous fission products emitted at the time of the incident were only a small fraction of the total. Thus, it appears that about 5% of the core inventory can be accounted for outside of the pressure vessel.*

A film badge from one of the victims was recovered from the operating floor seven months after the incident. The polyethylene picture was badly darkened from radiation damage. Tests on a similar polyethylene sheet showed that at least three million rad of ionizing radiation was received by the badge in question. This total far exceeds the general gamma levels in the region of the badge, and therefore, was probably produced primarily by beta contamination of the badge. Note that many of the personnel involved in the early cleanup operations received large beta to gamma dose ratios, some as large as 15 to 1.

Attempts to account for the amount of uranium on the operating floor were unsuccessful. Shoe covers of personnel entering the building, for instance, picked up trace amounts of uranium. The only specific identifiable quantity of fuel recovered was in the form of several small pieces of spongy metal containing only two grams of uranium, these being found in the fan room. All the evidence indicates that fuel and fission products were rather finely divided and scattered throughout the operating room.

4.4 Excess Reactivity

The central control rod was bound in its shroud at a position corresponding to 20 ± 1/2 inches withdrawn from normal scram. The other four control blades were found bound essentially in their scram positions. Details of the collapsed central shroud and imprisoned rod are given in Section III-1.1. The rod was grasped by the shroud at the time of the first high pressure surge, which developed at or very near to the time of peak power during the burst, and no motion of the rod relative to the blade occurred thereafter. The 20 inch withdrawn position does not necessarily represent the exact maximum reactivity of the excursion. However, the time during which most of the energy was released was quite short, so that during this time the rod would have been able to move less than 1/2 inch as a result of any plausible forces applied external to the core (see the following section, III-4.5). Therefore the 20 inch position of withdrawal corresponds to the approximate upper limit of the reactivity of the excursion, taking into consideration that it is unlikely that the control blade was being inserted when seized.

* Note added in proof: Both these measurements are obviously crude, and are prone to underestimate the fission product release. The apparent inconsistency with the uranium inventory is the subject of continued work.

The SL-1 core was normally operated with all five control rods banked (equally withdrawn), and there is very little data from which to estimate the excess reactivity of the central rod withdrawn by itself in a cold clean reactor. A summary of existing pertinent critical position data taken within several months of the incident is given in Table III - 8 . These values had been obtained during reactor physics measurements. Cadmium strips had been added to two of the outer T- shrouds in November to enhance the reactor shutdown margin.

Table III- 8

Summary of Critical Positions and Rod Worths (ambient temperature, no xenon)

September, 1960 - before adding Cd strips:	
5-rod bank critical at	10.5 inches
central rod alone critical at	14.3 inches
After adding Cd strip - November, 1960	
5-rod bank critical at	12.0 inches
central rod alone critical at	not measured

Thus, the addition of the cadmium strips in two of the outer T-shrouds raised the clean, cold critical position of the banked rods from 10.5 to 12.0 inches.

The effect of this change in rod position on reactivity has been obtained by reference to the differential rod-worth curves of zero power experiment loadings [1] #19 and #45, which were identical loadings, each with one full boron strip on each of the forty elements. The incident core had uranium burnup, high boron burnup on the 1/2-strips and on the lower part of the full strips, with lesser boron burnup near the top of the full strips. By calculating the variation of thermal neutron leakage in the boxes defined by the control blades, it was concluded that the central rod's differential worth would have been approximately 20% higher in the highest burnup region of the incident core compared to loadings #19 and #45. Assuming approximately the same increase would apply to the banked rod-worth, the effect of moving the bank from 10.5 to 12.0 inches, near the region of maximum burnup, is calculated to be 3.2 dollars (ref. cited, Figure 26, P. 56 showing 1.8 dollars/inch in this region for loading #45). Thus, the cadmium strips added about 3.2 dollars to the shutdown margin.

The differential rod-worth curve for the central rod operating with the other rods fully inserted is shown in Figure III- 95 . The solid curve is the general shape of a differential worth curve for loading #45 (ref. cited, Figure 24 and Figure 25) normalized to two data points for the central rod with the others fully inserted (ibid, P. 44). The dashed curve is the approximate correction made for the half-strips and the burnup between the incident core and loading #45. Note that the peak of the curve has been shifted to a lower position in the core. From this curve, it is

[1] ALPR Zero Power Experiments On the Argonne Low Power, D.H. Shaftman, ANL 6078

found that the 14.3 inch critical position, before adding cadmium to the T-shrouds, is raised to 16.7 inches with the cadmium. Prompt critical is at 17.6 inches. The 20 inch position is worth 3.4 dollars or 2.4% Δk/k above delayed critical. Some representative reactor periods in this range of K-excess are listed in Table III-9 , using calculated lifetime of 6.1 x 10-5 seconds for the SL-1.

Table III-9

Reactivity (% Δ k/k)	Period (milliseconds)
1.7	6.0
1.9	5.0
2.0	4.5
2.2	4.0
2.4	3.5
2.7	3.0
3.6	2.0

Estimated reactivity at 20 inches - 2.4% Δk/k

The results given above for the critical position and worth of the 20-inch position for the central control rod are derived from very limited applicable data. In particular, the differential rod worth curve indicates a very large total worth for the central rod, though it is probably not completely valid to interpret the integral of this complete curve, covering such a large variation in reactivity, as being a true total rod worth. The curve does imply a high shutdown margin existed. The small correction for burnup (and the 1/2 boron strips), amounting to less than 20%, is not precise, but is not likely to be far enough in error to effect the results significantly. No correction was applied for the effect of the added cadmium in the T-shrouds on the worth of the central rod, an effect which would probably be positive. It is estimated that the effect of all the uncertainties is to make the reactivity corresponding to 20 inch withdrawal certain by about ± 0.3% ΔK standard deviation. Since the rod may not quite have been at 20 inches, and since some plate expansion effects would have occurred at the time the major shutdown mechanism of steam formation began (see Section IV-1.2), the representative period was between about 3.3 and five milliseconds, with a best value of four milliseconds.

Between the time that the Cd strips were added and the time of the incident, it is assumed that the critical position of the banked rods did not change significantly, at least in reference to the position uncertainty of a banked rod measurement (within 0.3 inch). The change due to normal burnup of the uranium and boron would have been small during this six week period. There is no evidence to indicate that any significant amount of boron strip material had been physically lost from the reactor during this period, (2) as can be shown by a careful study of the rod positions corrected for variations in xenon poison and steam void effect.

(2) H. Cahn, Combustion Engineering, Inc., - SL-1 Control Rod Positions, November — December, 1960; September 18, 1961.

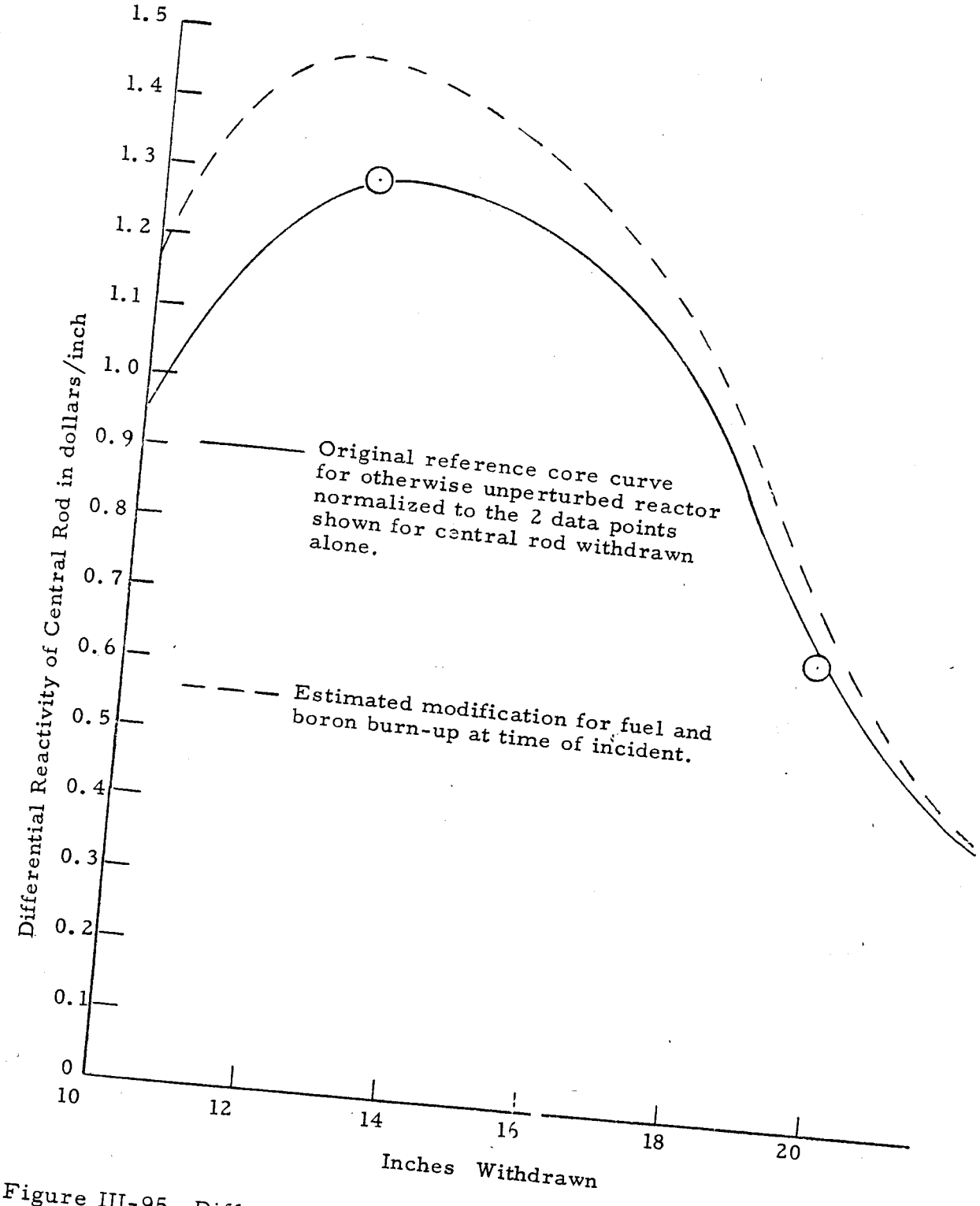

Figure III-95 Differential worth curve for central control blade with four blades completely inserted.

4.5 Central Control Rod Withdrawal

Motion of the central control blade from its inserted position, past the 16.7 inch critical position, and to the 20-inch withdrawn position must have been sufficiently rapid to permit the blade to reach the 20-inch position before significant steam was formed, about 1/10 second after delayed critical. As stated in Section III-2.3, the evidence will not support the hypothesis that the central control blade was ejected by a chemical explosion. The only known mechanism for getting the control blade to the 20-inch withdrawn position consistent with the physical evidence is manual withdrawal.

To evaluate the possibility of manual withdrawal of the rod, a mockup was made using a spare central control blade attached to the end of a control-rod and shield-plug mechanism, with the blade in a pool of water so as to simulate conditions of the incident (the blade was not enclosed in a shroud for the simulation). Using the actual "incident" handling tool, several different subjects withdraw the blade, under various conditions. The motion always commenced from the scram position or with the rod held up by a C-clamp, approximately three inches above the scram position.

A summary of the various conditions for which the subjects were told to expend maximum effort and the relative results obtained is shown in Table III-10

Table III-10

Manual Withdrawal of the Central Control Rod
With Maximum Effort

Conditions*	Average time from critical (16.7inches) to 20 inches	
1) C-clamp in place	49 m sec	
2) No C-clamp, rod resting on spring	46 m sec	375 m sec from fully inserted to 20 inches
3) No C-clamp, two men withdrawing rod	45 m sec	
4) Stuck rod, quickly released	56 m sec	
5) With C-clamp, Handling tool grasped at middle	77 m sec	Subject was unable to pull rod past 27 inches
6) With C-clamp, handling tool grasped at top	94 m sec	Subject was unable to pull rod past 22 inches

* Only one subject at a time pulled the rod. The handling tool was gripped near the bottom, unless otherwise noted.

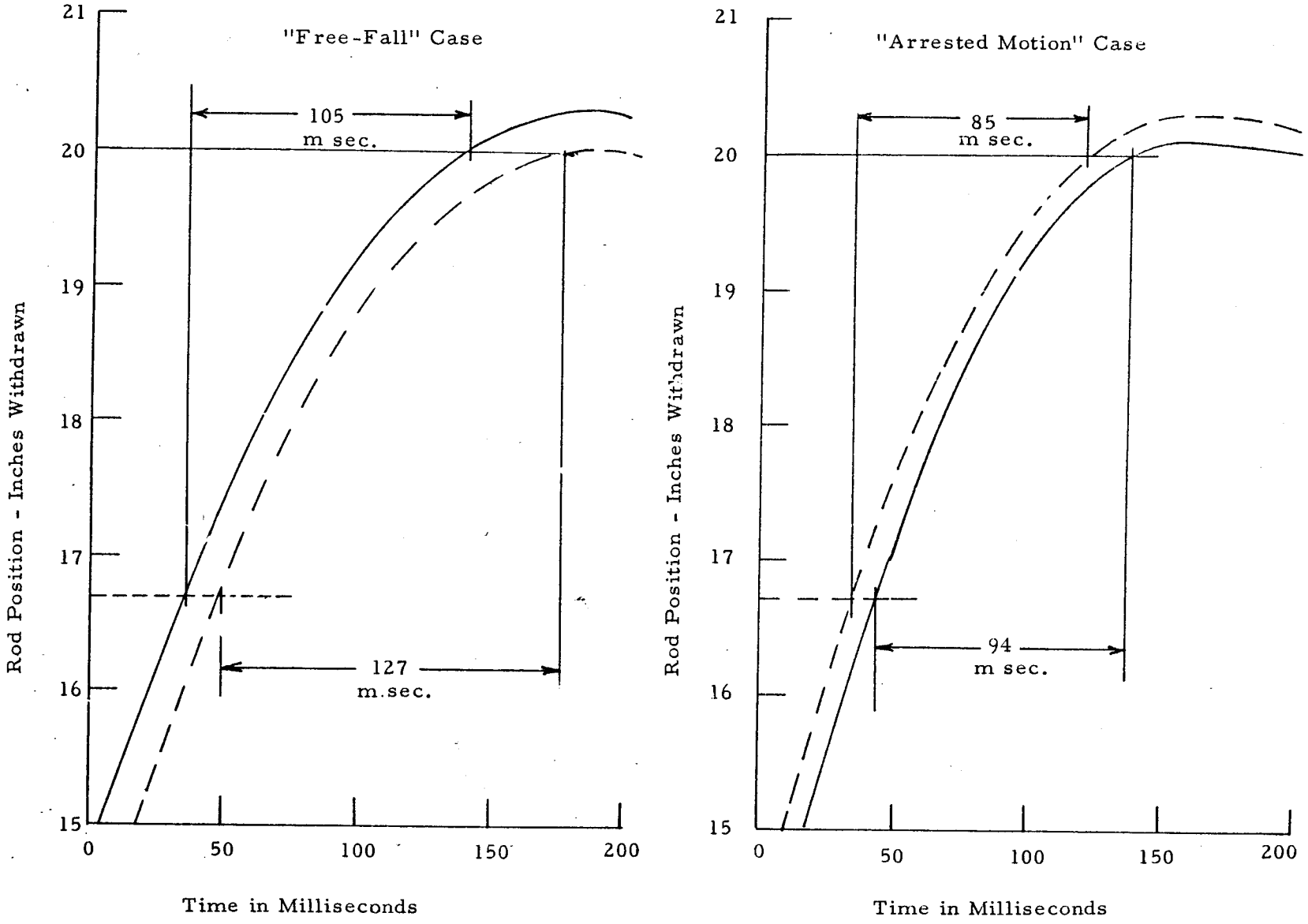

Figure III-96 Two experimental rod-withdrawal situations in which the rod was not pulled completely with maximum effort. Solid and dashed curves are results of two different tests.

As will be shown in the subsequent section, the control rod withdrawal times from critical to 20 inches of the order of 50 m sec are more than adequate to assure that the rod reaches the 20-inch position before steam is formed. The time differences between any of the first four cases, in which the handling tool was gripped near the bottom, are not significant. The less proficient gripping positions higher up on the handling tool resulted in significantly slower times of withdrawal.

Other motivations besides the expenditure of maximum effort to withdraw the rod as fast as possible were simulated. A "casual" but complete withdrawal of the rod averaged 75 m sec from the critical position to the 20-inch withdrawn position, about 60% longer than the time for maximum effort withdrawal.

A rapid pull, not followed through for complete rod withdrawal, might have caused the blade to rise to the vicinity of 20 inches, followed by a free fall trajectory. The data obtained for the simulation of such an event are presented in the left-hand graph in Figure III-96 . The blade would have been moving slowly near the 20 inch position, and the elapsed time from the critical position could have varied from the minimum possible 50 milliseconds to more than a hundred milliseconds, depending on the particular free fall trajectory. A curve within this range will certainly satisfy the excursion conditions rather accurately.

A rapid pull followed immediately by an attempt to stop the rod is shown in the right-hand graph of Figure III-96 . The subject would not have had time to respond to the occurrence of the nuclear excursion, but only to his realization that he should not have pulled the rod. This operation also provides considerable latitude in the possible time for the rod to move from the critical position to the 20-inch position, depending on the time at which the attempt was made to arrest the rod motion.

4.6 Reactivity Insertion Rate

To determine the ability of the various methods of manual withdrawal to produce the excursion, an analog simulation was set up on a G.E.D.A. Analog Computer. The computer circuitry for the problem and a more detailed discussion of the system is given in Appendix F . For the purpose of studying reactivity insertion rates, ramp rod-withdrawals of various speeds from critical (16.7 inches) to the 20 inch position were used, for which the reactivity insertion rate became a modified inverted parabolic section because of the decreasing worth of the rod near the higher withdrawn positions. The rod withdrawal was limited to 20 inches. The three shortest lived groups of delayed neutrons were used. The reactor power level at critical was generally set at about 300 to 400 watts. The power was integrated and a portion fed back for reactivity compensation due to plate expansion. The excursion was shut off rather abruptly by a large feedback reactivity proportional to the generated energy, at such a time that the total accumulated energy would be 130 Mw-sec.

Typical results of the simulation are shown in Figures III-97 , 98 , and 99 . Each figure contains the analog computer plot of: 1) reactivity inserted, 2) log of power, and 3) inverse period. Figure III-97 contains the results of the 75 millisecond ramp (16.7 inches to 20 inches withdrawal) which approximates the casual rod withdrawal rate. The rod reached the 20-inch position (actually set for 2.5% $\Delta K/K$ in the computer) approximately 30 milliseconds before the peak of the excursion, at which point the computer amplifier maintained the 2.5% Δ K/K inserted reactivity until the end of the excursion. Had the rod withdrawal not been terminated at 20 inches but continued on the same ramp, it would have reached 21.2 inches (including consideration for the faster period) corresponding to 2.9% Δ K/K by the time of peak power. This result is outside of the standard deviation of the reactivity estimates.

Figure III-98 shows the results of the 100 millisecond ramp, which brought the rod to the 20-inch position 13 milliseconds before peak power. This result is not unreasonable to within the error of the 20-inch reactivity estimate. Figure III-99 , showing the 125 millisecond ramp, found the rod just reaching the 20-inch position at peak power, and therefore is the best fit. The results indicate that the steady ramp rod withdrawal rate that best fits the conditions of the excursion is much slower than even the "casual" rod withdrawal rate. Note that a lower starting power at critical (below the nominal 400 watts used) makes the casual rod withdrawal rate an even worse fit for the excursion. The "maximum effort" rate is obviously much too fast. Had it been employed, the rod would have gone far past the 20-inch position.

Based on the reactivity estimates for the 20-inch position, which in themselves are subject to the uncertainty previously discussed, the analog simulation indicates there is little doubt that the central control rod could be withdrawn rapidly enough to produce the excursion. In fact, the results indicate that even a casual (average) effort to completely withdraw the rod exceeds that rate consistent with the known and estimated conditions of the excursion. Comparison of these rates is shown in Figure III-100.

However, the rod withdrawal curves corresponding to either the "free fall" case or the "arrested motion" case (Figure III-96 Sec. III-4.5) can, if properly selected, produce the excursion and permit the rod to be at or very near to the 20-inch position at the time of peak power. The reactivity insertions which these create insert the major portion of the total reactivity well in advance of peak power, and thus amount to essentially step insertions of reactivity.

In fact, a variety of ways (such as gripping the handling tool near the top, pulling of a stuck rod, etc.) exist in which the rod could be withdrawn manually to the observed 20-inch position in the time interval indicated by the analysis of the reactor kinetics. There seems to be no way of choosing between these various ways, since all of them can result in the same final reactor period.

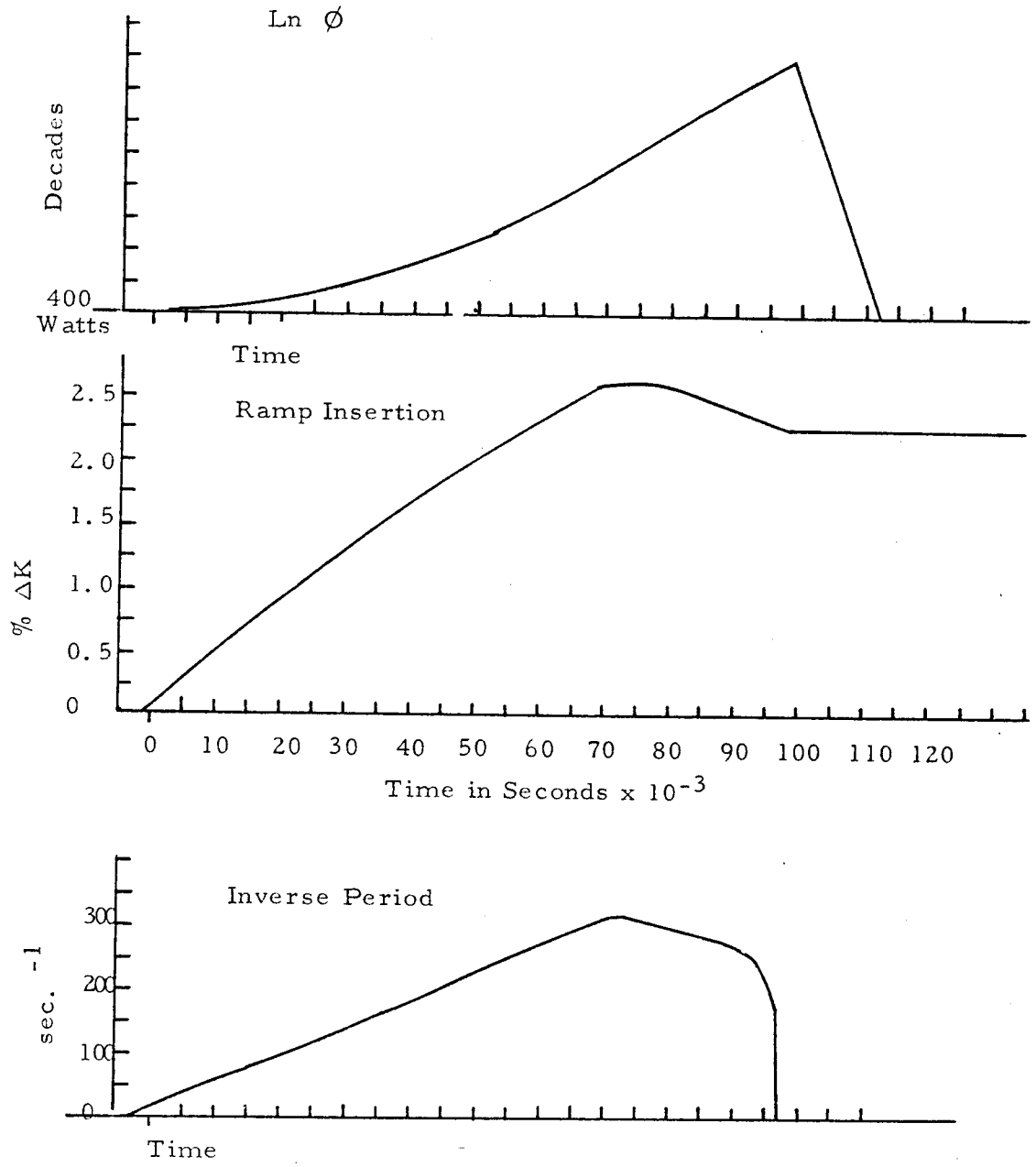

Figure III-97 Analog computer traces of 75 millisecond rod-withdrawal ramp (from critical to 20 inches)

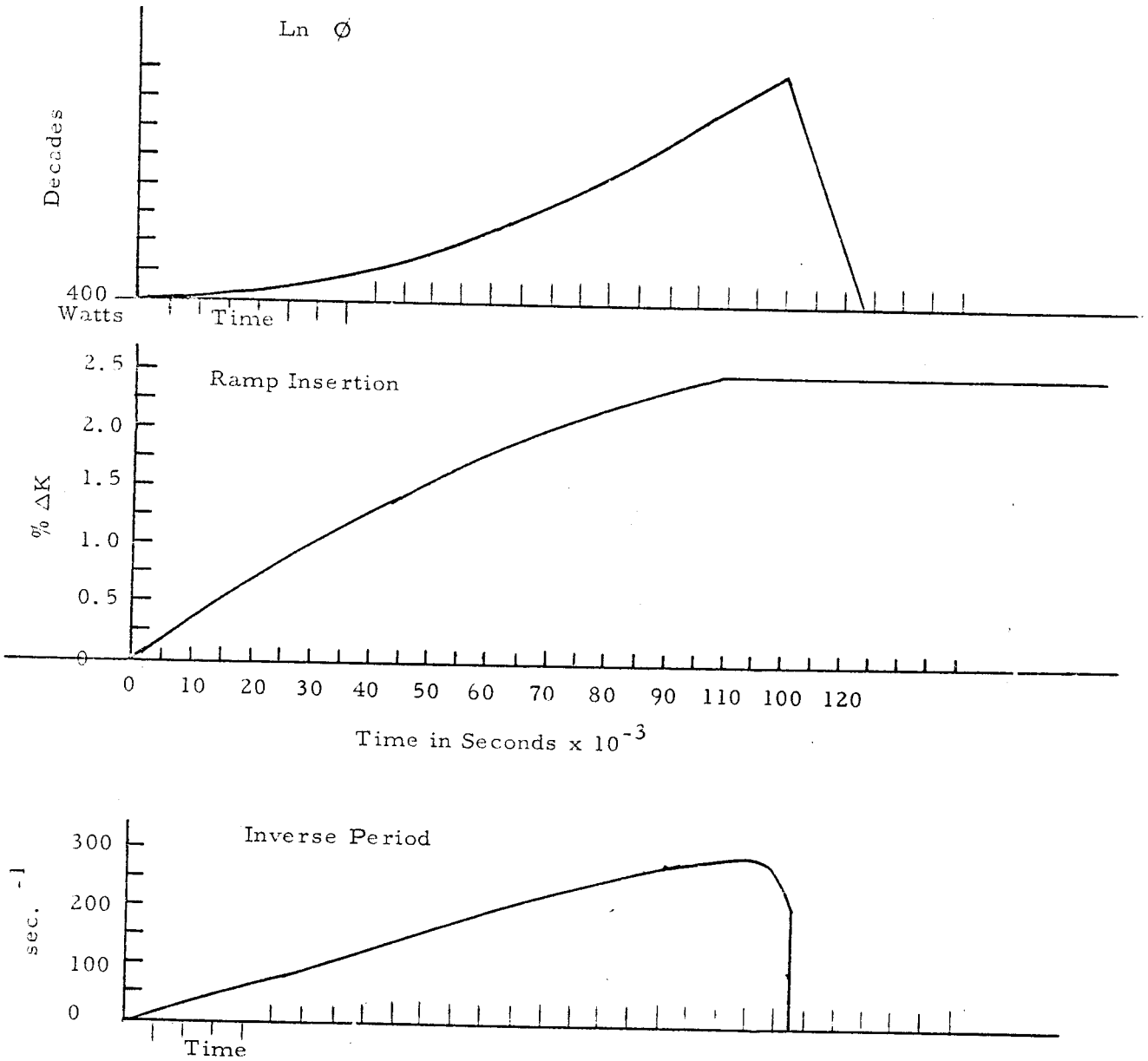

Figure III-98 Analog computer traces of 100 millisecond rod-withdrawal ramp (from critical to 20 inches)

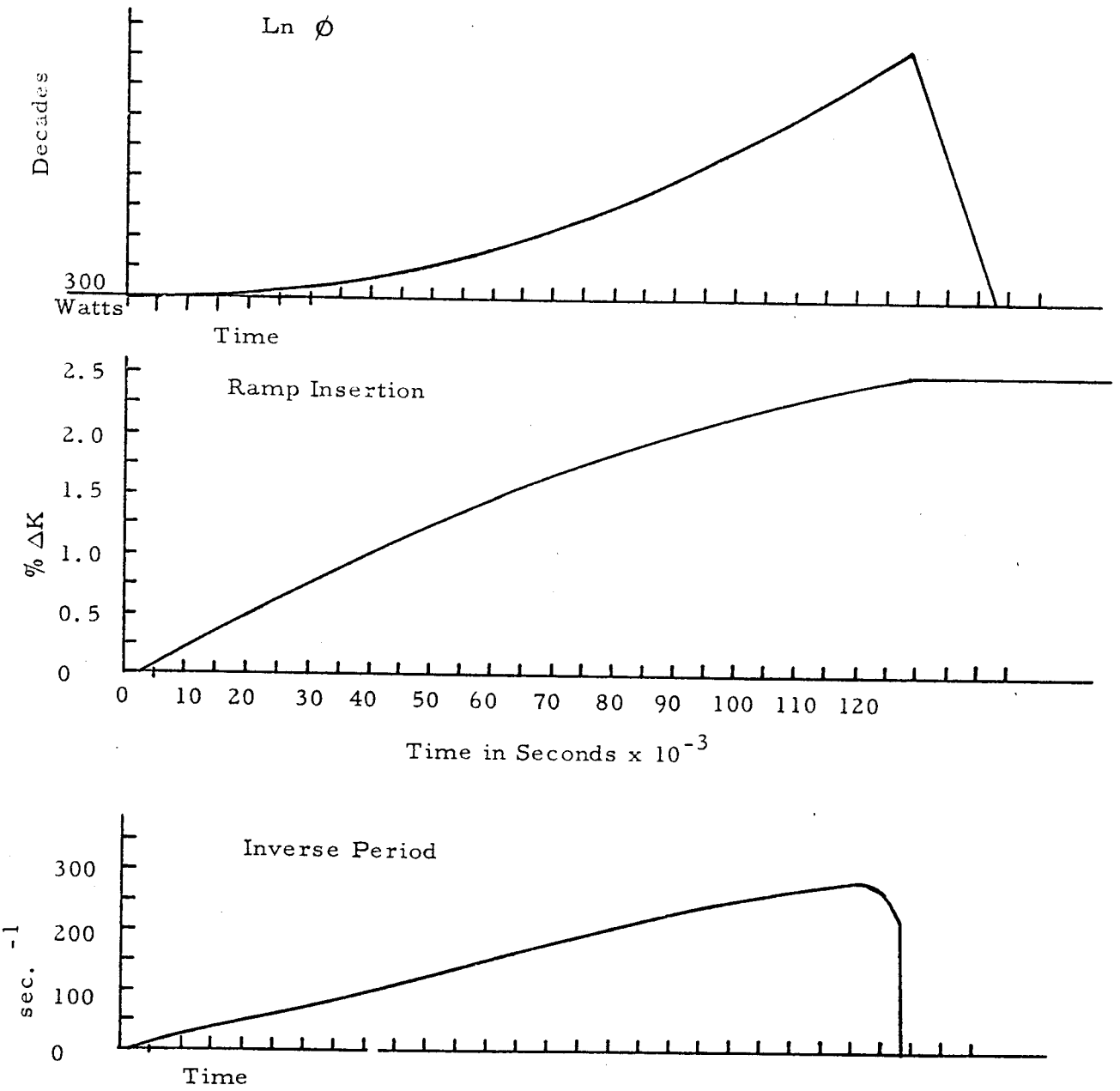

Figure III-99 Analog computer traces of 125 millisecond rod-withdrawal ramp (critical to 20 inches)

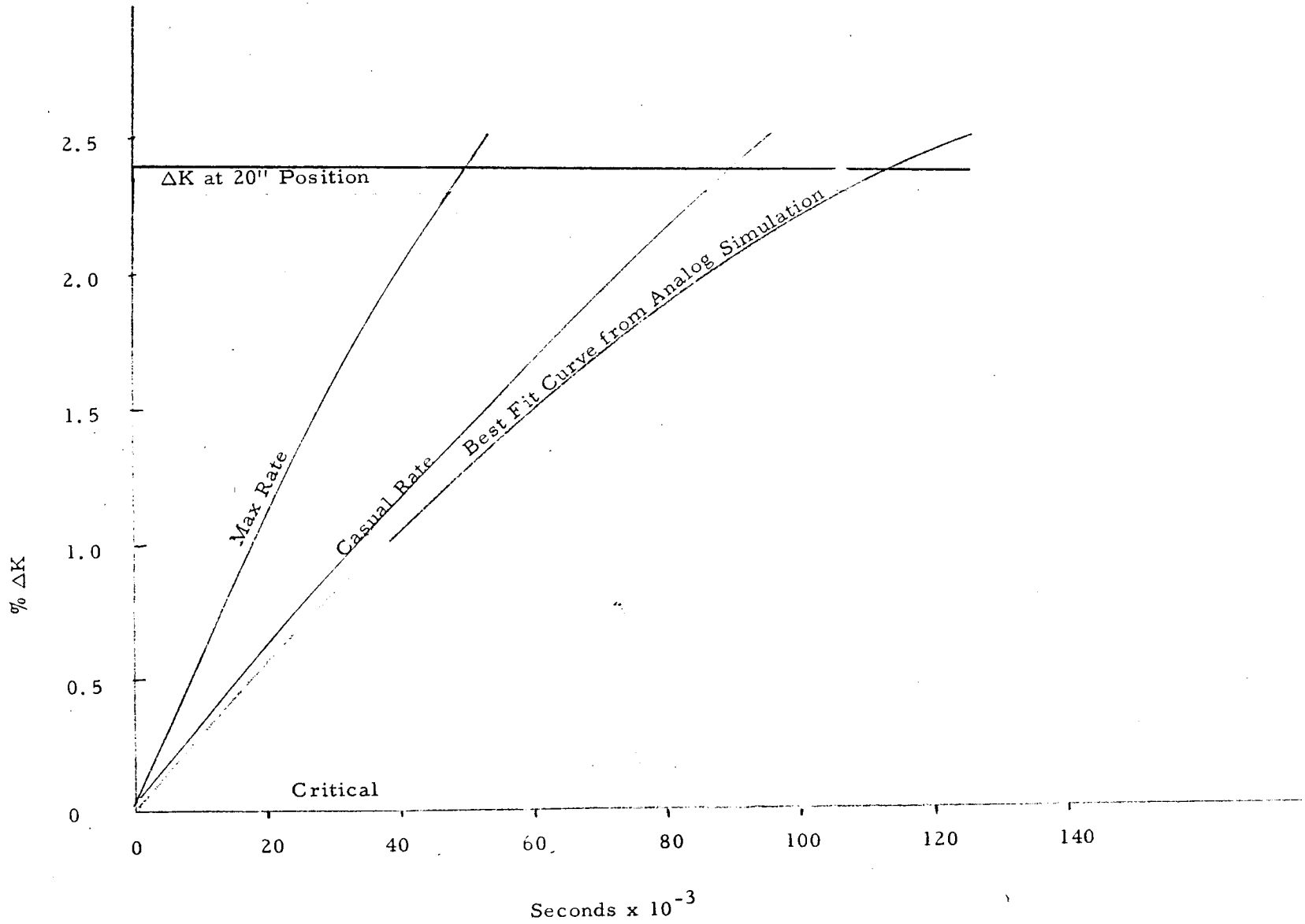

Figure III-100 Comparison on maximum and "casual" rod-withdrawal rates with the best fit obtained on the analog computer.

4.7 Critical Experiment Results

The experimental arrangement for the critical experiment on the post-incident core in the Hot Shop is described in Section II-2.6. The experiment was intended to determine if the destroyed core was capable of sustaining a chain reaction, or if not, how close to criticality it was. The possibility of a subsequent excursion following the initial excursion would have explained the high activation on the reactor operating floor. Since boron oxide from the reactor head had found its way into the vessel, it may have contributed ultimately to ending the sustained reaction, as could have either the loss of water moderator, loss of fuel, or the geometrical deformation of the core. Therefore, it was decided to attempt to wash out any boron compound deposits during the course of the critical experiment, without, however, distrubing metallic boron present in the poison strips.

During the first and last fillings with water and the three intermediate fillings with dilute acetic acid, no total multiplication effect was observed on any of the three scintillation chambers.

In each case the counters did show the normal increase in count rate due to moderation of source neutrons as the water moved between the source and the counter. Each filling removed some boron compound from the core and pressure vessel, for a total boron content removal of about 150 grams for the five fillings. The multiplication curves for successive fillings showed no significant difference which could be attributed to the removal of boron. When the reactor was disassembled, very little boron was found on the active fuel plates, apparently less than one gram on the total plate surface area.

The multiplication curves for the counter located furthest below the core are shown in Figure III-101. The major cause of the decreasing count rate with increasing water height is merely the attenuation of the water between the counter and source, and subsequently the shielding of the scattered source neutrons by the water above the source. It was completely impractical to remove just the fuel from the core and determine the overall attenuation created by filling the tank, pressure vessel, and core structure with water. The cadmium in the control blades certainly had a pronounced effect on the attenuation observed by the counters. However, the empty critical experiment tank was filled with water with source and counters in place in an effort to estimate the attenuating effect of the rising water height in the critical experiment configuration.

In the region from water level of 45 inches above the bottom of the critical experiment tank (where some fuel could have been lying on top of the bottom support structure) to the 58 or 60 inch level, the slope of the actual critical experiment multiplication curves was decidedly less than the slope of the "empty tank" multiplication curve. Above and below these levels, the two types of curves have similar slopes. This general appearance of the curves was observed with all the counters. However, since the #2 counter

was 21 inches below the bottom of the fuel in the intact outer elements, and about 18 inches below the cadmium, this counter was least influenced by the presence of the cadmium control blades. It was also least influenced by scattered neutrons from the source. Therefore, the difference between the slopes of the curves with the reactor in place and of the "empty tank" curve for this counter is due, in part, to a multiplication effect of the fuel in the core's central region, which was largely concentrated below the 60 inch level. From this data, a crude estimate of the multiplication factor of the reactor was obtained. The core, when full, had a k-effective of about 0.6. This is not to be construed as an accurate number, but only as an indication of how far from criticality the core was. Some cobalt foils had been dropped into the core and were allowed to remain there throughout the critical experiment. When removed, the foils showed a total thermal flux of 5×10^{10} n/cm^2. This result is an order of magnitude above what was expected from the source in a non-multiplying medium during the time it was surrounded by water moderater, as well as for the time it was unmoderated. Therefore, it appears that these foils may have been located near a concentration of fuel where significant local multiplication was occurring.

The post-incident critical experiment showed that the reactor was grossly subcritical and that this condition was apparently independent of the presence or absence of boron in the core region.

In view of the other facts discussed in previous sections, it appears that the subcritical condition was due in part to the radial displacement of the core and the resulting increase in water volume fraction, resulting in over moderation, i.e. poisoning. It was also subsequently found that nearly 50% of the fuel from the center section of the reactor was missing, resulting in a very low thermal utilization for this region. Furthermore, the intimate proximity of the collapsed cadmium control blades with the outer 24 elements made these elements very ineffective contributors to the overall multiplication of the core. In general, overall conditions in the core were not conducive to creating neutron multiplication.

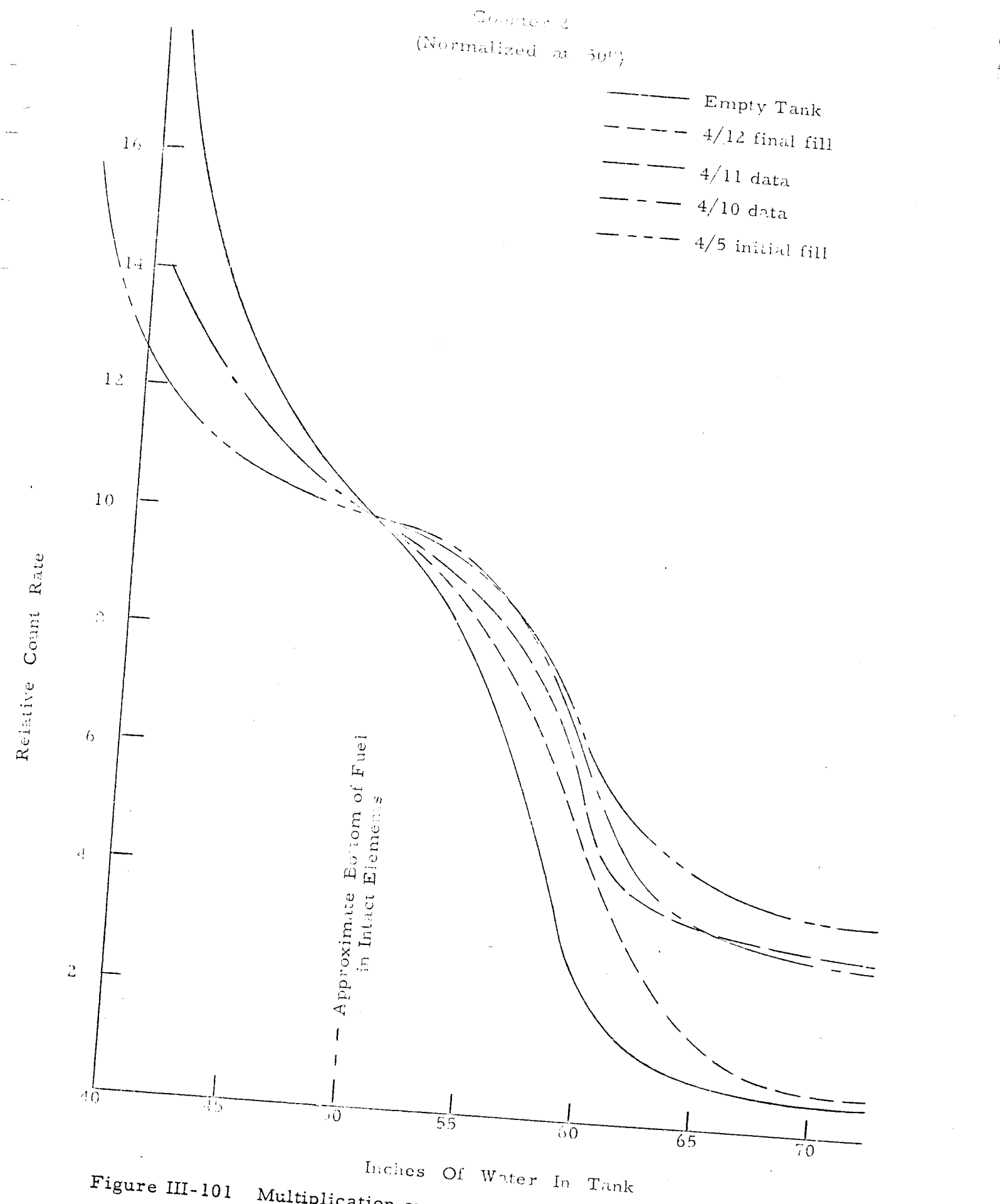

Figure III-101 Multiplication curves obtained during post-incident critical experiment.

IV- ANALYSIS AND CONCLUSIONS

1. Nuclear Excursion

1.1 Initiating Mechanism

The key fact determined in the investigation was that the central control rod was found bound in its shroud at the 20 inch withdrawn position, as described in Section III-1.1 and 1.8. The reactivity associated with this position, while not known precisely for the conditions existing, has been estimated in Section III-4.4 to be 2.4% Δ K/K. This is enough reactivity to account for the observed damage to the core. It is not necessary to postulate any additional mechanism to add reactivity, for example by loss of boron strips, although the condition of the core after the accident precludes direct determination of the location of the strips from the center of the reactor. To explain the accident it is, therefore, necessary and sufficient to explain how the central rod got to the 20-inch position.

One mechanism has been discussed in Sections III, 4.5 and 4.6, namely, manual withdrawal of the rod. It was shown in that section that the rod could be withdrawn manually in a variety of ways to produce the observed effects. In addition, the position of the bodies indicates that two men were standing on the reactor head at the time of the accident. Furthermore, the presence of the nut, washer, and handling tool on the central control rack at the time of the accident, and the probable presence of the C-clamp on the rack, make it appear that the operation being carried out at the instant of the accident was to raise the central rod manually a sufficient amount to remove the C-clamp. No attempt has been made to suggest possible motivations for pulling the rod 20 inches instead of 2.

One alternative mechanism which has been proposed is the use of chemical explosives in or under the core. Explosives experts from the Standford Research Institute examined the core. Their report, given in full in Appendix C, makes it clear that chemical explosives were not the agent responsible for the withdrawal of the central rod.

A second possibility, sometimes mentioned, is concerned with the explosion of hydrogen formed by the radiolytic decomposition of water. Experimental information quoted in the literature indicates that it would be credible for sufficient hydrogen gas to produce an explosion to have been formed in several hours time by the fission product activity present in the core. The explosion of a hydrogen-air mixture between the pressure vessel head and the top of the water above the core would have created a uniformly high pressure in this region. The five loose shield plugs would have then been ejected. It is known that nuts and washers were in place on the racks of all five of these control rod mechanisms at the time of the incident. Ejection of a shield plug would then result in the lifting of the control blade. It is inconceivable that only the central control blade, the heaviest of the five, would have been lifted by the hydrogen explosion. Since the other blades were found in their normal scram positions after the incident, it

is immediately apparent that the initiating mechanism was not a hydrogen explosion or any other explosion in the space between the water and the vessel head. (Note, the black coating on the extension rods, originally attributed to a high temperature reaction, was identified as chromous acid which accrues during long operation in a steam atmosphere. The product of a high temperature reaction produced in a laboratory test was a green coating of chromium oxide.)

In conclusion, the various proposed methods for initiating the mechanism without requiring manual withdrawal of the central control rod, are definitely inconsistent with the facts. The motivation for withdrawing the rod is not known, but the analysis indicates that the action was not a maximum effort attempt to withdraw the rod completely (reference Section III-4.6.).

2 Power Behavior

Since there was no direct record of the reactor power behavior during the excursion, a correlative method has been used to obtain an estimated power behavior using the results of SPERT experiments and analysis (the appropriate references cited in the text refer to SPERT documents).

The burst approximation equation for a reactor transient given in SPERT Quarterly Report (July-September, 1958, IDO 16512) assumes the power burst can be represented by a two term exponential expression. It has been decided to adopt this model for the SL-1 to facilitate the calculation of temperature distributions.

The two-term power burst equation is:

$$\text{I} \qquad \phi(t) = \phi(0)\left[r \exp(\alpha t) - (r-1) \exp\left(\frac{r}{r-1} \alpha t\right)\right]$$

where:

$\phi(0)$ = measured peak power

α = [reactor period]$^{-1}$

$\phi x(0)$ = extrapolated peak power

$r = \dfrac{\phi x(0)}{\phi(0)}$

Peak power occurs at $t = 0$

Using equation I, the total energy, E (T), energy in the water, E (W), and energy in the plate, E(P), becomes:

II $$E(T) = \frac{\phi(0)}{\alpha}\left[r \exp(\alpha t) - \frac{(r-1)^2}{r} \exp\left(\frac{r}{r-1} \alpha t\right)\right]$$

III $$Ew(T) = \frac{AC\rho\sqrt{d}\ \phi(0)}{\overline{H}\ \alpha^{1.5}}\left[r \exp(\alpha t) - \frac{(r-1)^{2.5}}{r^{1.5}} \cdot \exp\left(\frac{r}{r-1} \alpha t\right)\right]$$

IV $$Ep = E(T) - \frac{AC\ d\ \phi(0)}{\overline{H}\ \alpha^{1.5}}\left[r \exp(\alpha t) - \frac{(r-1)^{2.5}}{r^{1.5}} \cdot \exp\left(\frac{r}{r-1} \alpha t\right)\right]$$

where:

A = heat transfer area

C = specific heat of water

ρ = density of water

H = average effective heat capacity of core

$d = \frac{K}{\rho C}$ = the diffusivity of water

K = the conductivity of water

The two term approximation is limited in its application to sharp power bursts (short periods) (IDO-16636, by R. W. Garner). The value of r which best seems to fit the SPERT power burst shapes is r = 1.5 (r = 1 is a sawtooth; r = ∞ is a symmetrical burst). The resulting two-term exponential usually has a more rapid drop from peak back to zero power than was generally observed with the SPERT and BORAX non-destructive tests. However, this difference is actually believed to exist between these tests and the SL-1 excursion (see Section V-3.1).

The remaining terms in equation I through IV are self explanatory, except the value of $\overline{H}$. This was calculated using the following: (Ref. IDO-16489, page 75);

$$\overline{H} = Fw\ Hw + Fs\ Hs + Fp\ Hp;$$

where:

Hw = total heat capacity of water

Hs = total heat capacity of aluminum

Hp = total heat capacity of fuel plates

$Fw = \frac{lw}{d_w}$ = fraction of moderator heated

$Fs = \frac{ls}{d_s}$ = fraction of structure heated

F_p = ratio of actual heat content of fuel plate to that indicated by surface temperature

d_w = half thickness of water channel

d_s = half thickness of structural aluminum fuel plate

The above equations and assumptions were used along with the data available from the reactor designers to shed some further light on the incident.

From the design information and the position of the central control rod after the incident, the reactivity insertion was obtained. From this the associated period could be determined. The flux wires gave the total integrated power and the energy distribution. Using this information and the above stated assumptions, the values shown in Table IV-1 were calculated from equations I through IV. Of particular significance is the high peak power (19,000 Mw) and the small amount of energy transferred from the plates to the water up to the peak of the excursion (0.92 Mw sec). In contrast, approximately eight times as much energy is deposited uniformly in the water by nuclear heating.

TABLE IV-1

SL-1 Excursion Values Calculated from SPERT Model

α sec^{-1}	t_1^* sec.	$\phi(0)$ Mw	E (0) Mw-sec	$\overline{H}$ cal/^oC	EW (0) Mw-sec	EP (0) Mw-sec	EM[1] Mw-sec	Eg[2] Mw-sec
250	2.2x 10-3	19000	100 Mw-sec	5.39 x 10^4	0.92	99	45	78

$^*t_1$ = time at end of excursion. $t = 0$ is time of peak power

(1) EM = energy required to bring center 16 elements to 640^oC (melting temperature)

(2) Eg = energy generated by center 16 elements.

The energy generated in the center 16 elements was 60% of the total energy generated in the core.

1.3 Shutdown Mechanisms

The primary shutdown mechanism in the SL-1 (short of fuel loss or geometrical deformation) is moderator displacement, which can occur in four ways.

1. Expansion of fuel plates due to temperature increase - Reported void coefficients for the SL-1 are:

   a. -1 x 10-4% $\Delta K/cm^3$ for average steam void[1]

   b. -6 x 10-4% $\Delta K/cm^3$ for void throughout central region of a center element[2]

   The fuel plate expansion effect, at peak power, would be a maximum of about -0.5% ΔK, but would more likely be around the -0.1% ΔK given by the average steam void coefficient, since plate expansion is a similar "average" effect.

2. Moderator expansion due to both nuclear heating of the water and transfer of heat from the plates to the water - Both create "average" void effects. At the peak of the burst, approximately 6 Mw-sec. of energy will be in the water, creating a -0.7% ΔK effect.

(1) IDO 19300 - May 15, 1961 - SL-1 Report

(2) D. H. Shaftman, ANL, - private communication

3. Bubble Dilation - Recently Zivi[3] has demonstrated that dilation of adsorbed bubbles on the surface of fuel plates will precede boiling and insert a small amount of negative reactivity into the system. The total effect of bubble dilation is about -0.1% ΔK.

4. Steam Production - This process, under transient conditions from a non-boiling state, is little understood. However, some of the work at the University of California on void volume development in transient boiling of water[4] presents some helpful points.

The void growth due to steam formation occurs at a time when sufficient heat has been transferred to the water to bring it to the saturation temperature. However, the temperature measurement that is made in most systems is not the water temperature but the plate surface temperature. This problem, along with the predicted temperature distribution in the water under transient conditions shown in Section IV-1.4, Figure IV-2, creates some difficulty in defining a water volume, and an average temperature from which to compute steam formation. Complicating the problem further is the heat transfer coefficient after steam formation has begun. The curves of temperature and void formation given in reference (4) are produced by an exponential power source. The data taken from the above was used to predict a delay time. The delay time from plate saturation temperature until the beginning of void volume formation appeared to become asymptotic for short periods; approaching a value of approximately 3 milliseconds.

SPERT data[5] for very short periods (α greater than 150 seconds^{-1}) was examined for SPERT I aluminum cores "A" and "B" and the stainless steel core in order to obtain further information on the delay in void formation. From the data, it has been concluded that there will be a temperature overshoot, the amount depending upon the period, and that the delay time between plate-surface saturation temperature and the beginning of boiling is, for very short periods, approximately three milliseconds.

This temperature overshoot could cause two effects. The first is superheated water. The amount of superheat would, of course, depend on the period, and may allow an initial surge in the void volume formation. This is indicated in the curves contained in reference (4). However, of more significance is the effect of fuel plate temperature overshoot. If the period is sufficiently short, the amount of energy generated in the three millisecond delay may be sufficient to produce internal plate melt. This is indicated by the temperature distributions in Section IV-1.4. Since the center temperature is approximately 4.5 times the surface temperature, a 100°C overshoot would produce melt in the center region before steam would be formed on the surface of the plates.

(3) S.M. Zivi - Trans. of Amer. Nuc. Socl, Vol. 5, No. 1, p. 161.
(4) V.E. Schrock, et al, Series 163, Issue #2, January, 1961.
(5) Private communication - courtesy of R.W. Miller, G.F. Brockett, E. Feinauer, - Phillips Petroleum Company.

In summary, it appears as though there is a fixed time delay between saturation temperature and the beginning of void formation. This delay has been interpreted to be approximately 3×10^{-3} seconds for reactor periods less than 10 milliseconds. The delay produces problems in two areas. It delays the formation of void to produce shutdown, and it allows internal plate temperatures to rise to very high values.

1.4 Temperature Distribution (Fuel Plate)

Fuel plate temperature distribution as a function of time plays an important role in the shutdown mechanism postulated for the SL-1 incident. Since the exact transient power behavior is not known, it is not possible to accurately determine the plate temperature distributions. However, the two term burst discussed in Section IV-1.2 approximates the actual burst. Using this two term approximation the following equations were derived to approximate the temperature distribution.

I $$\theta_1 \text{ (meat temp.)} = \frac{Qo}{\alpha \rho c} \left[1 - \frac{D \cosh \mu_1 x}{D \cosh \mu_1 a + \frac{K_1 \mu_1}{K_2 \mu_2'} \sinh \mu_1 a} \right] e^{\alpha t}$$

$$- \frac{1}{9} \frac{Qo}{\alpha \rho c} \left[1 - \frac{D' \cosh \mu_1' x}{D' \cosh \mu_1' a + \frac{K_1 \mu_1'}{K_2 \mu_2'} \sinh \mu_1' a} \right] e^{3\alpha t}$$

II $$\theta_2 \text{ (clad temp.)} = \frac{Qo}{\alpha \rho c} \frac{K_1 \mu_1}{K_2 \mu_2} \sinh \mu_1 a$$

$$x \left[\frac{\cosh \mu_2 (x-a) - D \sinh \mu_2 (x-a)}{D \cosh \mu_1 a + \frac{K_1 \mu_1}{K_2 \mu_2} \sinh \mu_1 a} \right] e^{\alpha t}$$

$$- \frac{1}{9} \frac{Qo}{\alpha \rho c} \frac{K_1 \mu_1'}{K_2 \mu_2'} \sinh \mu_1' a$$

$$x \left[\frac{\cosh \mu_2' (x-a) - D' \sinh \mu_2' (x-a)}{D' \cosh \mu_1' a + \frac{K_1 \mu_1'}{K_2 \mu_2'} \sinh \mu_1' a} \right] e^{3\alpha t}$$

where:

$$D = \frac{\frac{K_2\mu_2}{K_3\mu_3}\sinh \mu_2 (b-a) + \cosh \mu_2 (b-a)}{\frac{K_2\mu_2}{K_3\mu_3}\cosh \mu_2 (b-a) + \sinh \mu_2 (b-a)}$$

$$D' = \frac{\frac{K_2\mu_2'}{K_3\mu_3'}\sinh \mu_2' (b-a) + \cosh \mu_2' (b-a)}{\frac{K_2\mu_2'}{K_3\mu_3'}\cosh \mu_2' (b-a) + \sinh \mu_2' (b-a)}$$

a = half thickness of meat

b = thickness of clad

K_1 = conductivity of meat

K_2 = conductivity of clad

K_3 = conductivity of water

$\mu = \sqrt{\frac{\alpha \rho c}{K}}$, and $\mu' = \sqrt{\frac{3\alpha \rho c}{K}}$ for the particular medium in question,

where:

ρ = density

c = specific heat

From the above equations and the energy density given by the flux wire analysis, the temperature distributions shown in Figures IV-1, 2, and 3 were calculated for a four millisecond reactor period (α = 250). Each figure shows the comparison between the maximum flux region and the "threshold of destruction" region. Figure IV-1 shows the temperature distribution four milliseconds (one period) before peak power, Figure IV-2 at the peak, and Figure IV-3 at the end of the excursion. The results are not exact, for there was no provision in the calculations to account for the constant temperature during the melting process (640°C).

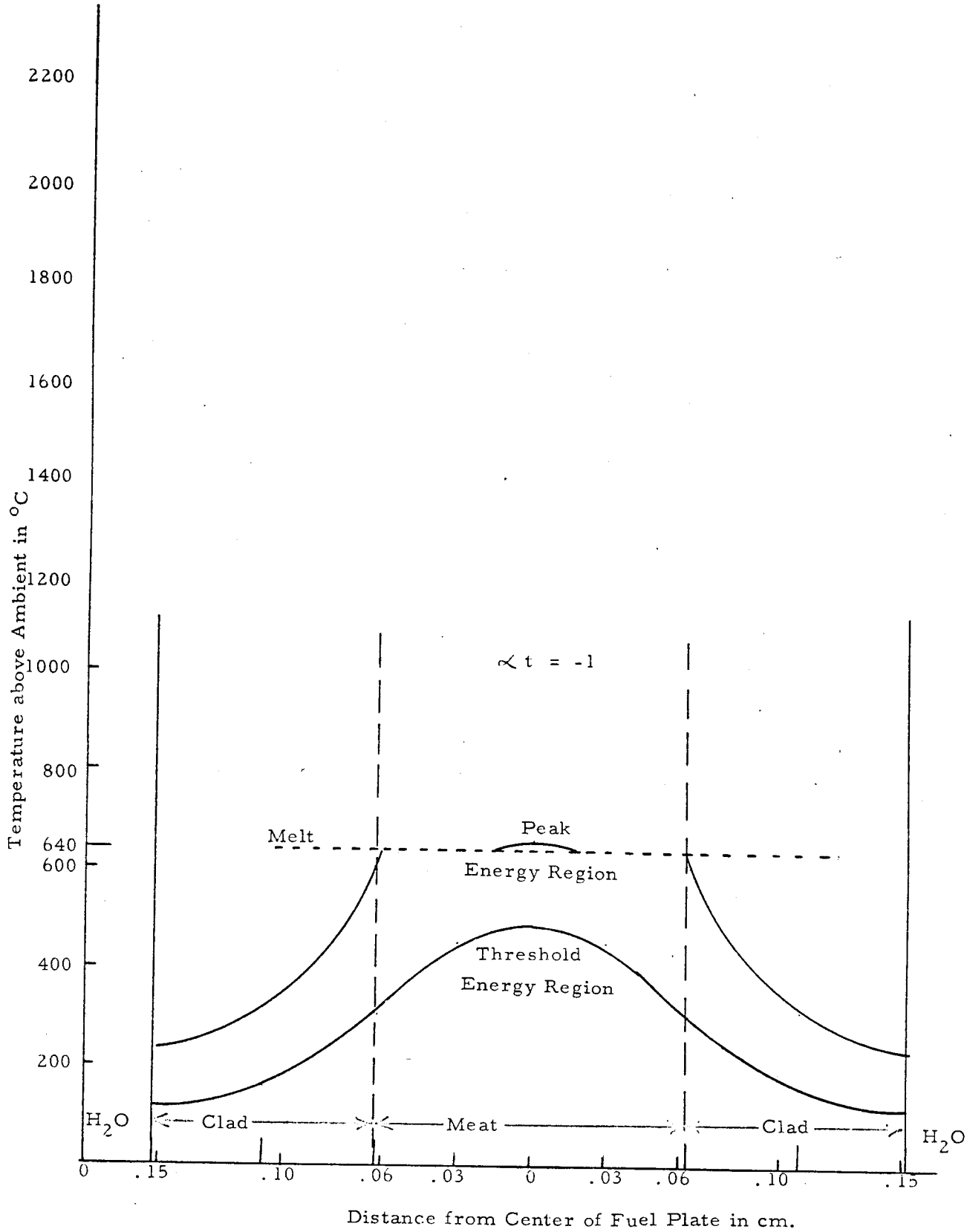

Figure IV-1- Temperature distribution in fuel plate, for 4 m sec transient, 4 m sec before peak power, for both peak energy density region and "threshold of destruction" region

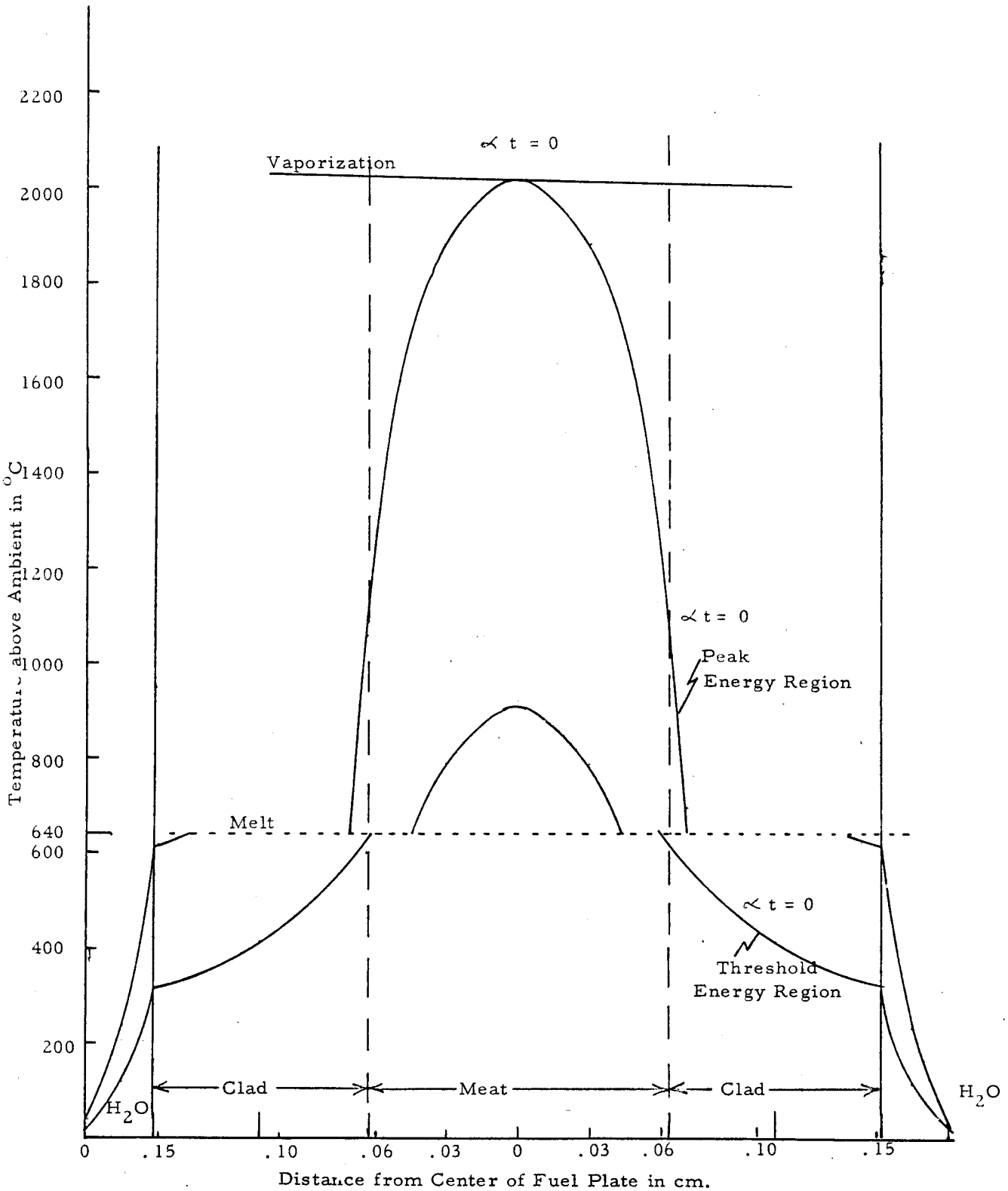

Figure IV-2- Temperature distribution in fuel plate, for 4 m sec transient, at time of peak power, for both peak energy density region and "threshold of destruction" region.

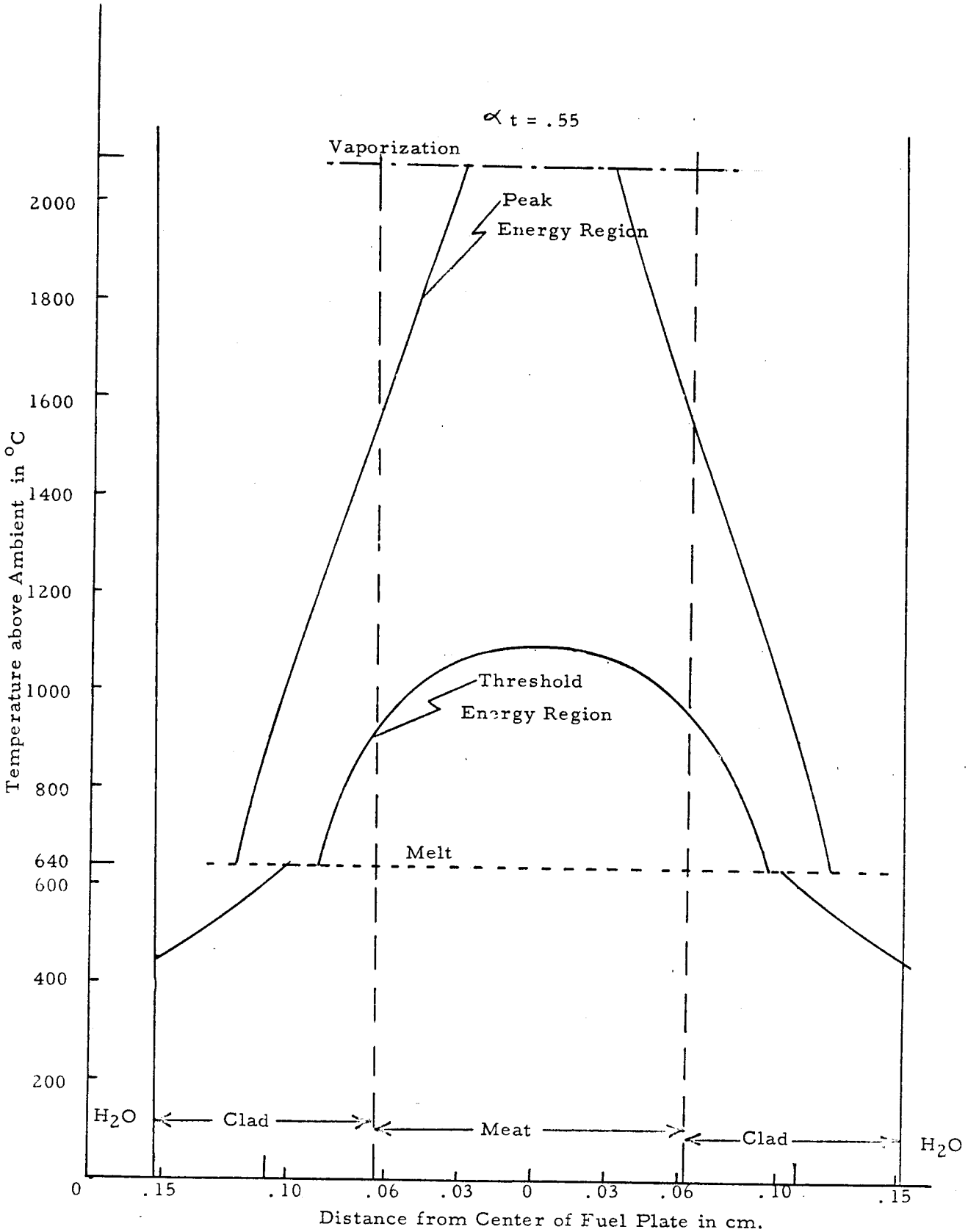

Figure IV-3- Temperature distribution in fuel plate, for 4 m sec transient, at end of excursion, for both peak energy density region and "threshold of destruction" region.

The highest energy density region just reached vaporization in the meat center at peak power. Thus a considerable potential existed to cause the explosive void formation and the resultant self-destruction.

The cladding surface in the "threshold of destruction" region was well below melting at peak power and only 490°C at the end of the excursion. The energy density in this region is just sufficient to melt the entire plate thickness. Since temperature equalization will occur quite rapidly (in a few milliseconds) after the end of heat generation, the cladding surface temperature must be significantly below melting at this time so that while the temperature is being equalized, sufficient heat can be removed to avoid destruction of the entire plate. Though a positive quantitative statement is not possible without more heat transfer information for transient conditions, it seems that the temperature distributions for a four millisecond transient are consistent with the observed core damage.

The temperatures at both the surface of the clad and the center of the meat are given at both peak power and the end of the excursion for three different transients in Table IV-2 below. These temperature distributions show that the five-millisecond period is too slow, permitting the cladding surface temperature to reach melting in the "threshold of destruction" region by the end of the prompt nuclear energy release. There is no latitude to allow for "drift" of this temperature up to melting during the temperature equalization process, while some heat is being removed from the plates. Thus, the five-millisecond "threshold of destruction" should have extended into a lower energy density region than was observed. The three-millisecond period resulted in temperature distributions that brought the center-of-meat temperature to vaporization (2060°C) by the end of the excursion in nearly 20% of the center section of the core. It is believed that such a large region of vaporization would have created much more metal-water reaction than seems to have occurred (see Section III-2.5 and IV-3.2).

Thus, it appears that there is sufficient evidence to conclude that the five-millisecond temperature distributions are such that this period is too slow to acccunt for the observed damage to the core. The three-millisecond period seems to be so fast that it would have vaporized more of the meat than one would assume occurred, on the basis of presently available information. The four-millisecond transient, however, creates temperature distributions which apparently account for the observed core damage. This period also is consistent with the estimates of the excess reactivity with the central control rod at the 20-inch position (Section III-4.4), with due consideration for the minor effects of plate expansion, moderator heating, and other reactivity compensating effects occurring before steam formation.

TABLE IV-2

Temperatures in SL-1 Fuel Plate in °C (above ambient) for Different Reactor Transient Periods

	3m sec Period	4m sec Period	5m sec Period
A) Region of Threshold of Destruction			
1. At peak of burst			
a) center of meat	945	853	792
b) surface of clad	254	310	440
2. At end of burst			
a) center of meat	1193	1147	973
b) surface of clad	393	491	melting+
B) Region of Peak Energy Density			
1. At peak of burst			
a) center of meat	2200*	2015	1895
b) surface of clad	508	619	melting+
2. At end of burst			
a) center of meat	2695*	2605*	2255*
b) surface of clad	melting+	671	1095

* Vaporization at one atmosphere occurs at 2060°C.

+ Melting occurs at 640°C.

2. Effects Following Excursion

1 Acceleration of Water Slug

The steam resulting from the nuclear excursion displaced water from the core and eventually from the region above the core. At the time of the incident, seven feet of water were above the fuel plates, leaving an air void of 40 cubic feet between the top of the water and the pressure vessel head. The water displaced from the core region pushed this water upwards against the head of the pressure vessel. The collision of the water column with the head resulted in the rapid conversion of the column's kinetic energy to potential energy of compression.†

An estimate of the pressure attained in the compressed water has been obtained from the damage sustained by the control-rod guide tubes extending from the end of the shield plugs. These 304-stainless steel tubes, 0.2 inches thick with 1.9 inches OD, yielded under the pressure. The static yield-pressure is 7000 psi. Because of the higher pressure required to yield material under transient conditions, an estimated 10,000 psi existed in the compressed water column surrounding the guide tubes.

If 10,000 psi was the peak pressure in the slug of water at the bottom of the head, the energy of compression in the entire slug was:

$$E_{comp.} = \frac{1}{3} V \beta (P_{max})^2$$

if a linear distribution of pressure between the head and the bottom of the slug is assumed. The kinetic energy of the column of water (in the center of mass system) is $1/2 \rho V v^2$, where

V = volume

ρ = density

v = velocity

β = compressibility = 5×10^{-5} atm^{-1}

Equating the kinetic energy and energy of compression gives a velocity of 130 ft/sec in the center of mass.* In the laboratory system,

v = 159 ft/sec.

† The air between the water and the head will have little effect on the analysis, since it will initially be forced into the space in the nozzles below the plugs. Also, the system was not tightly sealed.

* If a uniform pressure exists in the slug, the energy of compression will be $1/2 V \beta P^2$, giving a variation of less than 20% in the final result of velocity.

The time history of the steam pressure, in and above the core, that accelerated the column of water is not known. Had the pressure been uniform in time, it would have been 450 psi and the accelerating process would have lasted 34 milliseconds (for the 2.75 feet distance). This pressure represents only an average pressure that would accelerate the column of water to the required velocity. The peak steam pressure might have initially been several thousand psi for a short duration until pressure relief was obtained by propagation of the wave through the column of water and the resulting motion of the water occurred. Such exceedingly high pressures might occur because steam was probably formed, near the end of the excursion, quite rapidly and violently by contact of water with metal heated to beyond the critical temperature of water (374°C, with corresponding critical pressure of 3200 psi), in fact heated to the vapor temperature of aluminum (2060°C at atmospheric pressure).[1] Steam pressures of several thousand psi existed for no more than a few milliseconds, if at all, not long enough to actually rupture the thermal shield or pressure vessel.

The estimates of velocity of the water column and average steam pressure are not much different from the empirically measured values during the model - explosive tests (Section III-1.6). These tests indicate that a water velocity of about 165 feet/sec and an average sustained pressure of about 550 psi create effects similar to those produced by the incident.

2.2 Effects of Water Slug

2.2.1 Pressure Damage

The compression of the water column upon impact against the vessel head caused not only the collapse of the rod guide tubes but produced high pressure damage to other metal parts.

The nozzles in the vessel head were bulged, an effect requiring 3,500 psi to yield and 11,000 psi to break under static conditions.

The vessel wall was bulged outward about two inches on the radius in the region of highest pressure (near the head). The vessel should yield (under static conditions) at about 1000 psi and break at about 3000 psi. However, the high pressure compression-pulse had a width at half-maximum of about the propagation time of sound through the column of water, or about 1.4 milliseconds. The average excess pressure above that necessary to yield the vessel was about 4000 psi for that time, during which the wall would have been accelerated through a distance of five inches. Since the transient yield stress is generally higher than the static yield, it is quite conceivable how such a high pressure (peak of 10,000 psi) for such a short duration expanded the vessel wall only about two inches but failed to rupture it. The head nozzles and the rod guide tubes were much thinner, offering less mass to be transported by the pressure pulse,

(1) Kinetic Studies of Heterogeneous Water Reactors, Quarterly Report September 30, 1961, Space Technology Laboratories, Inc.

in contrast to their higher yielding pressures. Note also that the steam baffle plate was bent against the vessel by the same high pressure pulse.

2.2.2 Motion of Vessel

The impact of the fast moving column of water (mass about 200 slugs, velocity = 159 feet/sec) against the vessel head produced a transfer of momentum to the vessel. The model-explosive tests (Section III-1.6) have shown that essentially all of the water above the "core" was accelerated and left the vessel through the nozzles, indicating that the upward moving column of water was a complete piston, that it did not rebound into the core allowing the pressure to escape from the nozzles, and that the collision was, therefore, mostly inelastic. Transfer of the 32,000 slug feet/sec momentum of the water column to the 900 slug vessel (including water below the top of core) by means of an inelastic collision would impart a 29 feet/sec velocity to the combined 1100 slug mass.

The pressure vessel, however, was not free to move, being constrained by the outlet four-inch steam line and four smaller connecting pipes. It is estimated that these pipes could be sheared with about 60,000 ft-lb of energy, leaving the vessel with about 400,000 ft-lb of energy and an initial velocity of 27 feet/sec, with which it could rise 11.4 feet. The connecting piping was not ultimately the only constraining item, for the 1/4 inch steel insulation liner was constrained by the sheared piping so that the vessel was required to break the welds which connected the liner to the vessel flange. This action cost the vessel perhaps a foot of free rise, leaving about a 10 foot rise potential. The vessel's #5 seal housing apparently hit the bridge-crane drive shaft after a 9 feet-1 inch rise, limiting the height of the vessel travel, damaging the contacting components, but leaving no noticeable impact marks because of the very small relative velocity at the time of impact.

When the vessel rose nine feet out of its support cylinder, the thermal insulation (three-inch magnesia) from around the wall of the vessel generally rose with it. When the vessel struck the crane drive shaft, it may have become cocked toward the side that struck. As the vessel fell back into its support cylinder, the insulation on this side probably was stripped off and perhaps blown by the draft created as the vessel displaced air, thus accounting for the scattered insulation primarily in the region below the bridge crane. The steel punchings from the lid shielding were generally scattered toward the opposite side of the room. These were probably jarred loose and ejected by the initial impact of the water against the vessel head.

2.2.3 Shield Plug Ejection

Another effect of the water hammer was to eject the unbolted shield plugs from the vessel. If momentum transfer to the plugs vs. the vessel is assigned on an area basis, the shield plugs would receive twice the initial velocity of the vessel (each plug has 1/167 the mass of the vessel and 1/80

the area). It is estimated that the plugs would each lose 2000 ft-lb of energy in fracturing the rack and connecting rod fingers, leaving the plug with about 7000 ft-lb of energy. During the travel of the plugs out of their nozzles, they were further accelerated by the approximate 500 psi in the steam void below the water column. It is estimated that most of the plugs had 20,000 ft-lb of kinetic energy when they finally left the vessel nozzles. The #7 plug carried the third victim, who had been standing on the vessel. His mass was approximately equal to the mass of a shield plug. Had the victim not been partially accelerated by the rising vessel before meeting with the plug, the velocity of the combination man and plug would not have been sufficient for the plug with victim to leave the vessel, due to the impact of the water column alone. However, the water attempting to escape from the vessel promoted the separation of plug and vessel. A combination of these two effects was adequate for the #7 plug to become free of the vessel well in advance of the vessel hitting the ceiling, but such that this plug still trailed the others in flight.

2.3 Subsequent Excursions

Whether the reactor was rendered permanently subcritical by the initial excursion rests on the basis of pertinent evidence previously discussed and summarized below.

1. Critical Experiment

   The core (as received in the Hot Shop) was grossly subcrtical (k-eff about 0.6), a condition independent of the presence of boron poison.

2. Geometry

   The core was radially expanded and the center of the core was blown apart and upward (most of it eventually falling back), leaving the reactor larger, but well over-moderated.

3. Missing Fuel

   Approximately 2 Kg of U-235 was missing from the active core region, most of this from the center 16 elements, leaving this section with about 60% of its original fuel content and a resultant low thermal utilization.

4. Reactivity Insertion

   The rate at which the central rod could be manually withdrawn exceeds that necessary to get the rod to the 20-inch position well in advance of the peak of the power burst. The reactivity change can, therefore, be considered equivalent to a step insertion of reactivity.

5. Neutron Activation in Operating Room

The activation, both thermal and fast, at the position of the victims was many orders of magnitude above what can be accounted for by direct radiation from under the 7 ft. water head.

There seems little doubt, from the first three items above, that the core was rendered grossly subcritical by a very violent excursion. The withdrawal of the central control rod, regardless of the trajectory it followed, was such that motion near the 20 inch position was small over the time that the major portion of energy was developed during the excursion. Therefore, the shutdown mechanism developed while essentially the entire excess reactivity was inserted, and the resulting excursion was the most violent that could occur with this amount of reactivity (i.e. - a step insertion gives the worst excursion). Therefore, any subsequent excursions could have been no worse than the initial one provided they involved the same amount of excess reactivity.

With the control rods bound in their shrouds, the only means of enhancing reactivity was to remove the boron strips. The strips on the outer 24 elements were found in place, though generally unattached, during core disassembly. Therefore, it is unlikely that the small amount of boron remaining in the center of the core at the time of the incident would have been quickly removed by any action short of displacing the fuel elements from each other, such as was done in the final burst. Note that further evidence to support this contention is the fact that during normal operation, the fuel elements vibrated in the core structure, and yet this vibration apparently created no sudden detectable losses in boron. It is concluded that an insignificant amount of boron would have been quickly knocked out of the core by a mild excursion, and that such a mild excursion, therefore, did not precede the final violent one.

The high neutron activation on the operating floor is the one item that does not substantiate a single burst hypothesis. The fact that most of the water above the core would be blown out by even a mild excursion (model explosive tests, Section III-1.6) provides a reasonable mechanism for obtaining high floor-level activation on the subsequent burst. However, the fact that a dual excursion could conveniently explain the activation levels does not a priori eliminate other explanations which would still be compatible with a single burst. Such explanations are contained in Section IV-3.3.

The evidence for a single violent burst with no subsequent nuclear chain reaction seems overwhelming. The analysis of the predicted reactor behavior following the apparent reactivity insertion rate is completely self-consistent with the current data on reactor and fuel element transient behavior. It is quite certain that the final burst was a very severe and violent one, and it seems rather unlikely that this was preceded by a non-destructive, mild burst which precipitated the final one.

3. Core Damage

3.1 Temperatures, Destruction, Melt, and Vaporization

The fluxes recorded by the flux wires in the center 16 elements of the core were sufficiently high over approximately 50% of the plate area to heat the entire thickness of the fuel plate to the molten state. During the nuclear energy release, most of which occurred in about 10 milliseconds, a negligible amount of heat was transferred through the cladding to the water. At most, only 2% of the total heat deposited in the plates could have been removed under the most efficient nucleate boiling heat transfer conditions. Thus, the fuel plates initially retained essentially all of the prompt nuclear energy deposited in them except for those plates whose cladding surface did not remain intact.

As Figures IV-1, 2, and 3 show, if the energy is developed by an approximate four milliseconds excursion, the center of the meat can reach vaporization (at atmospheric pressure) while the surface of the clad is still below the melting temperature. Such apparent vaporization had occurred only over a small region of the reactor, less than 1% of the center 16 elements, by the time of the approximate peak of the power burst. By the end of the excursion, however, the center of the meat is about 5% of the central core region had reached vaporization temperature, based on the two term exponential model. The meaning of fuel "vaporization" at the high pressures which existed adjacent to the plates is somewhat nebulous. Nevertheless, once the meat region had reached 2060°C, conditions in the plate must have been extremely adverse to the plate maintaining its integrity, despite the existence of high pressures on the outer, still unmelted surface of the clad.

The disintegration of most of the destroyed plate area probably did not occur until the melting proceeded to the outer surface of the clad and therefore came after the peak of the power burst and did not contribute significantly to limiting the power rise, which may have been accomplished largely by normal steam formation from intact plates. However, before the nuclear excursion had been terminated by this latter mechanism, it is quite probable that very violent disintegration of a small fraction (approximately 5%) of the center section of the core had occurred, producing extremely fast steam formation, and terminating the excursion abruptly. It is this back side of the excursion power curve which probably differed most from the normal SPERT non-destructive power traces.

The two term expoential model, Power = $e^{\alpha t} - 1/3\, e^{3\alpha t}$, generally provided a sharper drop to the back side of the power curve than was observed in most SPERT and BORAX non-destructive tests. The more abrupt drop deduced for the SL-1 incident would, therefore, make this two-term model even more suitable for the SL-1. The model gives 77% of the total energy release before the peak power.

Most of the destroyed regions of the center 16 elements (47% destroyed 5% reached vaporization) resulted from normal melting which eventually spread to the outer clad surface and destroyed the integrity of the plate. Normal internal melting, resulting in a volume expansion of the order of 5%, would not be expected to destroy the plate. This melt spread relatively

slowly to the surface of the clad (for the unvaporized regions) so that even by the end of the excursion, the surface of the clad throughout most of the destroyed region had not yet become molten. Thus, it is believed that the destruction of the unvaporized portion of the plates occurred generally after the end of the nuclear excursion, and that this non-violent destruction did not contribute to the shutdown mechanism.

3.2 Energy Distribution and Metal-Water Reaction

3.2.1 Nuclear Energy Distribution

Of the total 130 Mw-sec released by the nuclear excursion, 50 Mw-sec was produced in the outer 24 elements. These elements easily absorbed this energy with little resulting damage. Therefore, transfer of heat from these outer 24 elements to the water occurred over a relatively long time by the slow process of nucleate or film boiling from smooth surfaces. This process would require a minimum of about two seconds, a time exceedingly long compared to the time scale of the incident.

Of the 80 Mw-sec produced by the center 16 elements 86 percent (69 Mw-sec) was promptly deposited in the plates and was distributed such that 12 of these elements suffered severe damage due to melting and possibly vaporization. Heating of the entire fuel plate material in these 16 elements to the melting temperature would require 45 Mw-sec. However, the energy was distributed so that half of the plate area was heated to melting or above while half of it was heated to less than the threshold of destruction. The portion of the plates that quickly disintegrated transferred heat very rapidly to the water. Approximately 44 Mw-sec of energy was deposited in the destroyed areas of the core, and most of this energy was transferred to the water when the disintegration of these regions occurred.

The amount of energy that could have been quickly deposited in the water and thus have contributed to the acceleration of the water column against the vessel head is listed in Table IV-3.

TABLE IV-3

Energy Rapidly Deposited in Water (within 30 milliseconds following peak power)

Prompt nuclear energy during the excursion (neutron heating of water)	7 Mw-sec
Normal heat transfer from smooth plates (approx. maximum)	4
From disintegration of plates (44 Mw-sec max.)	39
	50 Mw-sec

This is the energy which contributed to the mechanisms creating the mechanical damage of the incident. The explosive-model test (Section III-1.6) produced equivalent damage with a 1/2 pound charge of "Pentolite" in a 1/4 scale model. This would be equivalent to a 32 pound charge in a full scale model, depositing approximately 74 Mw-sec of energy in the water. However, the explosion of "Pentolite" conceivably produced more violent disturbance of the water, mixing it more thoroughly and permitting unvaporized water to absorb more heat than probably occurred in the SL-1 excursion.

An additional consideration requires that enough water be vaporized to produce the 500 psi approximate average pressure needed to accelerate the water column. This pressure endured for about 1/2 second until the water was ejected from the vessel. Using the 40 ft^3 of void into which the water vapor could expand with the water column against the lid, an energy of 52 Mw-sec is needed to vaporize sufficient water to produce a 500 psi pressure in this volume. Certainly, additional heat would be absorbed by unvaporized water. It appears, therefore, that of the total 130 Mw-sec of nuclear energy produced, 50 to 60 Mw-sec was rapidly inserted into the water, primarily by the portions of the fuel plates which disintegrated. It was this energy which created the steam that accelerated the column of water.

3.2.2 Metal-Water Reaction

In the peak energy density region of the SL-1 core, the energy deposited in the fuel plates was approximately 500 cal/gm (meat and clad). This is a little more than twice the energy density required to melt the plates (220 cal/gm). Experiments on fuel pins of aluminum and uranium oxide at TREAT(1) have shown that energy densities of 500 cal/gm produce an aluminum-water reaction in approximately 10% of the metal, while essentially no reaction occurs below energy densities of 220 cal/gm. However, not only did the fuel in the TREAT experiments differ from SL-1 fuel, but the reactor period was an order of magnitude longer than the SL-1 excursion period. At an energy density of 500 cal/gm, some of the SL-1 meat vaporized, while it is not certain that any vaporization of aluminum occurred in the TREAT experiments.

To obtain an estimate of the extent of an aluminum-water reaction in the SL-1 excursion, very liberal estimates were made using the TREAT experimental results as a guide. The reaction of aluminum with water, $2\,Al + 3\,H_2O \rightarrow Al_2O_3 + 3\,H_2$, releases 231×10^3 calories per mole of Al_2O_3 formed, or 18 Mw-sec per kilogram of aluminum metal reacting. It has been assumed that, in the portion of the plates which reached vaporization, 25% of the aluminum in the meat reacted with water; and for the remainder of the destroyed plate area, 5% of the aluminum has been assumed to have reacted with water. This amount of aluminum reacting with water would release 35 Mw-sec of chemical energy and produce 3.6 Kg of α - aluminum oxide.

(1) Liimatainen et al, ANL 6250

The aluminum oxide formed should be very finely divided. Presumably, it was distributed throughout the pressure vessel, and the major portion of it which did not leave the vessel would have settled to the bottom and would be found in the 53 Kg of material removed from that region. Diffractometer analysis of the fine material in the bottom of the vessel has indicated 1.5 kilograms of aluminum oxide (α -phase) existed in the fine material alone (see Section III-2.5).

The amount that was in the coarser material would be expected to be small because it is unlikely that particles of Al_2O_3 coalesced with each other. Since only one-half of the uranium particles not still in or on fuel plates was found in the bottom of the vessel (see Section III-3.3), it is conceivable that not much more than half of the total aluminum oxide formed would be found in the bottom of the vessel. If one kilogram escaped from the vessel, a total of 2.5 kilograms of α - aluminum oxide was produced.

Thus, the amount of metal-water reaction indicated from chemical analysis of the debris is about 2/3 of the value estimated, rather liberally, using the results of the TREAT experiments. The amount of energy released by this chemical reaction was (24 ± 10) Mw-sec, which is about one-fifth of the nuclear energy release. Table IV-4 lists the products of the apparent aluminum-water reaction.

TABLE IV-4

Aluminum-Water Reaction Estimated Effects
(± 40% uncertainty)

Energy generated	24 Mw-sec
Total aluminum oxidized	1.3 Kg
Al_2O_3 (α - phase) produced	2.5 Kg
Hydrogen gas produced	74 moles

The chemical energy generated is only a small fraction of the nuclear energy, despite the fact that some of the aluminum had reached vaporization temperature. The hydrogen gas formed would not have significantly boosted the average pressure under the column of water during its acceleration toward the vessel head, but might have inserted an initial high pressure surge compared to the rate at which steam was formed.

3.3 Activation

Since the 130 Mw-sec generated by the SL-1 excursion probably occurred in a single burst from under a seven foot, undisturbed column of water, it is difficult to account for the high neutron activation reported for various samples taken from the bodies of the victims. Through seven feet of water, the thermal and fast neutron fluxes from a 130 Mw-sec excursion would be between 10^3 and 10^4 n/cm^2, in sharp contrast to the

10^9 to 10^{13} n/cm^2 reported in the analysis of Phase I and II Operations and listed in Section III - 4.2 of this report.

With a much smaller column of water above the reactor, higher activation levels would occur, with each foot of water being worth about 1-1/3 decades of attenuation. However, the height of water above the core just prior to the incident is well known. Witnesses from the day shift of January 3, 1961, are certain that the water was within six inches of the head before the level was reduced to bring the level-instrumentation on scale. The water pumped from the vessel was in the contaminated waste tank (previously emptied) and was measured after the incident to be about 250 gallons, sufficient to reduce the water level in the pressure vessel 2-1/4 feet, leaving about seven feet of water above the core.

Since the critical experiment and certain other considerations strongly indicate that there was but one excursion (see Section IV-2.3), other explanations have been sought to explain the occurrence of such high neutron activation from under so much water. One consideration is the scattering of neutrons up the three inch insulation gap around the vessel after they have traveled through about ten inches of water and two inches of steel from the face of the reactor. However, from the top of the insulation gap the neutrons either must travel through sixteen inches of steel or undergo multiple scatterings to get to the operating floor. The resulting flux would be less than 10^8 (a liberal estimate), still much too low to account for the measured activations.

Other considerations are that the activation on the operating floor may have been produced predominantly by the delayed neutrons originating after the excursion, either (1) from fuel ejected from the reactor pressure vessel, or (2) from the core and its remnants inside the vessel while the vessel was above its rest position. These two hypotheses are considered below.

1. If delayed neutrons were emitted from 1% of the fuel at a distance of one foot from a detector, a fast flux of 6×10^{10} n/cm^2 would result. The same flux would result from 10% of the fuel inventory at a three foot distance. Lumps of fuel were not found in great quantity outside the pressure vessel (only a few identifiable lumps containing two grams of uranium were recovered). Therefore, most of the ejected fuel was probably in fine-particle form, easily and widely dispersed throughout the building. The uniform dispersing of fuel can explain why all the thermal receptors from the victims received similar doses. From the fission product and fuel escape estimates (see Section III-3.3 and 4.3), it is difficult to account for much more than 10% of the delayed neutrons being emitted outside of the pressure vessel, giving rise to fast fluxes certainly less than 10^{11} n/cm^2 and thermal fluxes (moderation by the bodies) which should be considerably less than 10^{10} n/cm^2 (assuming 10% moderation). The ejected fuel hypothesis is, therefore, somewhat insufficient to account for all the observed activation.

2. While the vessel was traveling upwards and falling back, the core was for a time close to the operating floor. In fact, most of the center section of the reactor was ejected upwards by steam and water and may have been well above the operating floor for part of the vessel's flight. Approximately 50% of the delayed neutrons are emitted within four seconds of fission. Though a freely falling body would go through a 10 foot high trajectory in 1.5 seconds, it is conceivable that the pressure vessel became cocked and remained out of the support cylinder for several seconds near the top of its trajectory. If such was the case, it can be shown that 50% of the delayed neutrons from the center section of the core (60% of total energy) would give a thermal dose of 5×10^9 n/cm^2, five feet from the core center, through the vessel wall, but not through the head. (Based on six inches of water and two inches of steel from reactor face.) The fast neutron dose would be less than the thermal dose.

It appears that a combination of hypotheses (1) and (2), above, probably explain thermal neutron activations of the order of 10^{10} n/cm^2, and fast neutron activations of less than 10^{11} n/cm^2.

The thermal flux near the #4 shield plug's Stellite bearing was an order of magnitude lower (10^9 n/cm^2 maximum). The plug and bearing were in the fan room at the time most of the delayed neutron irradiation occurred. Neutrons from inside the vessel would have had to penetrate the vessel head (except for the 8% open area) to reach the bearing; and of the ejected fuel and fission products, only a small fraction reached the fan room. Thus either hypothesis (1) or (2) correctly infers a lower activation for the #4 Stellite bearing than for the receptors on the victims.

The fast neutron activation of the hair samples from the victims (except the pubes of the first victim) is one to two orders of magnitude higher than can reasonably be accounted for by any combination of the above hypotheses. Furthermore, it is somewhat of an anomaly that, for the two victims for which data exists, activation at the head level was approximately 100 times the activation of the pubes. It is suspected that contamination of the samples by the ejected reactor water, a problem alluded to in reference 2 of Section III-4.2, was the cause of the exceedingly high apparent activation of the exposed head areas and the much lower apparent activation (but still unusually high for the second victim) of the clothed pubic areas.

In general, the thermal neutron activation data from outside the pressure vessel, levels of about 10^{10} n/cm^2 on the victims and 6×10^7 n/cm^2 from the Nuclear Accident Dosimeter at the doorway at the side of the operating room seem to have been caused by delayed neutrons. Whether these neutrons originated mostly from fuel ejected from the pressure vessel or from fuel inside the vessel during the time this fuel was above or near floor level is uncertain. Quite likely each source of neutrons made a significant contribution.

4. Summary of Excursion

The SL-1 excursion and its effects are summarized in graphical form in Figure IV-4. Despite the unfortunate nature of the incident, it has provided a valuable insight into the overall understanding of reactor excursions and the problems of reactor safety. The most significant items of information obtained from the analysis of the incident are listed below, with reference being made, when appropriate, of their relation to the BORAX destructive test. (1)

1) Reactivity Insertion - The withdrawal of the central control blade to the 20-inch position could have been performed manually with more speed than was actually necessary to create the excursion. Though the condition of the boron poison strips in the reactor at the time of the incident is not known, it appears unnecessary to postulate that any significant change in boron inventory occurred since the cadmium strips were added in the T-shrouds. The estimated reactivity of the 20-inch position was equivalent to the reactivity of a four millisecond transient.

2) Reactivity and Energy - The total energy generated by the SL-1 and BORAX-1 were about the same, yet considerably less reactivity was needed for the SL-1 excursion. (2.4% ΔK compared to 3.3% ΔK) Basic design differences between these two water-moderated, plate-type reactors created two opposite effects: one in which the SL-1 shutdown mechanism was less effective than that of the BORAX, followed by a potentially more rapid shutdown mechanism whereby the SL-1 excursion was terminated quite abruptly.

3) Shutdown Mechanism vs Energy - The SL-1 average void coefficient was small compared to BORAX and similar cores, thus reducing the effects of all non-destructive shutdown methods. The plate area, from which steam formation occurs, was also much smaller for the SL-1. Of more significance was the larger thickness of the plates and the cladding of the SL-1, permitting a larger amount of energy to be internally stored in the plates before significant heat transfer took place between the plate surfaces and the water.

4) Reactor period and temperature distributions - The large plate thickness of the SL-1 permitted a high ratio of center to surface temperature. The estimated four millisecond transient caused the fuel-meat in portions of the reactor to reach vaporization temperature before the surfaces of the plates had melted or had an opportunity to transfer much heat to the water. Due to these high center temperatures, the shutdown mechanism of steam formation suddenly became very rapid as portions of the plates exploded (presumably), resulting in an abrupt termination of the excursion.

(1) AECD-3668, BORAX-1 Experiments, 1954 - J.R. Dietrich

5) Fission product release - The empirical information, obtained during deliberate melt tests, of fission product release cannot, in general, be applied to the SL-1. For in this excursion, the primary method of fission product release occurred as a result of the bursting of internally vaporized plates, a condition that has not successfully been reproduced in controlled, out-of-pile tests. Furthermore, the partial containment provided first by the pressure vessel and secondly by the building shell obscured the correct interpretation of the amount of fission product release in an excursion of this magnitude.

6) External Effects - The damage outside of the pressure vessel was somewhat extraordinary, having been created primarily by the effects of a fast moving column of water slamming against the pressure vessel lid. This event had unusual consequences, strikingly destructive in view of the fact that the pressure vessel itself did not rupture but did jump nine feet into the air.

Thus the energy relationships between the nuclear, thermal, and mechanical phenomena can be cross-linked by the calculational methods of engineering physics. Moreover, the kinetics of the energy transformations are compatible with the behavior of other reactor systems in which destruction was deliberately produced by a similar rapid insertion of reactivity through control rod motion. As can be seen from the foregoing analysis, even differences that do exist between SPERT, BORAX and SL-1 behavior can be qualitatively explained in terms of physical differences in reactor structure.

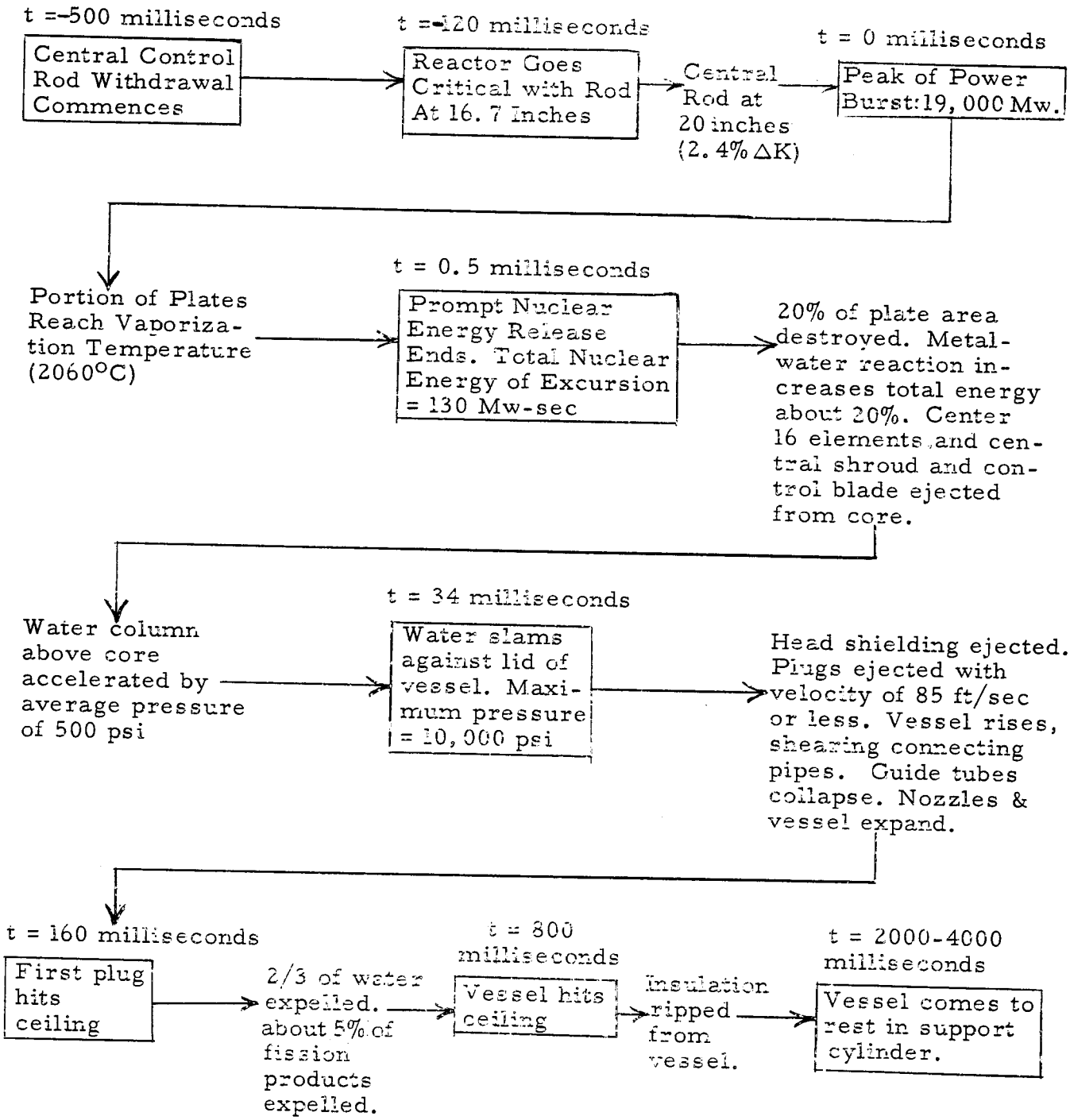

Figure IV-4 SL-1 Excursion Summary. Values are approximate (see text for estimated uncertainties). Time is in milliseconds.

APPENDIX A

Description of the SL-1

The SL-1, a small, natural circulation, direct cycle, boiling water reactor, was designed by Argonne National Laboratory and put into operation at the National Reactor Testing Station near Idaho Falls, Idaho. The first operation at significant power was on October 23, 1958. On February 5, 1959, operating responsibility of the reactor was transferred from ANL to Combustion Engineering, Inc. Figure A-1 shows the entire power plant. The large tank in back houses the reactor, power generating equipment, blower fans, etc. The concrete building in the foreground is the administration building, and the building between the reactor and administration building is the support facilities building. The remaining buildings shown in Figure A-1 are support and training buildings.

Figure A-2 shows a cutaway view of the reactor building and the north corner of the support facilities building. This cutaway shows the lower portion of the cylindrical building which contains the reactor pressure vessel surrounded by gravel shielding. The turbine generator and plant support equipment are located in the center portion of the building above the reactor pressure vessel proper. The upper portion of the building contains the air cooled condensor and its circulation fan.

At the time of the incident, the shield blocks were moved back. Except for this, the reactor floor was as shown in Figure 2.

The perspective cutaway shown in Figure A-3, depicts the pressure vessel, core, biological shield, and the control rod drive mechanisms. The lower portion of the cutaway shows the core support, support lugs, support grid, thermal shield, and thermal shield support. In the center cutaway of the core, the control rod shrouds, X-stanchions and fuel element positions can be seen. The upper left portion of the pressure vessel just below the head shows the steam and water lines. Above the head are the biological shield, still wells, cover assembly and the control rod drive mechanism. The biological shield contains steel punchings, sand, and 30 pounds per cubic foot of boric oxide. At the time of the incident, the #5 control rod drive mechanism, blind plugs #2 and #6, blind flange cover #8, and the still wells were secured as shown. The remainder of the rod drives had not been secured.

Figure A-4 is a top view of the core taken through the head showing the control rod coupling, shrouds, and the top fuel element hold down boxes.

The above gives the condition of the reactor at the time of the incident on January 3, 1961.

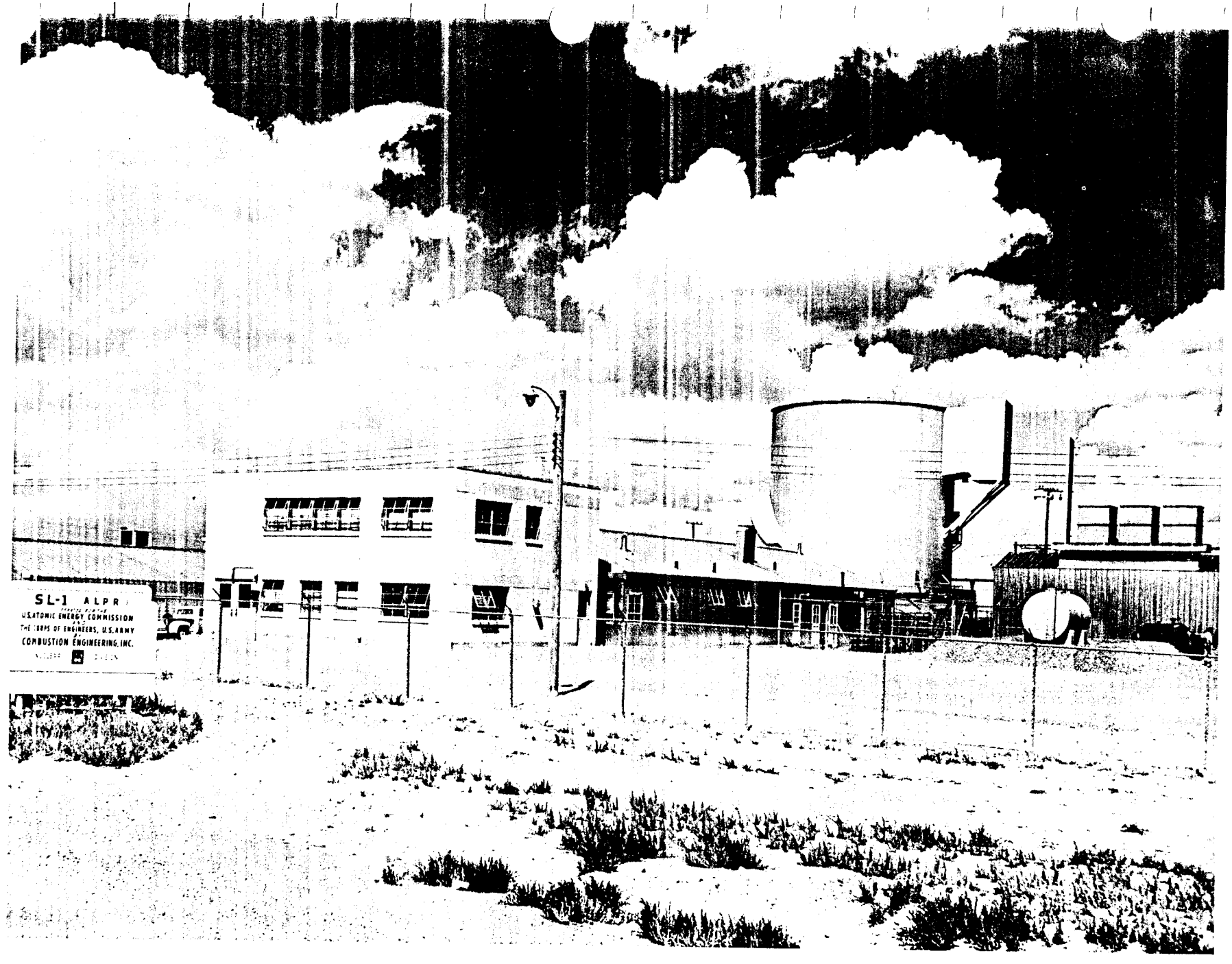

NRTS-60 4749

Figure A-1 SL-1 Plant Area

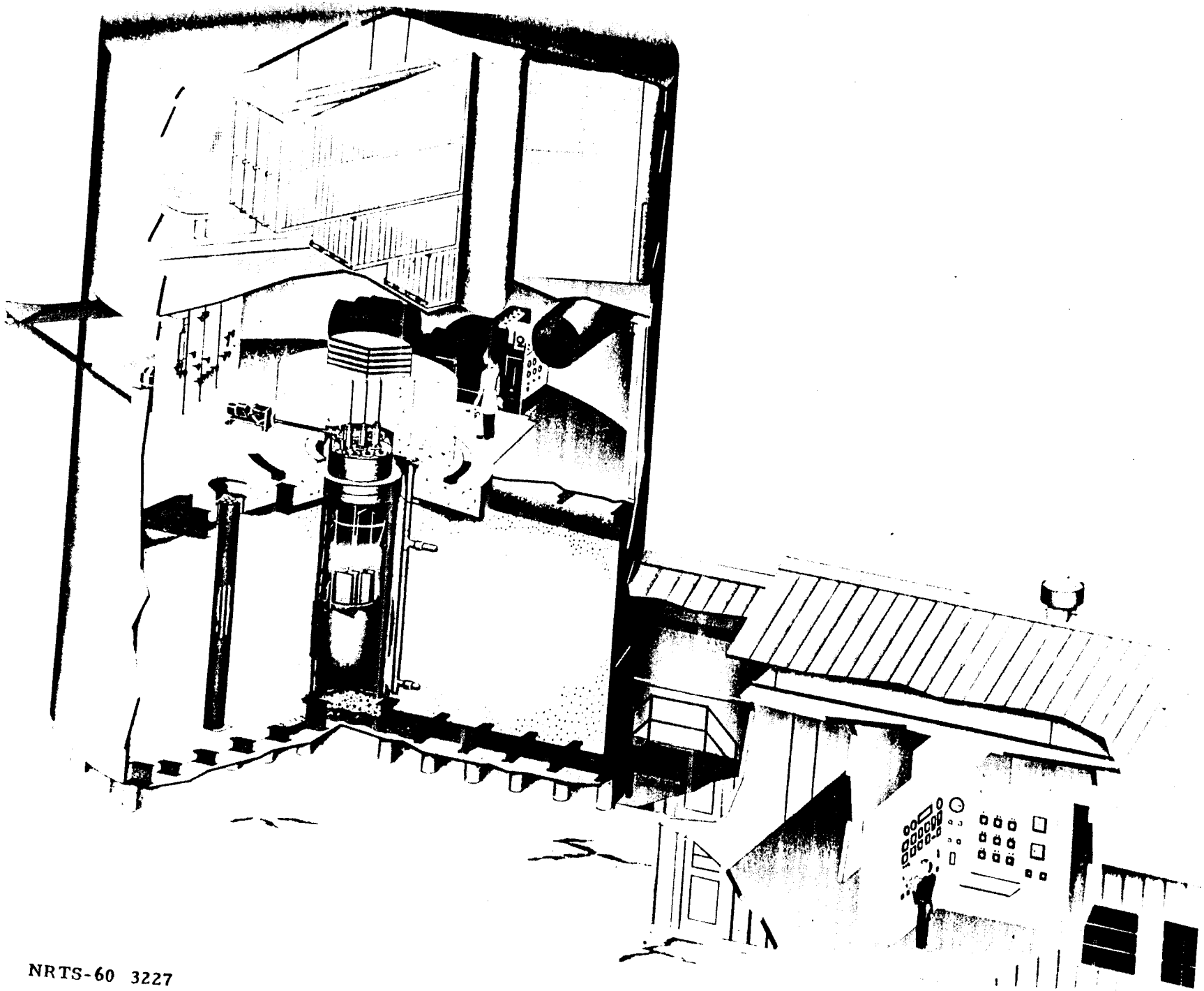

NRTS-60 3227

Figure A-2 SL-1 Plant Perspective

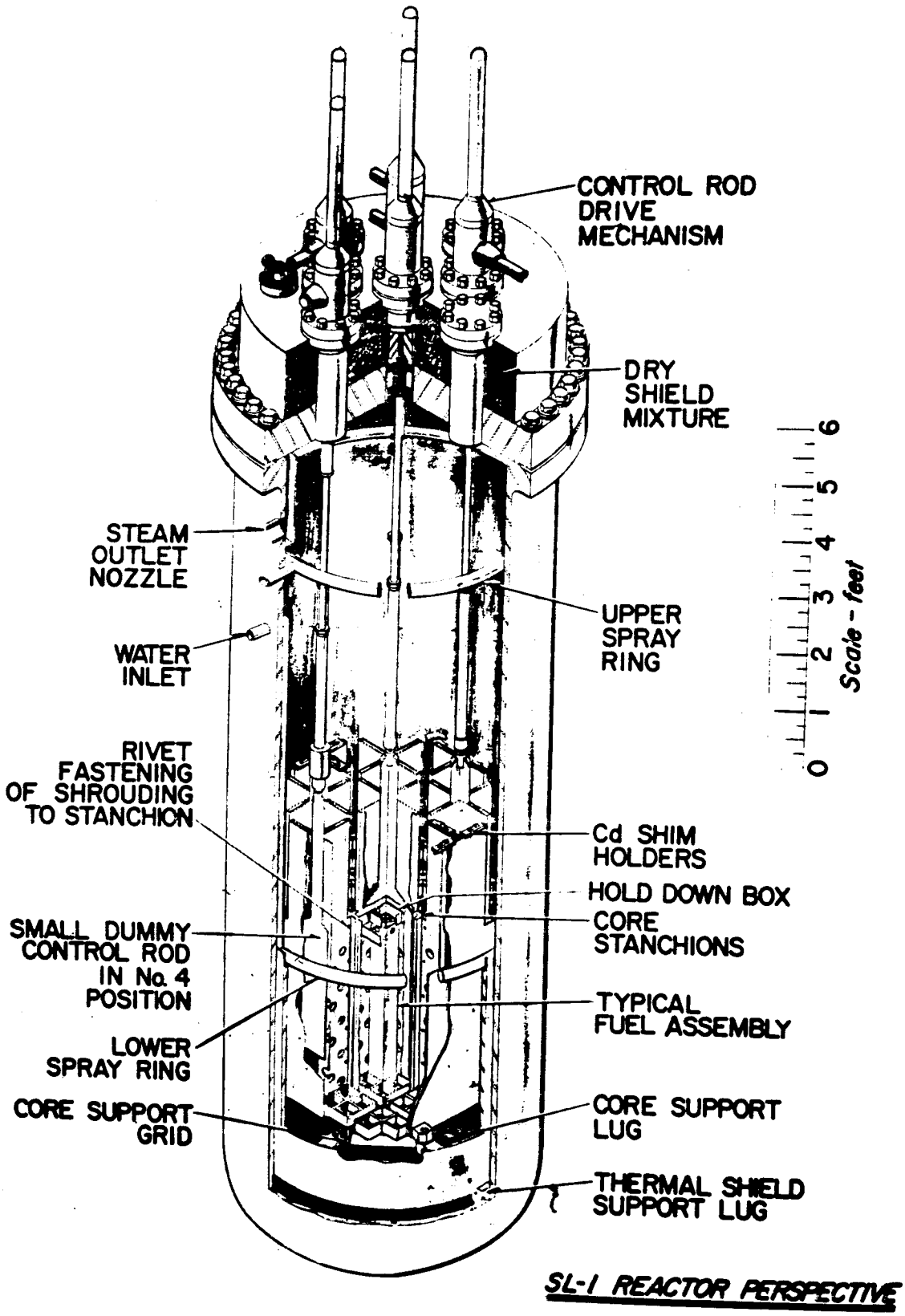
CONTROL ROD DRIVE MECHANISM
DRY SHIELD MIXTURE
STEAM OUTLET NOZZLE
WATER INLET
UPPER SPRAY RING
RIVET FASTENING OF SHROUDING TO STANCHION
Cd SHIM HOLDERS
HOLD DOWN BOX
CORE STANCHIONS
SMALL DUMMY CONTROL ROD IN No. 4 POSITION
TYPICAL FUEL ASSEMBLY
LOWER SPRAY RING
CORE SUPPORT GRID
CORE SUPPORT LUG
THERMAL SHIELD SUPPORT LUG
0 1 2 3 4 5 6
Scale - feet
SL-1 REACTOR PERSPECTIVE

Figure A-3

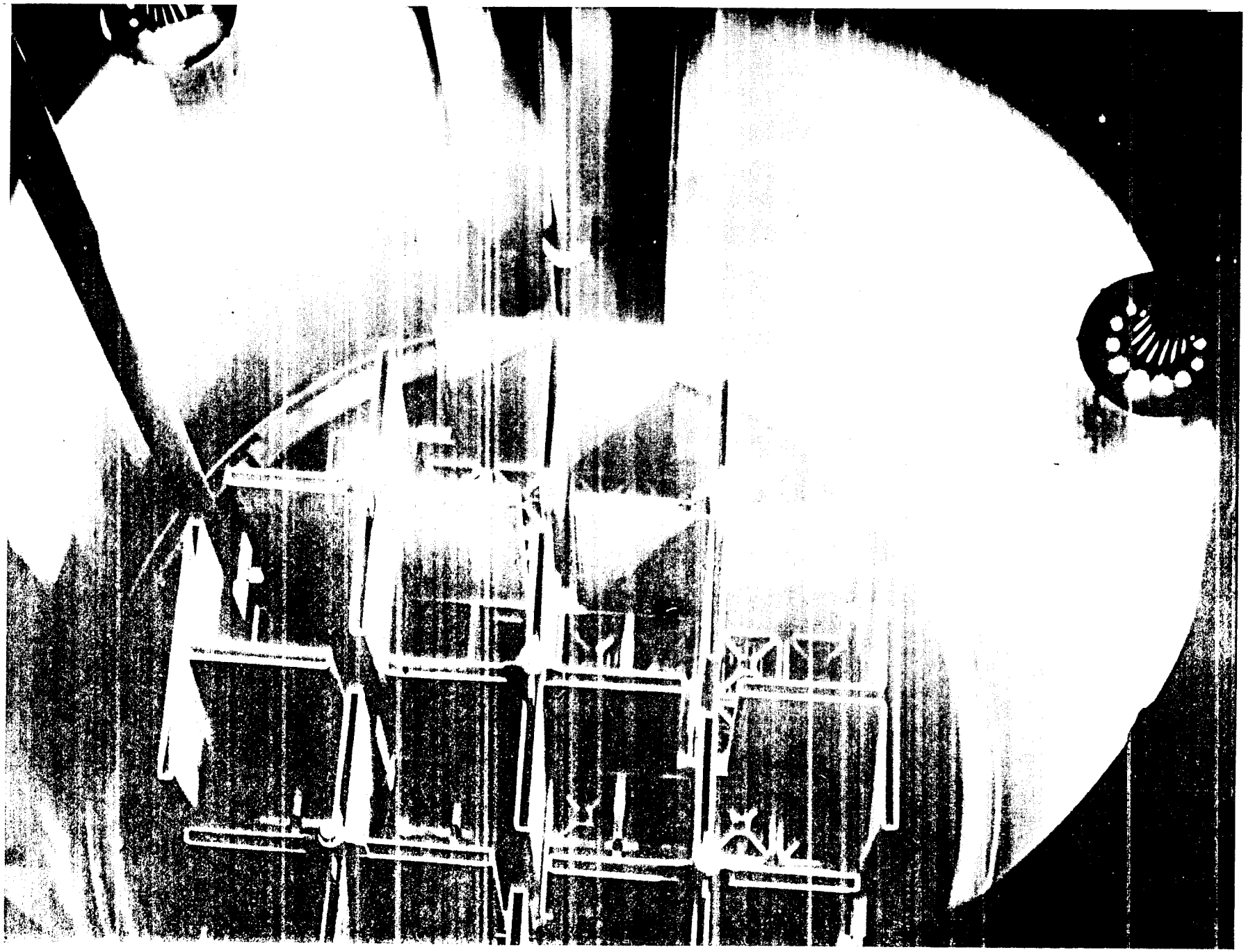

U-5116

Figure A-4 SL-1 Core Plan

APPENDIX B

List of SL-1 Photographs by Series Numbers

Site and in Transit

U-5003	Pictures of SL-1 and reactor floor
U-5004	Enlargement of movies frames
U-5005	Checkout on pin-hole camera
U-5006	Operating room photographs
U-5009	Photostat of flow diagram
U-5011	Operating room photographs (6-29-61)
U-5013	Operating room photographs (7-3-61)
U-5016	Operating room photographs (7-13-61)
U-5018	Operating room photographs (7-21-61)
U-5019	Fan room photographs
U-5020	Fan room photographs
U-5021	Fan room photographs
U-5027	Fan room photographs
U-5032	Fan room photographs
U-5035	Operating room photographs
U-5040	Fan room photographs
U-5041	Operating floor photographs
U-5042	Operating floor photographs
U-5043	Operating floor photographs
U-5047	Fan room photographs
U-5049	Pinhole camera pictures

Site and Transit (Continued)

U-5050	Pictures of Core
U-5051	SL-1 Building and Reactor
U-5053	Pressure Vessel
U-5054	Fan Room and Reactor Floor Ceiling
U-5055	Operating Floor
U-5056	Pressure Vessel
U-5057	Boroscope
U-5058	Boroscope
U-5059	Boroscope
U-5060	Pressure Vessel
U-5061	Mockup in 607
U-5062-3	Exterior of Core-Lift on Pressure Vessel
U-5068	Reactor Building
U-5071	Cask and Truck enroute to SL-1
U-5073	Reactor Building
U-5075	Removal of Core from Vessel
U-5076	Inside Pressure Vessel, Cocoon, Crane, Shield, Fan Room, Gravel Fill, etc.
U-5077	Moving Core to ANP
U-5078	Mockup - SL-1 Core
U-5101	Austin-Western Crane
U-5114	Facilities and Gravel Removal from Building
U-5145	SL-1 Area and Containment Vessel
U-5163	Final Area Inspection

Hot Shop

U-5008	Material from SL-1 Floor
U-5010	Component and Shield Plug
U-5017	Parts removed from SL-1 Floor
U-5079	Top of Core
U-5081	Control Rod #9
U-5083	Top of Vessel - Shield can removed
U-5084	Top of Vessel - Shield can partially lifted
U-5085	Core through binoculars
U-5086	Core through boroscope
U-5087	Bulged Control Nozzles
U-5089	Sand, boron, steel punchings shielding material on top of pressure vessel head
U-5090	Criticality test stand
U-5092	Inside pressure vessel (boroscope)
U-5094	Core removed from cask
U-5095	Inside pressure vessel (boroscope)
U-5096	Insulation in bottom cap
U-5097	Dished head
U-5098	Bulged nozzles
U-5099	Light leaks around head
U-5100	Control Rod #5
U-5103	Removing head from pressure vessel
U-5104	Inside pressure vessel - head removed

Hot Shop (Continued)

U-5105	Inside pressure vessel after removal of various parts
U-5109	Color photos - inside pressure vessel
U-5112	Inside pressure vessel
U-5117	Inside pressure vessel No Sun-Gun
U-5118	Inside pressure vessel No Sun-Gun
U-5119	Pressure Vessel head - elongated holes
U-5122	Before and after boric acid neutralization test
U-5123	Inside pressure vessel
U-5124	Boroscope - bottom of pressure vessel
U-5130	Bottom of pressure vessel (boroscope)
U-5131	Light coming through core from mirror
U-5132	Inside pressure vessel
U-5134	Criticality stand and cutting stand set up
U-5138	TV-Monitor views inside pressure vessel
U-5144	Critical control panels
U-5147	Core during cutting operation of pressure vessel
U-5148	Core disassembly
U-5150	Thermal shield and other reactor parts
U-5161	Pressure vessel in Warm Shop
U-5167	Hot Shop - final wash down
U-5170	Head nozzle deformation

Laboratories

U-5001	RML Photos of SL-1 Components
U-5002	Components HL-1 to 14
U-5007	Material in HCA
U-5010	Component and Shield Plug
U-5012	Hot Lab
U-5014	Film Badge (Legg)
U-5022	Shield Plug A
U-5023	Shield Plug B
U-5024	Misc. part, (Legg film badge)
U-5025	Seal control unit in disassembly position
U-5029	HL-64 to HL-79
U-5031	Shield Plug assemblies 3 and 4 and component parts
U-5034	Front and back views of boron poison strips
U-5038	Shield Plug #1
U-5039	Microscope photos (components)
U-5044	Rack assemblies
U-5045	Seal assembly
U-5046	Connectors
U-5048	Shield Plug A
U-5052	Shield Plug #7 and #9
U-5066	Boron metallograph

Laboratories (Continued)

U-5080	Mockup in 607 of Sl-1 ceiling
U-5102	Control rod parts
U-5125	Baffle plates
U-5137	#9 Control Rod Sketch
U-5157	Shield Plug Projectories
U-5162	Weld on pressure vessel

Miscellaneous

U-5135	Memory scope #9 rod pulling
U-5140	#9 Rod set-up in 607 pool
U-5143	Turbine - generator from SL-1
U-5146	Fan Room Floor section above Reactor
U-5149	Scale model pressure vessel
U-5160	Memory scope #9 rod pulling
U-5164	Mock-up and Fan Floor Section
U-5165	Aberdeen Model Test

APPENDIX C

Report from Stanford Research Institute

STANFORD RESEARCH INSTITUTE

MENLO PARK, CALIFORNIA

June 26, 1962

Dr. C. L. Storrs
P. O. Box 2147
Idaho Falls, Idaho

Reference: Project PLD-3959

Dear Dr. Storrs:

Stanford Research Institute has been asked to make an investigation into the possibility that the reactor runaway which destroyed the Sl-l reactor could have been a result of sabotage in the form of some type of explosive.

Three visits - one by Poulter and two by Poulter and Davenport, have been made to the Idaho Falls facility to inspect the various elements of the reactor as it has been dismantled. These first-hand inspections of the damaged reactor and a study of the extensive photographs that have been taken, have made it possible to establish a number of basic facts from which very definite conclusions can be drawn.

Absence of Explosive or Explosive Decomposition Products

(1) The entire interior of the reactor assembly was comparatively free of elemental carbon such as would most certainly have been present if most types of high explosives or propellants had been exploded within the reactor.

(2) A chemical analysis of both water and carbon tetrachloride extracts of the residue showed the absence of more than traces of nitro or nitrate groups which further shows that neither a high explosive nor a propellant type charge had been exploded inside of the reactor even though it be one of a carbon-deficient type.

(3) From an examination of control rod No. 9 after it was removed from the shroud, it can be stated definitely that it was not raised by means of a high detonating rate-type explosive charge located under it in the space below the reactor proper; otherwise it would definitely show characteristic high explosive damage marks on the lower end.

(4) Likewise, control rod No. 9 could not have been blown upward by means of any reasonable quantity of a low order detonating explosive or propellant-type explosive, because of the relatively large annular space between the reactor elements and the shell of the pressure chamber.

(a) The comparatively large volume of open space in the lower portion of the pressure chamber below the reactor elements would have allowed such a free radial distribution of pressure that a pressure gradient sufficiently high at the center to left control rod No. 9, and yet low enough so as not to lift the surrounding and lighter control rods, is physically impossible.

(5) The possibility of control rod No. 9 being raised by a very rapid pulse or steady state flow of water upward through and around the reactor elements can be eliminated on the following bases:

(a) The annular space around the reactor elements is too large and so much water would flow up through that route that pressure sufficient to raise element No. 9 could not develop.

(b) The four similar elements surrounding No. 9 would raise first because they all have the same cross-sectional area and are lighter in weight so would have moved first, and none of them did move.

(c) There is no inlet pipe opening in the bottom portion of the pressure chamber sufficiently large to admit a sufficient quantity to do this by many fold.

(6) An examination of control rod No. 9 after it had been removed from its shroud or control rod No. 9 plus its shroud, shows no evidence whatever of any explosive or propellant having been detonated or burned within the reactor proper in such a manner that could have caused rod No. 9 to have been raised the 20 inches, as is evident from the seizure marks.

(a) Any such explosive would have collapsed the shroud on the rod before it moved, rather than forcing it up 20 inches first.

(b) Neither the shroud encased control rod No. 9 nor any of the surrounding fuel elements exhibit the type of damage that could have been caused by any such explosion.

(7) An examination of the character of the failure of the fuel elements which were adjacent to control rod No. 9, plus the radially outward displacement of all reactor components surrounding control rod No. 9 and the adjacent fuel elements shows conclusively that the major destruction occurred in those fuel elements adjacent to control rod No. 9 and at a distance of from three to six inches below the center of the fuel elements.

(8) The fact that in almost all cases the surfaces of the fuel elements which were in contact with the control rod were the least damaged shows that the major reaction during the excursion took place in that portion of those fuel elements which would be affected if the excursion were caused by the central control rod No. 9 having been raised 20 inches, at which point the shroud was collapsed on the control rod. This would have been true if control rod No. 9 had been raised by any amount exceeding 16 inches.

(9) Not only does a physical examination of all fragments from the control rod system and the contents of the reactor pressure chamber show no evidence of any chemical explosive or propellant having been exploded in or adjacent to the reactor, but a chemical analysis of residues from within this chamber plus the absence of any black deposits or residues of free carbon show not only that no such chemical explosives were detonated but that they were not even present.

Not only do we not find any evidence of any chemical-type explosive or propellant having been exploded within this reactor, but there is very strong evidence that no such materials had been present, and there is certainly no evidence of any portion of the reactor having been within the immediate proximity of exploding propellant or high explosive.

We are therefore convinced from these facts that there was no sabotage involved in this event of the nature which could have been caused by a chemical type of explosion.

Sincerely,

Thos. C. Poulter
Senior Scientific Advisor

Donald E. Davenport, Director
Poulter Laboratories

APPENDIX D

TABULATION OF % AREA DESTROYED & % AREA UNMELTED ON OUTSIDE OF CLAD

Fuel Element No.	Plate No.	% Area Destroyed	% Area Unmelted
1.	E- 9	84.7	15.3
	E-82	78.0	5.0
	E-52	78.0	13.0
	E-69	76.0	14.0
	E-80	78.0	15.0
	E-11	78.0	14.0
	E-48	78.0	11.5
	E-25	76.0	13.0
	E-24	72.0	11.5
		Avg. 77.6	Avg. 12.5
2.	E-72	57.0	1.0
	E-26	63.0	13.0
	E-59	83.0	11.0
	E-81	76.0	12.0
	E- 6	87.0	7.6
	E-46	85.0	10.0
	E-79	85.0	10.0
	E-13	87.0	7.6
	E- 4	88.0	7.6
		Avg. 79.0	Avg. 8.9
3.	E-45	7.0	38.0
	E-34	5.0	35.0
	E-18	64.0	27.0
	E-74	68.0	20.0
	E-30	65.0	20.0
	E-66	66.0	20.0
	E-56	69.0	20.0
	E-47	70.0	20.0
	E-68	69.0	20.0
		Avg. 53.7	Avg. 24.4
4.	E-78	74.0	23.0
	E-33	74.0	19.0
	E-75	77.0	12.0
	E-85	81.0	12.0
	E-35	81.0	12.0
	E-62	85.0	11.0
	F-44	85.0	11.0
	E-73	85.0	11.0
	E-39	85.0	11.0
		Avg. 80.7	Avg. 13.6

TABULATION OF % AREA DESTROYED AND % AREA UNMELTED ON OUTSIDE OF CLAD

Fuel Element No.	Plate No.	% Area Destroyed	% Area Unmelted
5.	E- 8	30.0	70.0
	E- 88	0.0	100.0
	E-253	2.0	98.0
	E- 21	12.0	88.0
	E-280	12.0	88.0
	E- 31	12.0	88.0
	E- 16	0.0	100.0
	E- 7	0.0	100.0
	E- 57	0.0	100.0
		Avg. 7.6	Avg. 92.4
6.	E- 22	69.0	19.0
	E-163	69.0	11.2
	E- 28	69.0	15.0
	E-160	69.0	11.2
	E- 32	69.0	15.0
	E-165	69.0	15.0
	E- 83	69.0	15.0
	E-155	69.0	15.0
	E-166	69.0	17.0
		Avg. 69.0	Avg. 14.8
7.	E-164	70.0	27.0
	E-140	68.0	19.0
	E-162	72.0	10.0
	E-158	73.0	15.0
	E-141	73.0	14.0
	E-273	69.0	17.0
	E-139	70.0	16.0
	E-157	81.0	15.0
	E-137	78.0	6.0
		Avg. 72.7	Avg. 15.4
8.	E-250	0.0	100.0
	E-252	75.0	6.0
	E-256	80.0	4.0
	E-260	74.0	7.0
	E-264	70.0	8.0
	E-265	69.0	10.0
	E-269	69.0	9.0
	E-270	73.0	8.0
	E-274	72.0	8.0
		Avg. 64.7	Avg. 28.9

TABULATION OF % AREA DESTROYED AND % AREA UNMELTED ON OUTSIDE OF CLAD

Fuel Element No.	Plate No.	% Area Destroyed	% Area Unmelted
9.	All plates Complete - No melting		
			100
10.	E-255	3.0	24.0
	E-278	55.0	39.0
	E-279	66.0	21.0
	E-272	62.0	11.0
	E-261	62.0	6.0
	E-257	58.0	8.0
	E-244	58.0	7.0
	E-277	66.0	11.0
	E-281	65.0	8.0
		Avg. 55.0	Avg. 15.0
11.0 All Others	E-195	19.0	19.0
	--	--	100.0
			Avg. 91.0
13	E-147	8.0	30.0
	E-153	3.0	20.0
	E-145	0.0	20.0
	E-146	0.0	20.0
	E-143	0.0	23.0
	E-121	0.0	48.0
	E-123	0.0	46.0
	E-245	0.0	45.0
	E-167	0.0	34.0
		Avg. 1.2	Avg. 31.8
14	E- 99	24.0	40.0
	E- 96	24.0	50.0
	E-110	12.0	75.0
	E-119	12.0	75.0
	E-130	8.0	84.0
	E-134	0.0	100.0
	E-171	0.0	100.0
	E-131	0.0	100.0
	E-129	0.0	100.0
		Avg. 8.9	Avg. 80.4

TABULATION OF % AREA DESTROYED AND % AREA UNMELTED ON OUTSIDE OF CLAD

Fuel Element No.	Plate No.	% Area Destroyed	% Area Unmelted
17.	All Plates Complete	0.0	100.0
		0.0	100
18.	All Plates Complete	0.0	100.0
		0.0	100
19.	All Plates Complete	0.0	100.0
		0.0	100
20.	E-297	12.0	48.0
	E-290	5.0	57.0
	E-287	2.0	98.0
	E-304	0.0	100.0
	E-303	0.0	100.0
	E-307	0.0	100.0
	E-302	0.0	100.0
	E-299	0.0	100.0
	E-298	0.0	100.0
		Avg. 2.1	Avg. 89.2
35.	E-315	85.0	4.0
	E-458	85.0	5.0
	E-472	84.0	7.0
	E-439	83.0	4.0
	E-442	80.0	4.0
	E-441	73.0	5.0
	E-445	65.0	7.0
	E-327	65.0	8.0
	E-464	43.0	15.0
		Avg. 73.7	Avg. 6.6
39.	E-550	3.0	17.0
	E-516	0.0	100.0
	E-551	0.0	100.0
	E-525	0.0	100.0
	E-553	0.0	100.0
	E-546	0.0	100.0
	E-555	0.0	100.0
	E-527	0.0	100.0
	E-528	6.0	97.0
		Avg. 1.3	Avg. 90.4

TABULATION OF % AREA DESTROYED AND % AREA UNMELTED ON OUTSIDE OF CLAD

Fuel Element No.	Plate No.	% Area Destroyed	% Area Unmelted
41.	E-519	51.0	17.0
	E-466	40.0	19.0
	E-455	51.0	19.0
	E-463	57.0	16.0
	E-465	65.0	13.0
	E-473	68.0	12.0
	E-470	73.0	11.0
	E-474	75.0	10.0
	E-540	80.0	4.0
		Avg. 62.2	Avg. 13.4
43.	All Plates Complete	Very Slight Melting	100.0
			100
44.	All Plates Complete	0.0	100.0
		0	100
45.	All Plates Complete	0.0	100.0
		0	100
46.	All Plates Complete	0.0	100.0
		0	100
47.	All Plates Complete	0.0	100.0
		0	100
48.	E-573	0.0	23.0
	All Other Plates Complete	0.0	100.0
			Avg. 91.4
49.	All Plates Complete	0.0	100.0
		0	100

TABULATION OF % AREA DESTROYED AND % AREA UNMELTED ON OUTSIDE OF CLAD

Fuel Element No.	Plate No.	% Area Destroyed	% Area Unmelted
50.	E-618	70.0	24.0
	E-625	70.0	21.0
	E-631	63.0	23.0
	E-628	61.0	25.0
	E-676	54.0	19.0
	E-672	53.0	15.0
	E-619	40.0	15.0
	E-677	15.0	68.0
	E-674	16.0	19.0
		Avg. 49.1	Avg. 25.0
51.	All Plates Complete	0.0	100.0
		0	100
52.	E-673	9.0	16.0
	E-634	10.0	22.0
	E-669	11.0	23.0
	E-627	10.0	19.0
	E-624	15.0	20.0
	E-718	24.0	19.0
	E-663	20.0	18.0
	E-626	27.0	21.0
	E-689	28.0	12.0
		Avg. 17.1	Avg. 18.9
53.	All Plates Complete	0.0	100.0
		0	100
54.	All Plates Complete	0.0	100.0
		0	100
55.	All Plates Complete	0.0	100.0
		0	100.
56.	E-723	0.0	75.0
	All other Plates Complete	0.0	
			Avg. 97.2

TABULATION OF % AREA DESTROYED AND % AREA UNMELTED ON OUTSIDE OF CLAD

Fuel Element No.	Plate No.	% Area Destroyed	% Area Unmelted
57.	All Plates Complete	0.0	100.0
		0	100
58.	All Plates Complete	0.0	100.0
		0	100
59.	E-777	0.0	40.0
	E-695	0.0	40.0
	E-811	0.0	40.0
	E-815	0.0	30.0
	E-788	0.0	30.0
	E-790	0.0	30.0
	E-813	0.0	30.0
	E-809	0.0	30.0
	E-749	0.0	40.0
			Avg. 34.4
60.	All Plates Complete	0.0	100.0
		0	100
61.	All Plates Complete	0.0	100.0
		0	100
62.	E-704	0.0	30.0
	E-765	0.0	30.0
	E-699	0.0	30.0
	E-728	0.0	30.0
	E-709	0.0	30.0
	E-702	0.0	30.0
	E-661	0.0	30.0
	E-732	10.0	3.0
	E-774	10.0	2.0
		Avg. 2.2	Avg. 24.9

Total Core: 19.8% Destroyed; 68.0% "ostensibly" unmelted
Core Center (16 elements): 47.4% Destroyed
Core Center 4 corner elements: 1.2% Destroyed

APPENDIX E

Tabulation of Flux Measured by Each Cobalt - Aluminum Pellet

(Pellets not reported were either unrecovered or unidentified)

Element	Wire Number	Position Between Fuel Plates	Position from top of fuel plate Inches	Thermal Flux $n/cm^2 \times (10^{-14})$
1	2157	G	-8.5	3.05
			-5.5	1.84
			-2.5	1.54
2	1368	B		
	1403	G		
3	1251	B	0.5	1.7
			3.5	1.9
			6.5	
			9.5	3.8
			12.5	
			15.5	5.2
			18.5	5.1
			21.5	4.7
			24.5	4.0
			27.0	3.9
	1563	G	0.5	1.54
			3.5	1.66
			6.5	2.17
			9.5	3.17
			12.5	4.19
			15.5	4.06
			18.5	4.01
			21.5	3.93
			24.5	2.70
			27.0	2.55
	1830	E	0.5	2.0
			3.5	2.3
			6.5	2.5
			9.5	3.2
			12.5	4.7
			15.5	5.2
			18.5	6.0
			21.5	5.1
			24.5	3.7
			27.0	
4	2027	B	0.5	1.95
			3.5	1.74
	1533	D	0.5	1.42
			3.5	1.78
			6.5	4.85
			9.5	4.13

Element	Wire Number	Position between Fuel Plates	Position from top of fuel plate Inches	Thermal Flux $n/cm^2 x(10^{-14})$
5	2144	G	0.5	1.07
			3.5	1.42
			6.5	1.70
			9.5	2.73
			12.5	3.28
			15.5	3.03
			18.5	3.21
			21.5	2.88
			24.5	1.72
			27.0	1.91
	2054	B	0.5	
			3.5	.84
			6.5	1.90
			9.5	2.47
			12.5	2.52
			15.5	3.16
			18.5	2.79
			21.5	2.83
			24.5	2.11
			27.0	1.92
6	1339	B	-8.5	.68
			-5.5	.94
			-2.5	1.56
			0.5	3.00
			3.5	3.83
			6.5	5.40
			9.5	
			12.5	
6	1685	G	-8.5	.20
			-5.5	.38
			-2.5	1.06
			0.5	1.19
			3.5	1.21
			6.5	3.75
			9.5	6.18
			12.5	
	1349	E	3.5	1.70
			6.5	2.21
			9.5	4.70
			12.5	6.50
7	1799	B	0.5	1.46
			3.5	2.03
			6.5	2.80

Element	Wire Number	Position between Fuel Plates	Position from top of fuel plate Inches	Thermal Flux $n/cm^2 x(10^{-14})$
	1252	G	3.5	2.15
			6.5	3.58
			9.5	4.90
			12.5	6.91
			15.5	6.41
			18.5	5.67
			21.5	5.39
			24.5	4.03
8	1409	G	0.5	3.1
			3.5	2.9
			6.5	
			9.5	5.6
	1435	B		
9	1258	G	0.5	
			3.5	.89
			6.5	1.17
			9.5	1.54
			12.5	2.31
			15.5	2.50
			18.5	2.78
			21.5	1.98
			24.5	1.84
			27.0	1.01
10	1243	E	0.5	1.67
			3.5	1.54
			6.5	2.67
			9.5	3.95
			12.5	5.37
			15.5	5.78
			18.5	6.17
			21.5	4.94
			24.5	4.00
11	1274	B	0.5	1.38
			3.5	1.17
			6.5	1.69
			9.5	1.96
			12.5	2.68
			15.5	3.45
			18.5	2.84
			21.5	2.88
			24.5	1.89
			27.0	1.88

Element	Wire Number	Position between Fuel Plates	Position from top of fuel plate Inches	Thermal Flux $n/cm^2 x(10^{-14})$
	1872	D	0.5	1.16
			3.5	1.75
			6.5	3.32
			9.5	3.20
			12.5	3.55
			15.5	2.88
			18.5	1.92
			21.5	1.87
			24.5	1.30
			27.0	
	1972	G	All pellets missing from wire	
13	2162	E	0.5	
			3.5	.91
			6.5	1.82
			9.5	+
			12.5	+
			15.5	+
			18.5	+
			21.5	+
			24.5	+
			27.0	1.25
18	1605	E	0.5	.64
			3.5	.84
			6.5	.90
			9.5	1.58
			12.5	1.63
			15.5	2.18
			18.5	2.33
			21.5	1.97
			24.5	.89
			27.0	.96
19	2010	B	0.5	*
			3.5	.84
			6.5	.82
			9.5	+
			12.5	3.39
			15.5	2.23
			18.5	1.70
			21.5	1.27
			24.5	.95
	1247	G	0.5	*
			3.5	*
			6.5	*
			9.5	.64

+ Contaminated during chemical separation
* Below threshold of detection

Element	Wire Number	Position between Fuel Plates	Position from top of fuel plate Inches	Thermal Flux $n/cm^2 x(10^{-14})$
			12.5	.32
			15.5	1.06
			18.5	1.06
			21.5	.74
			24.5	.64
			27.0	.53
39	1257	G	0.5	1.28
			3.5	1.52
			6.5	
			9.5	2.30
			12.5	3.03
			15.5	3.31
			18.5	2.74
			21.5	
			24.5	2.28
			27.0	2.33
	2013	B		
41	1249	G		
	1433	B		
43	1278	E	0.5	.59
			3.5	.80
			6.5	.97
			9.5	1.08
			12.5	2.18
			15.5	1.94
			18.5	1.79
			21.5	1.24
			24.5	1.03
			27.0	1.02
47	1388	D	0.5	.25
			3.5	.50
			6.5	.63
			9.5	.70
			12.5	.76
			15.5	1.02
			18.5	.94
			21.5	.76
			24.5	.56
			27.0	.68

Element	Wire Number	Position between Fuel Plates	Position from top of fuel plate Inches	Thermal Flux $n/cm^2 x(10^{-14})$
47	1526	G		
	1905	B	5.5	.08
			2.5	.48
			0.5	.64
			3.5	1.17
			6.5	1.27
			9.5	2.01
			12.5	2.17
			18.5	2.37
			21.5	2.09
			24.5	1.74
				1.46
48	1242	G	0.5	1.16
			3.5	1.18
			6.5	1.72
			9.5	2.76
			12.5	3.12
			15.5	3.04
			18.5	3.01
			21.5	2.86
			24.5	1.88
			27.0	1.60
51	1272	B		
52	2187	E	-8.5	.65
			-5.5	.39
			-2.5	4.2
			0.5	4.5
			3.5	3.6
53	1784	B	0.5	.82
			3.5	.84
			6.5	1.04
			9.5	1.15
			12.5	1.35
			15.5	1.64
			18.5	1.72
			21.5	1.35
			24.5	.74
			27.0	.37
55	1201	E		

Element	Wire Number	Position between Fuel Plates	Position from top of fuel plate Inches	Thermal Flux $n/cm^2 x(10^{-14})$
56	2074	D	0.5	.64
			3.5	.61
			6.5	.97
			9.5	1.23
			12.5	1.53
			15.5	1.78
			18.5	1.50
			21.5	1.33
			24.5	1.06
			27.0	.94
58	1245	G	0.5	.71
			3.5	.53
			6.5	.50
			9.5	.49
			12.5	.65
			15.5	.99
			18.5	.90
			21.5	.65
			24.5	.54
			27.0	.50
58	1236	B	0.5	.62
			3.5	1.22
			6.5	1.87
			9.5	1.79
			12.5	1.94
			15.5	1.51
			18.5	1.34
			21.5	1.26
			24.5	.81
			27.0	.49
59	1426	D	0.5	.44
			3.5	.58
			6.5	1.0
			9.5	1.44
			12.5	1.60
			15.5	2.68
			18.5	3.0
			21.5	2.27
			24.5	2.06
			27.0	2.05
60	1766	D		
62	1546	E		

APPENDIX F

ANALOG COMPUTER STUDY OF REACTOR INCIDENT

The analog study, conducted using the setup shown in Figure F-1, allows a 10 decade power excursion without re-scaling. Since the calculated values from the SPERT model predicted a peak power of less than 40,000 megawatt seconds, the critical level could be as low as 4 watts and still be within the 10 decade range of the computer.

The nuclear portion of the simulation was contained in amplifiers 1, 3, 9, 13, 25, and integrating amplifiers 5 and 23. Amplifiers 1 and 3, coupled with their multipliers, comprise the three shortest-lived delayed groups. The other delayed groups were eliminated by a series of trial runs which showed that they contributed no noticeable effect to the results. The system gain was established such that potentiometers P1, P2, and P3 could be set to the λ_i values (delayed neutron group decay constants) directly. In like manner potentiometers P11, P12, and P13 were set to the β_i values (delayed neutron group fraction) directly. Integrating amplifier 5 along with P8 was used to generate the various ramps of reactivity (ΔK) used in the simulation. This circuit was modified to produce the non-linear ramp functions which are shown on the traces in Figures III-97, 98, and 99 of Section III, 4.6. The potentiometer P10 was used to set the value of $\Sigma \beta_i$ directly. Summing the above variables produces ℓ/τ at amplifier 13. Amplifier 14 permitted varying the generation time (ℓ). The output of 14 is $1/\tau$. The negative value of $1/\tau$ is integrated by amplifier 23, producing ln ϕ. (ϕ = reactor flux or power.)

The remainder of the setup is used to simulate the temperature in a fuel plate, converting ln ϕ to ϕ, integrating ϕ, then inserting a feed back of ΔK proportional to energy, both linear and delayed. Only the top four decades of linear power are employed. Amplifier 12 covers two decades, and then amplifier 6 switches in producing the top two decades of linear power. This approximation of the total power trace is very good since the first 6 decades do not contribute an appreciable amount of energy (approximately 1/100% of total.) The output of integrating amplifier 17 is the total energy. This unit is used to supply the linear energy feed back through the 2 megohm summing resistor plus the delayed energy feed back through the multiplier.

The temperature simulation represents the following equations:

$$\text{I} \qquad \frac{dT_o}{dt} = 3.18\, Q_o - 630\,(T_o - T_1),$$

$$\text{II} \qquad \frac{dT_1}{dt} = 3.18\, Q_1 + 630\,(T_o + T_2) - 1260\, T_1,$$

$$\text{III} \qquad \frac{dT_2}{dt} = 605\,(T_1 + T_3) - 1210\, T_2,$$

$$\text{IV} \qquad \frac{dT_3}{dt} = 300\,(T_2 - T_3)$$

where:

T_o = centerline of meat temperature,

T_1 = temperature at meat clad interface,

T_2 = temperature at 0.030 cm from surface,

T_3 = surface temperature.

The output of amplifier 24 represents surface temperature. This temperature is used to drive the switch and delay circuit consisting of amplifiers 15, 16, 18 and 31.

The system described allows simulation of the incident based on a gross reactor behavior. The overall system calibration is performed by the ratio of peak meat source energy and energy required to bring the peak section to 100°C (85°C above assumed ambient temperature of 15°). This value was calculated by simulating the enrgy deposited in a unit volume of meat. The source energy in the maximum flux region is known from the flux wire analysis; and the energy required to bring the surface to 100°C can be calculated, using the average plate temperature as shown in Section IV-1.4. The ratio of these two energies is approximately 10.

Using the system as described, a number of runs were made, each recording the total energy for several different ramp rod-withdrawal rates and different delay times. These results can be seen in Figure III-97, 98, and 99 of Section III-4.6. As shown in these figures the critical power level was determined to be approximately 400 watts. This value produces a conservative estimate for the time from critical to the occurrence of the peak power. The temperature output of the peak energy density region was used to calibrate the total energy output, which in turn was used to calibrate the power trace and establish the value of the initial power. The calibration between energy and log of power could be changed by varying the gain of amplifier 17, thus, in essence, changing the initial power.

Figure F-2 is a typical run, showing outputs of energy, log of power, and reactivity, which consisted of the ramp input plus the two feed back terms. A reactivity feed back becomes apparent approximately 10 milliseconds before the peak of the burst. This is, of course, the plate expansion term. With the assumed void coefficient of 0.0039% ΔK/megawatt second, the total effect of the plate expansion, based on a linear coefficient of expansion, would be less than 0.55%. This linear energy feed back term is small in comparison to the total reactivity to be overcome by the shutdown mechanism.

The major remaining portion of the shutdown must come from steam void formation. As discussed earlier, this mechanism is quite complicated, but is evidently delayed by approximately 3 milliseconds, for short period excursions, from the time the

plate surface temperature reaches 100°C until the appearance of any steam voids. The 130 Mw-sec total energy generated in the excursion was used as a constraint on the shutdown mechanism. It was found that without a delay between saturation temperature on the plate surface and the beginning of void formation, it was impossible to achieve a reasonable power trace in which the feedback was proportional to energy and the total accumulated energy was about 130 Mw-sec. For the tests of simulated rod-withdrawals, discussed in Section III-4.6, the excursion was made to approach a chopped exponential, a condition approximating the bursting of plates due to vaporization. Such an approximation will have little influence on the conclusions derived concerning the rate of reactivity insertion and the position of the central control rod at the peak of the excursion.

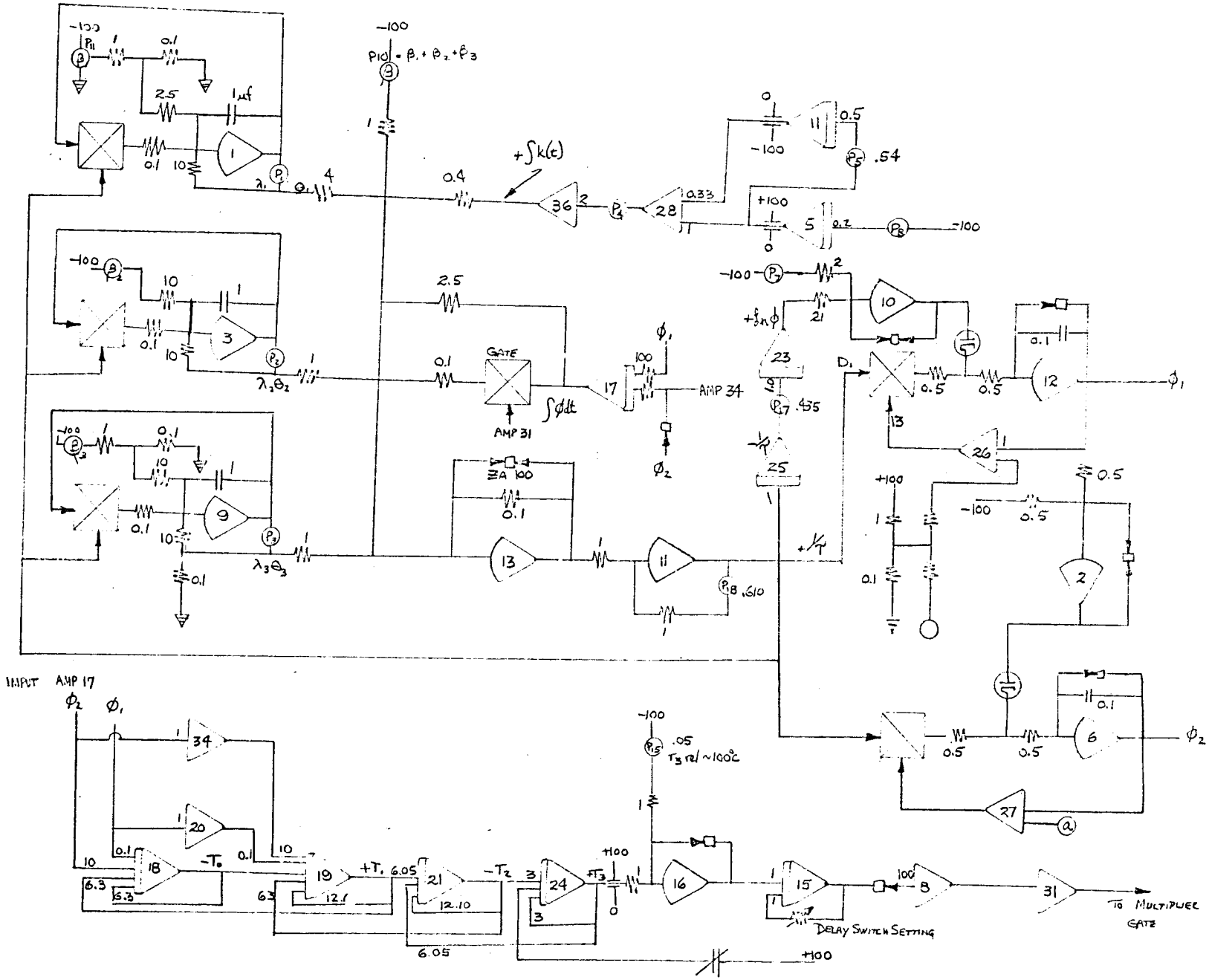

Figure F-1 Analog Circuit Used for Excursion

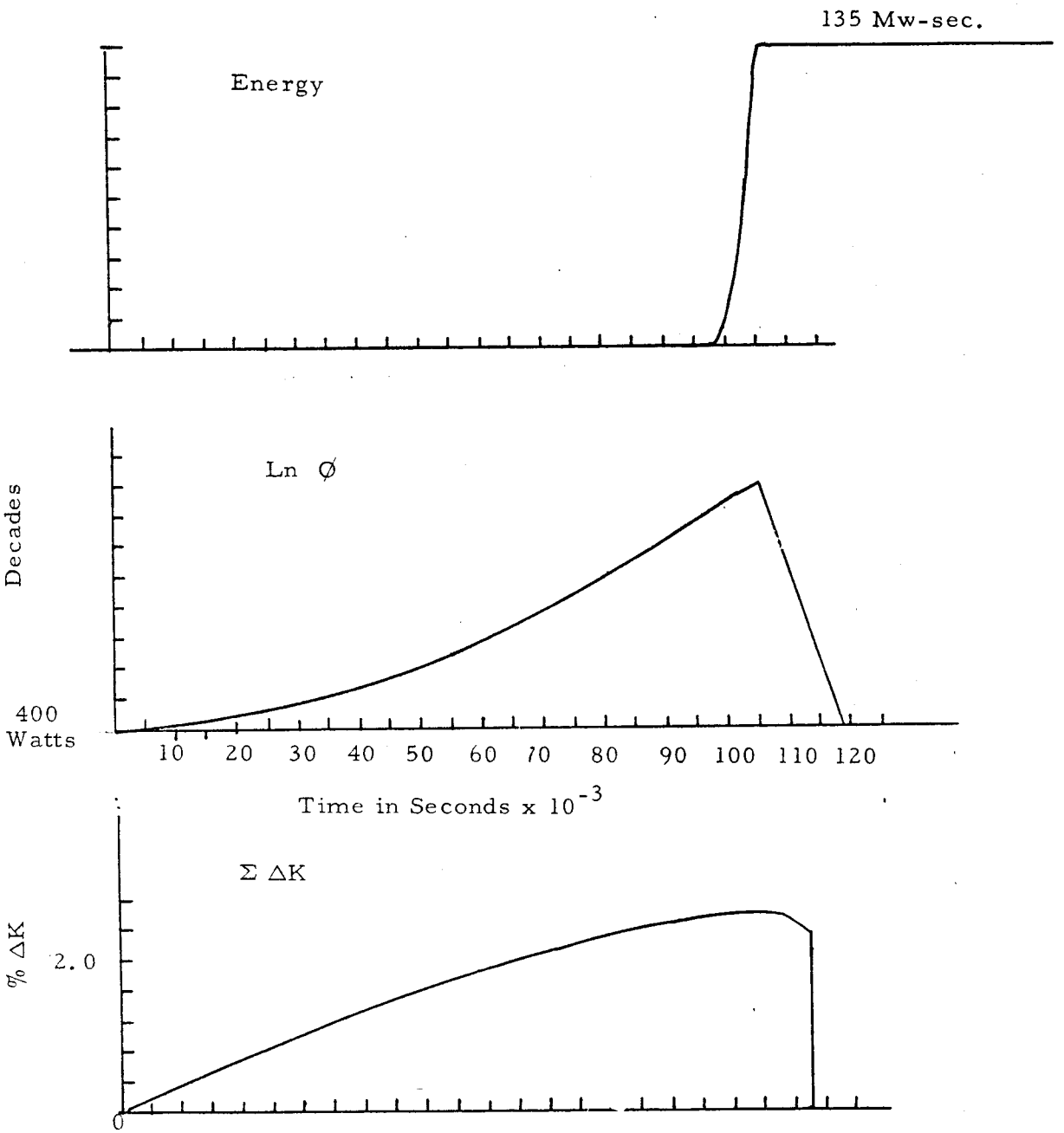

Figure F-2 Typical Transient Power Run